SURFACE WATER – GROUNDWATER INTERACTIONS AND THEIR CONTROL ON GROUNDWATER REDOX PROCESSES

A THESIS
SUBMITTED TO THE FACULTY OF THE
UNIVERSITY OF MINNESOTA
BY

AUBREY JUSTINE DUNSHEE

IN PARTIAL FULFILLMENT OF THE REQUIREMENTS
FOR THE DEGREE OF
MASTER OF SCIENCE

Gene-Hua Crystal Ng

FEBRUARY 2020

Acknowledgements

I would like to thank my adviser, Crystal Ng, for her amazing support and encouragement over the last two plus years; it has been a delight being your student. I would also like to thank Cara Santelli for being my surrogate co-adviser and for her valuable insights and support over the final year of my graduate career, and Brandy Toner for kindness, support, and advice during my time in her lab as an undergraduate researcher as well as during my time as a graduate student.

I would also like to thank our collaborators without which none of this work would have been completed. I would like to thank Doug Kent, Deborah Repert, Richard Smith, Tim McCobb and Robert Hull for collecting and analyzing valuable data that was used in the first chapter of this thesis. I would also like to thank Dan Kaplan, John Seaman, and Michael Liard for their immense support in the field and in the lab as we completed our field investigations in Aiken, SC. I would like to thank every member of the Cara Santelli Lab, especially Mary Sabuda, Jackie Mejia, Chris Schuler, and Tingying Yu, who helped me in any way they could while I worked in the Santelli lab. I would like to extend a special thank you to Alex Waheed, whose collaboration and aid during geochemical analyses was essential to the completion of this thesis. I would also like to thank Joshua Torgeson for paving the way on the geochemical analyses used in the second chapter of this thesis. Without his invaluable work and SOPs, the second chapter of this thesis would likely not exist.

Finally, I would like to thank my family for their unwavering support throughout this process. Without them, I would not be the person or scientist that I am today.

Dedication

I dedicate this thesis to my partner, who has endured all the hardships of graduate school along with me over the past two and a half years with admirable strength, grace, and patience. He has and continues to give the support and inspiration I need to do and be my best, and I would not have made it here without him.

Abstract

Interactions between surface water and groundwater promote sharp geochemical and redox gradients, diverse microbial metabolisms, and the transformation of contaminants. Due to the impact on water quality, it is important to develop a greater understanding of surface water-groundwater interaction and hyporheic zone systems. Here, two projects are discussed, both focus on investigating surface water-groundwater interactions and their impacts on biogeochemical cycles occurring in the subsurface. In chapter one, a reactive transport model was developed to simulate seasonal temperature variability in an aquifer downgradient from a nutrient impacted lake. Model results indicate that As release is temperature dependent and implementing temperature variation results in As concentrations above maximum contaminant levels (MCL). Above MCL As concentrations were unable to be reproduced in scenarios where temperature was simplified to an averaged value. Chapter two outlines field and lab-based methods used to observe hydrologic, geochemical, and microbial drivers of "cryptic" sulfur cycling within a heterogeneous and diverse riparian wetland of the Savannah River in Aiken, SC. Results indicate that dynamic hydrologic conditions have a marked impact on subsurface geochemistry. Subsites which experienced periods of inundation and non-inundation had higher dissolved and solid Fe concentrations and elevated sulfate concentrations. Additionally, hydrologic flux direction appears to be linked to the production of Fe oxide microbial mats. Sites which experienced upward flux of groundwater contained flocs, whereas sites which experienced downward flux did not. Finally, sites containing microbial mats were found to contain S intermediates, indicating the presence of "cryptic" sulfur cycling.

Table of Contents

List of Tables

List of Figures

1.0 Introduction

Since the enactment of the Clean Water Act in 1972, water quality standards set by local, state, or federal agencies have brought about valuable research into surface water and groundwater chemistry for both naturally occurring and anthropogenically introduced contaminants. Often, surface water and groundwater are seen as separate pools, however; these two water sources are intrinsically linked via the surface water-sediment interface (Sophocleous, 2002). Depending on the hydraulic gradient of the system, surface water can have a marked impact on groundwater chemistry, and vice versa, through flow or mixing across this interface (Sophocleous, 2002). The study of surface-water groundwater interactions lends itself to a wide variety of disciplines depending on the research question. Some have utilized heat transport to quantify flow across a surface water-sediment interface (Anibas et al., 2009; Engelhardt et al., 2011; Hatch, Fisher, Revenaugh, Constantz, & Ruehl, 2006; Rau, Andersen, Mccallum, & Acworth, 2010), others have observed microbial communities that exist within these interfaces (Ayuso, Acebes, López-archilla, Montes, & Guerrero, 2007; Stern et al., 2017), while others have inspected geochemical or hydrologic impacts that occur downgradient (Costa, Burlando, & Liong, 2016; Scanlon & Cook, 2002).

Surface water-groundwater interfaces, otherwise known as hyporheic zones, are hotspots of activity. Advection, steep geochemical gradients, and microbial metabolisms drive transformations of pollutants, sometimes resulting in the removal of the pollutant from the mobile phase (Boano et al., 2014; Boulton, Findlay, Marmonier, Stanley, & Valett, 1998). Sharp redox gradients often occur due to contact between oxic surface water and suboxic or anoxic porewaters (Boano et al., 2014; Boulton et al., 1998).

Hyporheic zone characteristics can cause the net removal of contaminants such as organic micropollutants (Burke et al., 2014), and trace metals via precipitation of sorptive minerals (Fuller & Harvey, 2000; Gandy, Smith, & Jarvis, 2007; Lynch, Batty, & Byrne, 2014; Winter, Harvey, Franke, & Alley, 1998). However, hyporheic zone processes have also been observed to result in the release of contaminants such as arsenic (Nagorski & Moore, 1999). Due to the impact on water quality, as well as their inherent heterogeneity and complexity, it is important to develop a greater understanding of surface water-groundwater interaction and hyporheic zone systems.

A plethora of literature exists relating to surface water-groundwater interactions and hyporheic zone processes, but questions remain about specific processes both within and downgradient of these systems. For example, evidence suggests that surface water-groundwater interactions may play a role in seasonally variable arsenic concentrations downgradient of a nutrient impacted lake, however research into arsenic release often focuses on areas with little seasonality or on deeper groundwater where seasonal temperature changes have little effect. Also, evidence of "cryptic" sulfur cycling, in which the oxidation/reduction pathways of sulfur are believed to be more complex and linked to processes such as abiotic Fe(III) reduction, have been found in several hyporheic zones, though the mechanisms of this "cryptic" sulfur cycle remain poorly understood.

Here, two projects are discussed which differ in both motivation and methods. Both, however, focus on investigating surface water-groundwater interactions and their impacts on biogeochemical cycles occurring in the subsurface. Chapter one will observe surface water-groundwater interactions in the lens of seasonal variation in naturally occurring aqueous contaminants, specifically arsenic. A reactive transport model was developed to observe arsenic concentrations in an aquifer downgradient of a nutrient impacted lake, where arsenic concentrations were seemingly affected by seasonal changes in temperature. In this case, surface water transports both organic carbon and increased or decreased temperatures (depending on the season) to the downgradient aquifer. Research into this topic was driven by the hypothesis that recharge from surface water may introduce water impacted by atmospheric temperatures into aquifers, affecting processes such as arsenic release.

Looking more closely at the hyporheic zone, chapter two outlines field and laboratory-based methods used to observe hydrologic, geochemical, and microbial characteristics within a heterogeneous and diverse riparian wetland of the Savannah River in Aiken, SC. Utilizing a suite of multi-disciplinary methods, an investigation into “cryptic” sulfur cycling was conducted on this wetland, in hopes to capture a glimpse at the mechanisms that drive this sulfur cycle.

2.0 Temperature-dependent reactive transport modeling of arsenic release downgradient of a eutrophic lake

2.1 Introduction

2.1.1 Motivation

Exposure to arsenic in drinking water is a major global health concern. Acute exposure above toxic levels can lead to destruction of red blood cells, vertigo, and death (Mandal & Suzuki, 2002). Chronic exposure, even at concentrations below toxic levels, have been linked to hyperkeratosis, reduced neuron and motor function, and skin, liver, and kidney cancers (Mandal & Suzuki, 2002). Inorganic arsenic has been identified by the U.S. Environmental Protection Agency (EPA) as a known carcinogen (Mandal & Suzuki, 2002), and the World Health Organization (WHO) has set a provisional maximum contaminant level (MCL) for arsenic at 10μg/L (0.133 μM) (World Health Organization, 2011). Many studies throughout the world have noted arsenic concentrations in drinking water above this standard, often in economically vulnerable communities (A. H. Smith, Lingas, & Rahman, 2000). Due to health risks and widespread contamination, it is important to understand the mechanisms that attenuate and release arsenic into drinking water.

2.1.2 As Chemistry – Mobile Phases

Inorganic arsenic (As) exists in solution primarily in two forms, the oxidized form arsenate (As(V)), and the reduced form arsenite (As(III)). Arsenic acts as a weak acid oxyanion, ranging from the fully deprotonated forms (AsO_4^{3-}, AsO_3^{3-}) to fully protonated forms (H_3AsO_4, H_3AsO_3). At most environmentally relevant pH values (6-8), the most common mobile forms of As are H_2AsO^{3-} and $HAsO_3^{2-}$ for arsenate, and H_3AsO_3 for arsenite (Smedley & Kinniburgh, 2002).

2.1.3 *As Attenuation: Sorption Reactions*

Arsenic can be readily immobilized from solution by poorly crystalline, positively charged mineral surfaces, most commonly on ferric iron (Fe^{3+}) oxyhydroxide mineral phases (Bauer & Blodau, 2006; Bauer, Fulda, & Blodau, 2008; Oremland & Stolz, 2003). Processes such as adsorption of As on poorly crystalline Fe^{3+} oxide minerals (e.g., hydrous ferric oxide (HFO), such as ferrihydrite), as well as co-precipitation of As with Fe^{3+} oxide minerals and ferrous iron (Fe^{2+}) sulfides, have been observed (Farquhar, Charnock, Livens, & Vaughan, 2002; Goldberg & Johnston, 2001; Pierce & Moore, 1980, 1982; Raven, Jain, & Loeppert, 1998). As(V) is much more readily sorbed onto positively charged mineral surfaces than its reduced counterpart (Oremland & Stolz, 2003), and thus, redox conditions play a major role in the mobility of arsenic in aquatic systems (Ascar, Ahumada, & Richter, 2008).

2.1.4 *As Mobilization*

Arsenic can be mobilized from mineral surfaces through processes such as competitive ion sorption on and reductive dissolution of hydrous ferric oxide (HFO) (Smedley & Kinniburgh, 2002).

Arsenic often competes with other ions for the same sorption sites on mineral surfaces. Ions such as phosphate (PO_4^{3-}), carbonate (CO_3^{2-}, HCO_3^-), and Fe^{2+} are common competitors (Appelo, Van Der Weiden, Tournassat, & Charlet, 2002). If concentrations of any of these ions increase, arsenic may competitively desorb from the mineral surface and re-enter porewater.

In the case where there is a reductant present, a shift towards lower redox potentials can also result in a net release of sorbed As into porewater. In porewater downgradient from lakes, a common reducing agent is particulate or dissolved organic carbon (POC and DOC, respectively) (Bauer & Blodau, 2006; Bauer et al., 2008). Oxygenic microbial organic carbon oxidation can rapidly consume dissolved oxygen in porewater, forcing reliance on alternative electron acceptors, such as Fe^{3+}, to complete this reaction. The utilization of Fe^{3+} results in the dissolution of Fe^{3+} minerals, and the release of ions once sorbed onto the mineral surface, including As. Further, low redox potentials (100mV to -400mv at environmentally relevant pH values) can also result in the reduction of As(V) to As(III), which has reduced affinity for sorption on remaining ferric oxide minerals (Smedley & Kinniburgh, 2002).

2.1.5 Lake Eutrophication and Temperature Dependence of Organic Carbon Oxidation

Porewaters downgradient from lakes or ponds can be susceptible to delivery of high organic carbon concentrations, depending on the trophic level of the lake or pond (Williamson, Morris, Pace, & Olson, 1999). Lakes of a higher trophic level, such as eutrophic lakes, are nutrient-impacted, and often result in high organic carbon concentrations advected to downgradient porewaters (Williamson et al., 1999). The introduction of increased organic carbon concentrations can result in the rapid consumption of dissolved oxygen in downgradient aquifers and lead to increased concentrations of reduced forms of redox sensitive species as organic carbon oxidation utilizes alternative electron acceptors.

Additionally, the temperature of the incoming surface water can also affect the impact of organic carbon in downgradient porewaters. Clear links have been made between seasonal air temperature changes and variation in groundwater temperature due to surface water – groundwater interactions (Anibas et al., 2009; Rau, Andersen, Mccallum, Roshan, & Acworth, 2014). Heat transfer is often used to quantify rates of hyporheic flux (Briggs, Lautz, Mckenzie, Gordon, & Hare, 2012; Constantz, Eddy-Miller, Wheeler, & Essaid, 2013; Lautz, Kranes, & Siegel, 2010). Studies have also shown a clear link between temperature and microbial respiration – with an increase of a factor of 2-5 with an increase in temperature by 10°C (Arnosti, Jorgenson, Sagemann, & Thamdrup, 1998; Fierer, Colman, Schimel, & Jackson, 2006), with similar trends occurring with degradation rates of terrestrial organic carbon (Lloyd & Taylor, 1994; Singh & Gupta, 1977). Studies show minimal amounts of respiration at temperatures of 0°C, with respiration rates increasing and reaching maximum values at 60°C (Singh & Gupta, 1977).

2.1.6 Temperature and As Mobilization

Observed effects of organic carbon concentration on As release (Bauer & Blodau, 2006; Bauer et al., 2008), together with links found between temperature and microbial respiration, suggest a potential connection between variable temperature and As release into porewater. Some studies have investigated this link, focusing on flooded contaminated soils (Simmler et al., 2017; Weber, Hofacker, Voegelin, & Kretzschmar, 2010), the rhizosphere below rice paddies (Neumann, Seyfferth, Teshera-levye, & Ellingson, 2017), stratified lakes and lakebed sediments (Barrett et al., 2019), and groundwater sediments (Bonte, Breukelen, & Stuyfzand, 2013). In all studies, a positive correlation was identified between temperature and mobile arsenic concentrations. Many studying this link utilized laboratory microcosm experiments, placing soils and sediments under varying temperature conditions (Bauer & Blodau, 2006; Neumann et al., 2017; Simmler et al., 2017; Weber et al., 2010), while fewer have utilized field observations (Barrett et al., 2019; Bauer et al., 2008).

Currently, little is known about the temperature dependence of As release in shallow groundwater adjacent to temperate lakes, due to the relative lack of field studies in such settings. Field-based investigations of As have generally not focused on temperature and often examine warm-climate settings that undergo little temperature variation. In fact, many As studies take place in tropical and sub-tropical environments, particularly southeast Asia (Bose & Sharma, 2002; Charlet et al., 2007; Harvey et al., 2002; Dieke Postma et al., 2007), where temperatures are relatively constant year-round. Arsenic contamination, however, is not exclusively a problem in tropical climates. Temperate climates, including the Midwest and Northeast regions of the United States, also experience above-MCL As concentrations due to contact between lithologic facies of differing redox conditions (Erickson & Barnes, 2005a, 2005b; Nicholas et al., 2017). Additionally, groundwater arsenic contamination in the western United States has been potentially linked to irrigation occurring in areas laden with volcanic sediments (Welch, Lico, & Hughes, 1988). High dissolved arsenic concentrations have also been linked to dissolution within arsenopyrite-rich igneous and shale beds in Alaska and California (Nordstrom, 2002). Similarly, the occurrence of arsenic-contaminated aquifers has been linked to As-rich sulfide deposits in the northeastern portion of the United States (Welch, Westjohn, Helsel, & Wanty, 2000). The prevalence of groundwater As contamination throughout the United States motivates the need for examining the effect of seasonal temperature variability while studying As mobilization. This is especially important in shallow groundwaters adjacent to lakes, which, compared to deeper aquifers, are more strongly influenced by varying atmospheric temperature and tend to experience more dynamic redox conditions that facilitate As attenuation and mobilization.

Temperature dependence of mobile As has been observed in the field within lakebed sediments in the context of lake stratification (Barrett et al., 2019). It was found that increased lake stratification resulted in more constant temperatures in lakebed sediments as compared to weakly stratified lakes where lakebed sediment temperatures more closely matched atmospheric temperature. This difference in lakebed sediment temperature led to decreased As mobilization in sediments within beds of strongly stratified lakes as compared to weakly stratified lakebeds (Barrett et al., 2019). Our study builds off these findings on the temperature sensitivity of As release in lakes but focuses on seasonal rather than spatial temperature variability and examines As mobilization in groundwater farther downgradient of lakes, where it can affect drinking supplies.

2.1.7 Objective and Hypothesis

The objective of this study is to investigate temperature-dependent arsenic release mechanisms in the context of shallow aquifers downgradient from heavily nutrient-impacted lakes. We hypothesize that temperature influences on organic carbon degradation will have impacts on dissolved oxygen concentrations in downgradient aquifers, such that shallow groundwaters will experience more reducing conditions during warmer periods due to increased organic carbon consumption of dissolved oxygen, and more oxidizing conditions during colder periods due to decreased organic carbon degradation. We then anticipate that the difference in redox conditions will result in reductive dissolution of Fe^{3+} oxyhydroxides and release of sorbed As during warmer conditions, and the precipitation of Fe^{3+} oxyhydroxides and attenuation of mobile As during colder conditions.

To test this hypothesis, we investigate geochemical data from an As-impacted aquifer downgradient from a nutrient-dense lake on Cape Cod, Massachusetts (USA), and we assess the mechanisms controlling geochemical conditions using a multi-component reactive-transport model. We specifically hypothesize summer months to result in the delivery of high temperature, organic carbon rich waters to the downgradient aquifer, resulting in the dissolution of As-sorbing Fe-oxide minerals and corresponding release of As into the mobile phase. During colder months, we expect the delivery of low temperature oxic waters, leading to the re-precipitation of Fe-oxide minerals and the removal of As species by these sorptive minerals.

2.2 Field Investigations

The model is motivated by aquifer-lake systems located on Cape Cod, Massachusetts (USA), where arsenic concentrations above the MCL have been observed. Cape Cod is underlain with mostly glacial outwash sands, and many of its lakes are impacted by wastewater and residential runoff resulting in lakes with trophic levels ranging from oligotrophic to hypereutrophic (R. L. Smith, Repert, Barber, & Leblanc, 2013). Previous studies at and nearby our aquifer-lake systems of interest have characterized Fe phases within mineral grain coatings (Zhang et al., 2011), examined Pb and Zn sorption on aquifer sand grain coatings (Coston, Fuller, & Davis, 1995), and performed genomic analysis of nitrogen-based organic carbon degradation pathways (Stoliker et al., 2016).

Field investigations into mobile As concentrations within and downgradient from Cape Cod lakes were conducted by collaborators at the US Geological Survey. Methods for collection of groundwater and surface water samples follow those described in Kent & Fox (2004). Major and minor ion concentrations and trace metals concentrations were determined via ICP-AES, and total As concentrations were determined by ICP-MS (Kent & Fox, 2004). Observations indicate As concentrations above the MCL in shallow groundwater downgradient from the hypereutrophic lake Santuit Pond, and they appear to show a loose temperature correspondence (Figure 2.1). Additionally, there is evidence of reductive dissolution of Fe oxides downgradient of Santuit Pond, based on the notable concentrations of aqueous Fe^{2+} (Figure 2.2).

Santuit Pond is known to be a flow-through lake, but its flow field has not been well-characterized. Ashumet Pond, a nearby oligotrophic flow-through lake, has been extensively studied for temperature and flow parameters and is assumed to represent a similar physical setting as Santuit Pond.

Conceptually based on the two Cape Cod lakes, a reactive-transport model is implemented for a scenario in which an aquifer downgradient from a flow-through hypereutrophic lake receives waters of seasonally varying temperature. The implementation of seasonally varying temperatures advecting into downgradient porewaters is supported by data from Ashumet Pond (Figure 2.3). Temperature data downgradient from this pond indicate that seasonal surface water temperature variations are heavily influenced by atmospheric temperatures and quickly reach shallow groundwaters (up to about 29 m depth) at least 10 meters horizontally downgradient from the lake (at well F-722) (Figure 2.3). Temperature and flow parameter data from Ashumet Pond served as inputs into our model. Dissolved As concentrations downgradient from Ashumet Pond are well below the MCL (Figure 2.4), consistent with the low organic carbon concentrations typically associated with its oligotrophic classification. Geochemical data from hypereutrophic Santuit Pond served as the basis for our geochemical model results.

2.3 Reactive-Transport Model

2.3.1 Reactive-Transport Modeling

Reactive transport modeling makes it possible to examine different control mechanisms, such as transport, geochemical processes, and microbially based temperature drivers – as well as their combined influence – on the spatiotemporal release of As into groundwater.

Reactive transport modeling has proved to be a useful tool for examining arsenic in contaminated aquifers (Jung, Charette, & Zheng, 2009; Manning & Goldberg, 1996; Pierce & Moore, 1980; Dieke Postma et al., 2007; Wallis et al., 2011). Reactive transport modeling studies have aided in assessing arsenic attenuation mechanisms in coastal aquifers (Jung et al., 2009), arsenic variation under the influence of remediation techniques (Wallis et al., 2011), processes behind heterogeneous groundwater As distribution (Charlet et al., 2007), and shallow groundwater As release mechanisms within vulnerable communities (Dieke Postma et al., 2007). Reactive transport modeling has also aided in assessing the effects of surface water-groundwater interactions on general redox processes (Bardini, Boano, Cardenas, Revelli, & Ridolfi, 2012; Boano et al., 2014; Engelhardt et al., 2014; Lautz & Siegel, 2006; Runkel & Kimball, 2002; Zarnetske, Haggerty, Wondzell, Bokil, & González-Pinzón, 2012)

2.3.2 Model Description

2.3.2.1 Model Framework

The model is implemented using the reactive-transport model PHT3D (Prommer et al., 2003), which couples transport components of MT3DMS (Zheng and 217 Wang, 1999) and geochemical components of PHREEQC-2 (Parkhurst and Appelo, 1999). The model was run for 10 model years, with alternating cold seasons at 2°C and warm seasons at 25°C. The choice of a 10-year model run was based on anecdotal evidence of decade-long elevated arsenic concentrations occurring downgradient of Santuit Pond.

2.3.2.2 Transport Component

The model represents a 1-dimensional steady-state flow path in a 15-meter domain discretized into 50 grid cells, extending horizontally from the sediment-water interface into the downgradient shallow aquifer (Figure 2.5). In the 50-grid cell domain, the first grid cell represents surface water and the remaining 49 grid cells represent downgradient groundwater. MODFLOW simulations using hydraulic conductivity and head gradient parameters from Ashumet Pond were applied to generate the flow field. This was then implemented in PHT3D to simulate solute transport, along with dispersivity parameters appropriate for the 15-m length domain size (Garabedian, Leblanc, Gelhar, & Celia, 1991). Porosity typical of the region's glacial outwash sands (R. L. Smith et al., 2013) was also used. Table 2.1 summarizes flow and transport parameters.

2.3.2.3 Temperature Component

The temperature range set in the model is based on temperature measured in and downgradient of Ashumet Pond (Figure 2.3). Implementing a two-season temperature pulsing (180 days at 25°C and 180 days at 2°C) rather than a true annual cycle helped produce more distinct geochemical responses that facilitated interpretations of the effect of seasonal changes. PHT3D does not simulate heat transport, and instead, isothermal temperature was applied to the domain for each alternating hot/cold time period. Observations around Ashumet Pond showed similar temperatures in shallow groundwater (down to 6.1 m.a.s.l.) at 10m horizontally downgradient of the lake as within the lake water (Figure 2.3), supporting this simplified implementation in which temperature transport through 15 m of aquifer downgradient of the lake is assumed to be fast compared to seasonal changes in surface water temperature.

2.3.2.4 Partial-Equilibrium Geochemistry Implementation and Initial Geochemical Conditions

For the geochemical component of the model, we implemented a partial equilibrium approach for oxidation-reduction reactions, in which the reduction portion of the reaction occurs rapidly compared to the oxidation half. Specifically, we represented organic carbon oxidation as a kinetic reaction, while corresponding terminal electron accepting processes (TEAPs) proceed according to their equilibrium reactions. This method has been used in previous reactive-transport modeling studies (Jakobsen & Cold, 2007; G.-H.

C. Ng, Yourd, Johnson, & Myrbo, 2017; G.-H. C. Ng et al., 2015; Postma et al., 2007; Prommer, Barry, & Davis, 2002), and we consider it to be a reasonable simplification when competition among TEAPs is not a focus of the model implementation.

Fe^{3+} oxyhydroxides were represented in the model as $Fe(OH)_3$, and concentrations for this phase were based on previous extraction experiments on Cape Cod aquifer sediments (Fuller et al, 1996; Kent and Fox, 2004). Fe^{3+} oxyhydroxide dissolution was represented by the following equilibrium reaction:

$$Fe(OH)_3 + 3H^+ \rightarrow Fe^{3+} + 3H_2O$$

The log K_{sp} value of for the mineral goethite (FeO(OH)) was used for the above reaction (-1.0), based on the dominant form of Fe^{3+} oxyhydroxide coating found at the site, Al-substituted goethite (Zhang et al., 2011). Organic carbon measurements are not available, and so we initialized the groundwater portion of the model domain without organic carbon and with fully oxygenated conditions throughout the domain to ensure that initial As concentrations were sorbed onto ferric oxides - as would be expected for As conditions before the onset of eutrophication. Organic carbon concentrations in the surface water for subsequent times in the model are calibrated, as discussed below (Section 2.3.2.6). Geochemical observations prior to the onset of eutrophication in Santuit Pond are generally not available, so initial condition concentrations for other major cations and ions in the model are mostly based on current day (2015-2016) observations in Santuit Pond surface water (for the first grid cell) and downgradient groundwater at well M229 (for all other grid cells) (Table 2.2). Use of current day concentrations for initialization of major ions ensures internally consistent geochemical conditions, and we assume that it is a reasonable approach given that eutrophic conditions rapidly develop throughout the domain under high groundwater velocities and high incoming organic concentrations from surface water.

2.3.2.5 *Sorption Component*

Hydrous ferric oxide (HFO) minerals act as the primary sorbent in aquifer sediments (Kent & Fox, 2004; Zhang et al., 2011). PHT3D simulations include a double-layer, electrostatic surface complexation model. Sorption reactions and corresponding equilibrium sorption parameters for "weak" sorption sites from Dzombak and Morel (1990) were used to represent sorption of arsenic and other cations and anions such as calcium, magnesium, and sulfate. In our implementation, we excluded "strong" sorption sites that are also included in the model by Dzombak and Morel (1990), due to the lack of simulated As sorption on these "strong" sites during initial testing of the model with the data from Cape Cod. The "weak" sorption site model also incorporates sorption of ferrous iron and carbonate species using reactions and equilibrium parameters from Appelo et al. (2002), because this has also been found to impact arsenic sorption (Arai, Sparks, & Davis, 2004; Bauer et al., 2008; Brechbühl, Christl, Elzinga, & Kretzschmar, 2012; Radu, Subacz, Phillippi, & Barnett, 2005). All sorption reactions and their corresponding equilibrium constants can be found in Table 2.3.

The surface complexation module of PHT3D calculates the concentration of available HFO sorption sites as a function of site density, HFO concentration, and calculated surface charge (a function of pH). Site density is set to the value presented in Dzombak and Morel (1990) (0.2 mol weak sites per mol HFO). HFO concentrations change over time through reductive dissolution coupled to organic carbon degradation and/or oxidative re-precipitation of ferrous iron. HFO is represented in our model as $Fe(OH)_3$, which we implemented with initial concentrations based on literature values, as discussed in Section 2.3.2.4.

2.3.2.6 Organic Carbon Degradation

Organic carbon oxidation acts as the main electron donor in this model implementation. The uncharacterized, complex mix of labile organic carbon in the aquifer is represented in the model using the generic model form of CH_2O. Oxidative organic carbon degradation (Eqn. 1) will consume oxygen in the model until DO concentrations become sufficiently low (threshold at $1x10^{-5}$M), at which point the rate of this reaction rate drastically decreases, representing the shift from oxygen as the electron acceptor to alternative electron acceptors, such as ferric iron (Eqn. 2).

$$CH_2O(aq) + 1.5O_2(g) \rightarrow CO_3^{2-} \quad (1)$$

$$4Fe(OH)_{3(s)} + CH_2O + 7H^+ \rightarrow 4Fe^{2+} + HCO_3^- + 10H_2O \quad (2)$$

We implement the partial equilibrium approach through use of a first-order rate equation with decay parameter *k* for organic carbon oxidation (Eqn. 3):

$$\frac{d[CH_2O]}{dt} = -k[CH_2O] \quad (3)$$

where $[CH_2O]$ is the concentration of labile organic carbon.

A key component in this model is the temperature dependence of *k* to represent the temperature sensitivity of microbially mediated organic carbon oxidation for both aerobic and anaerobic processes. Temperature dependence of degradation rates is implemented via an Arrhenius model (Eqn. 4):

$$lnk = -m\left(\frac{1}{T}\right) + b \qquad (4)$$

where k is the first order degradation parameter and T is temperature. Arrhenius models have been commonly used to represent the temperature dependence of microbially mediated organic carbon oxidation (Davidson & Janssens, 2006; Lloyd & Taylor, 1994; Singh & Gupta, 1977). Experiments using sediments from Ashumet Pond provide evidence that rates of organic carbon degradation were temperature-dependent. Aerobic rates increased by a factor of two with a 10°C increase in temperature (Repert et al., 2020), whereas anaerobic denitrification rates increased by a factor of 5 over a 10°C increase temperature (Figure 2.6). These anaerobic denitrification experiments are used as the basis for our anaerobic Fe reduction model due to a lack of data on temperature dependency for specifically Fe reduction. The implementation of this log-linear Arrhenius model uses an observed aerobic decay constant of $4.4\text{x}10^{-8}$ hr^{-1} at 9°C (Repert et al., 2020). Initial anaerobic degradation rates at 9°C were determined based on a $k_{anaerobic}/k_{aerobic}$ ratio of 10^{-6} (Stoliker et al., 2016). The slope and intercept (m and b) for the log-linear Arrhenius model were then calculated using these degradation rates at 9°C and the above temperature-dependent rates of increase. The first-order decay parameter k was set based on these degradation observations, while the initial organic carbon concentration served as a model calibration parameter to match current-day measured concentrations of mobile As at Santuit Pond within an order of magnitude. Organic carbon was used as a calibration parameter due to a lack of labile organic carbon concentration observations within our example sites. A summary of parameter values can be found in Table 2.4.

2.3.3 Model Results

The first two years of the 10-year simulation are used to spin up the model from the approximate initial conditions to solute concentrations consistent with the flow field and alternating temperature conditions. Our discussion focuses on years 6 to 10 of the simulations, which are shown in Figures 2.7 through 2.10.

2.3.3.1 Calibration Results

While the ultimate goal of this study is to increase understanding of As release mechanisms rather than to capture site-specific processes, we compare model results to observations at Santuit Pond to ensure that the model provides insights grounded in actual field conditions.

pH remains circumneutral both spatially and temporally throughout the model simulation (Figure 2.7b), which is consistent with data for Santuit Pond surface water and porewater (Table 2.2). Reproducibility of observed pH conditions is key to ensuring that sorption processes are realistic in model simulations, because of their high sensitivity to pH.

Model results for maximum total aqueous As concentrations match reasonably well with observations (Figure 2.11). The maximum observed total aqueous As concentration at Santuit Pond (0.2 μM, which occur only above 15°C) (Figure 2.1) is similar in magnitude as the maximum simulated concentrations of total aqueous As during the hot period (0.18 μM). Additionally, the temperature dependence of As release suggested by

Santuit Pond observations is apparent in the model results, with high simulated mobile As concentrations during hot periods and low simulated mobile As during cold periods (Figure 2.11). Ultimately, speciated aqueous As observations would be needed to further determine whether model predictions of As speciation or sorbed As are consistent with conditions downgradient of Santuit Pond.

We should note that simulated Fe^{2+} concentrations are several or orders of magnitude lower than observed (Figure 2.2 and Figure 2.8). This is likely due to over-simulated depletion of the Fe mineral phase at x = 7 meters to the end of the domain (where x=0 is at the surface water-groundwater interface). Depletion of our Fe mineral phase acts the main driver of continued As mobilization downgradient, as As lacks a sorbent in which to be immobilized. The occurrence of Fe mineral depletion within our simulations may be due to an underestimation of Fe mineral concentration. Alternatively, our simulated system may be more eutrophic than actual Santuit Pond conditions, leading to more extreme reducing conditions and increased reductive dissolution of the Fe mineral phase. Interestingly, high concentrations in observations of total aqueous As suggest that there is some depletion of the Fe mineral phase in the downgradient aquifer, which is needed to allow for high concentrations of aqueous As to advect downgradient after mobilization. However, from the model simulations, it is unclear how to simultaneously achieve high concentrations of both As and Fe, as is observed. Finally, model simulations suggest little to no temperature dependence of aqueous Fe^{2+} concentrations past x=9 m, which is also seen in observations (Figure 2.8). There is a spatial lag between the onset of reductive Fe dissolution between the hot and cold temperature periods, but simulated concentrations between these two periods only differ by 25%, much lower than would be expected given the factor of 10 difference in anaerobic degradation rates between the two temperatures (2°C vs 25°C, with a factor of 5 difference in anaerobic degradation rate per 10°C). This constant Fe concentration is also likely attributed to Fe mineral depletion, as the same amount of Fe mineral is being reductively dissolved between the two temperatures.

Simulated organic carbon concentrations reach steady-state both temporally and spatially past 1 m from the sediment-water interface (Figure 2.7a). The lack of change in organic concentration past the first 1 m indicates that throughout the rest of the domain, organic carbon degradation rates are effectively 0^{th} order in our implementation. This suggests that with our calibrated organic carbon concentrations, the simulated As release mechanisms are not organic carbon limited, even during hot periods when organic carbon degradation rates are high.

An important note is that geochemical observations of Santuit Pond are obtained from a multi-level sampling well located 30 meters downgradient – twice the length of our domain. It is unknown whether the spatial trends of the model results are consistent with conditions 0-15 m downgradient of Santuit Pond due to a lack of observations. In order to test the spatial trends of the model results against spatial distributions of observations, another iteration of this model with at least a 30-meter domain is needed. However, increasing the model domain would extend it beyond what can confidently be simulated with spatially isotropic temperature changes with each season. Heat transport would likely need to be included in the model to capture time lags and/or attenuation of temperature changes at 30 m distance from the lake.

2.3.3.2 Temperature Controls on As Release Mechanisms

Model results support the proposed hypothesis that delivery of oxic surface water with seasonally changing temperatures can drive spatiotemporally variable release of As in shallow groundwater through anaerobic, reductive dissolution of ferric oxides.

Oxygen concentrations near the surface water-groundwater interface (x=0 to 5.5 m during the warm period and x=0 to 7.5 m during the cold period) become suboxic despite fully oxic surface water infiltrating the downgradient groundwater domain. The persistence of suboxic conditions in that region even during cold periods indicates that calibrated organic carbon concentrations consume significant amounts of oxygen despite lower degradation rates with cooler temperatures. However, importantly, the region from x=5.5 to 8 m alternates seasonally from suboxic to anoxic conditions, because colder temperatures allow DO to penetrate a few meters farther downgradient before being completely consumed by organic carbon degradation. The seasonal pulsing of DO in this intermediary region triggers corresponding alternating conditions in Fe. During the warm period, $Fe(OH)_3$ reductively dissolves over the domain starting at x=5.5 m, while in the cold period, farther penetration of DO allows re-precipitation and replenishment of ferric oxides from x = 5.5 to 8 m. Downgradient of x=8 m, anoxic conditions and reductive dissolution of Fe(OH)3 prevail year-round, and this leads to the near-depletion of $Fe(OH)_3$ in those downgradient areas. Correspondingly, over x = 5.5 to 8 m, aqueous Fe^{2+} alternates between near 0 to $4x10^{-8}$ M based on the re-precipitation versus dissolution of $Fe(OH)_3$, while aqueous Fe^{2+} remains elevated past x=8 m due to constant $Fe(OH)_3$ dissolution. Note that although Fe(OH)3 concentrations approach concentrations of 0, small concentrations remain over the 10-year simulation and are sufficient to maintain Fe^{2+} concentrations past x=8 m.

Seasonally pulsing of DO and of reductive dissolution of $Fe(OH)_3$ over x = 5.5 to 8 m has important implications for the spatiotemporal variability in As mobilization. The onset of reductive dissolution of ferric oxides during hot periods over x=[X] to [X] is mirrored by an increase in dissolved aqueous As(V) concentrations up to 0.15μM (above the MCL of 0.133 μM) due to the release of As that is sorbed on $Fe(OH)_3$. As(V) then appears to reduce to As(III) past x=7 m where conditions are strongly reducing, shown by a decrease in aqueous As(V) concentrations and an increase in aqueous As(III) concentrations up to 0.15 μM. The reduction to As(III) affects the mobility of As within the model, as the neutral As(III) is far less sorptive than oxyanion As(V). Furthermore, beyond x = 8 m, ferric oxides are mostly depleted through reductive dissolution, and this allows mobile As(III) in the warm months to advect through the entire domain due to a lack of sorbate. During cold months, reducing conditions subside, $Fe(OH)_3$ dissolution mostly ceases, and there is no longer a source of mobilized As. After the warm season As(III) advects out of the domain, aqueous As concentrations drop to 0 throughout the domain.

To check our hypothesis that reductive dissolution of Fe oxides is the main driver for As mobilization, we consider an alternative mobilization mechanism – competitive desorption. Based on Santuit Pond geochemical data, the solutes most likely to compete with arsenic are ferrous iron and carbonates based on concentration. Model results for sorbed components of these molecules can be found in Figure 2.10. Sorbed ferrous iron species (Figure 2.10a and b) occur at very low concentrations (10^{-11} and 10^{-13}), several orders of magnitude lower than sorbed arsenic concentrations predicted by our model and are therefore unlikely to have a significant impact on arsenic sorption. Sorbed carbonate and bicarbonate species in the model (Figure 2.10c and d) reach relatively high concentrations (10^{-5} M), but concentrations drop to near-zero from x=6 to 15 m, where we see seasonal arsenic pulsing. This is likely due to depletion of the main sorbent in this model simulation, Fe^{3+} oxyhydroxide, over this same spatial area. In conclusion, due to the amount of Fe^{3+} mineral depletion in this system, it is unlikely that competitive ion sorption is a main driver for As mobilization.

In summary, the model shows that delivery of oxic surface water and seasonal temperatures causes a temporal pulsing of anoxic/suboxic conditions over a dynamic transition region (x = 5.5 to 8 m), triggering alternating reductive dissolution and re-precipitation of $Fe(OH)_3$ in that region, and correspondingly As release. Because of the near depletion of $Fe(OH)_3$ in downgradient, constantly anoxic parts of the aquifer, mobilized As from the transition region is able to advect throughout the domain in the warm season. However, because of fast groundwater velocities, mobile As flushes out of the domain, and concentrations drop to near 0 under cold temperatures, when As is no longer released from the transition region. These results indicate that temperature seasonality in eutrophic systems can play an important role in the spatiotemporal occurrence of groundwater As concentrations that could be averse to human health.

2.3.3.3 Alternative Scenarios

Additional model simulations were run to determine the sensitivity of variable As release on organic carbon concentrations (Figure 2.12) and temperature changes (Figure 2.13).

Low organic carbon simulations were carried out to capture conditions downgradient from a lake of a low trophic level. In this scenario, organic carbon concentrations were lowered from 15M to 1.75M, with all other variables remaining the same. Model results indicate that As mobilization and reduction would be drastically reduced. Simulated aqueous As concentrations are dominantly in the form of As(V), and concentrations are far below the MCL (0.02 μM simulated vs 0.133 μM MCL). This difference from the base model seems to be driven by a lack of DO depletion; concentrations of DO never fall below 5μM. This leads to a lack of reductive dissolution of Fe mineral, and therefore a lack of As mobilization. This conclusion is supported by sorbed As(V) data, which shows that concentrations of sorbed As are several orders of magnitude higher than mobile As. From x = 0 to 0.3, DO drops to 0, which causes small amounts of Fe mineral dissolution and As(V) reduction. This signal is likely simply due to edge effects and can be discounted. These model results show that eutrophication of the upgradient surface water source is necessary to drive the simulated effects on As release.

Simulations with a constant temperature of 13.5°C (an average of temperature end members used in the base model) were used to determine the consequences of not taking into account seasonal temperature changes for evaluating As mobilization. Results from this scenario simulation indicate that DO does not deplete, and instead reaches 1μM by the end of the domain, resulting in a lack of reductive dissolution of the Fe mineral phase and a lack of As mobilization. Maximum mobile As concentrations only reach 0.001μM, which is both below the MCL and below detection of commonly used analysis methods. Additionally, the maximum As concentration in this alternate simulation is lower than the average concentration between simulated hot and cold periods in the base model (0.075 μM). This indicates that the implementation of seasonally variable temperature produces non-linear effects that cannot be captured by simplifying seasonal temperatures as an average temperature. Furthermore, this indicates that temperature variability should be taken into account to determine whether concentrations may exceed MCL As concentrations.

2.3.3.4 Model Uncertainties

To assess model uncertainty, major parameters were altered, and the corresponding percent change in total aqueous As concentration throughout the domain was determined during both hot and cold periods (Figures 2.14 to 2.17).

The model appears to be most sensitive to organic carbon concentration, as this had the greatest percent difference from baseline model results, up to 150% in total aqueous As concentration change per 1% change in organic carbon concentration (Figure 2.14 and 2.15). As discussed earlier (Section X), due to the lack of direct measurements, organic carbon concentration was calibrated based on the agreement between simulated As concentrations and observations. Given its importance for controlling As results, further data constraints on organic carbon would be valuable for future reactive-transport studies on As release.

In contrast, total aqueous As does not appear to be as sensitive to changes in Fe mineral concentration (Figure 2.16 and 2.17). A large order of magnitude change (+/-1000%) was needed to yield differences of 100% between sensitivity test results and baseline results. The highest changes in simulated As concentration were observed when Fe mineral concentration was decreased by an order of magnitude, which led to Fe mineral depletion and large decreases in aqueous total As. Additionally, this test can help determine if ferric oxide concentration is indeed the source of simulated Fe^{2+} concentrations being lower than observed (Figure 2.18). Simulations with an increase in ferric oxide by an order of magnitude resulted in an increase in simulated Fe^{2+} concentrations by over an order of magnitude, matching more closely to observed concentrations, though still lower by 1-2 orders of magnitude. This further indicates that concentrations of ferric oxide within the model are underestimated, and that future iterations of this model should increase the concentration of this variable.

2.4 Conclusions and Future Work

Overall, our model demonstrates that interactions between temperature and organic carbon can play a significant impact on arsenic release mechanisms downgradient of nutrient impacted lakes. With our simulations, depletion of dissolved oxygen during warmer periods results in the reductive dissolution of ferric oxide minerals, which then leads to the release of sorbed As(V) into the mobile phase and reduction of As(V) into the less-readily sorbed As(III).

This model, however, is still a simplified representation of a complex hydrologic and geochemical system. Future iterations of this model would benefit from a more complex flow network and kinetic mineral dissolution. A more complex representation of groundwater flow is needed to better represent mechanisms occurring downgradient of nutrient impacted lakes. Components such as 2-dimensional groundwater flow, surficial groundwater recharge, and heat transport would greatly increase model accuracy, and would allow for better representation of arsenic plume transport both spatially and temporally. The inclusion of kinetic mineral dissolution would allow for the coexistence of multiple Fe(III) mineral phases such as goethite and ferrihydrite, which often co-occur in nature, which is not possible under the current equilibrium-based geochemical modeling system.

Overall, future work at both this site and other arsenic-impacted areas in temperate climates would be benefited by the collection of data during cold time periods. Collection of this data would provide valuable insight into cold-temperature arsenic release (or more likely, attenuation) mechanisms. The collection of such data would also aid in the future development of both more robust models and a better understanding of arsenic release mechanisms.

3.0 Investigating the impact of hyporheic flux on Fe-S redox cycling in a riparian wetland

3.1 Introduction

3.1.1 Motivation

Wetlands are diverse and dynamic ecosystems that provide valuable ecosystem services and are key components of the global carbon cycle (Mitra, Wassmann, & Vlek, 2005; Mitsch, Bernal, Nahlik, Jørgensen, & Brix, 2013). Biogeochemical and hydrological interactions within wetlands improve water quality through the transformation of nutrients (Gutknecht, Goodman, & Balser, 2006; Lamers et al., 2012; Neubauer, Emerson, & Megonigal, 2002; Roden, Wetzel, & Dec, 2007) and the immobilization of contaminants such as heavy metals (Al-Sid-Cheikh et al., 2015; Fuller & Harvey, 2000).

In riparian wetlands, the interfaces of surface water and groundwater, or hyporheic zones, are hotspots of hydrologic, geochemical, and microbial activity. Hydrologic fluxes, steep geochemical gradients, and microbial metabolisms can drive transformations and sequestration of pollutants (Boano et al., 2014; Boulton, Findlay, Marmonier, Stanley, & Valett, 1998). For example, hyporheic zone processes can cause the net removal of contaminants such as organic micropollutants (Burke et al., 2014) and trace metals via precipitation of sorptive minerals (Fuller & Harvey, 2000; Gandy, Smith, & Jarvis, 2007; Lynch, Batty, & Byrne, 2014; Winter, Harvey, Franke, & Alley, 1998). Due to their impact on water quality, as well as their inherent heterogeneity and complexity, it is important to develop a greater understanding of hyporheic zone processes. Currently, the effect of hyporheic processes on iron (Fe) – sulfur (S) cycling in wetlands is not well understood. In this study, we seek to better understand how these dynamic systems can affect redox processes of Fe and S, which play critical roles in the transformation and sequestration of pollutants and trace metals (Gandy et al., 2007; Lynch et al., 2014; Ng et al., 2017; Ng et al., in review).

3.1.2 Fe-S cycling in wetlands

Fe and S are commonly found in wetland systems and are known to interact with one another through a variety of abiotic and microbially mediated reactions (Figure 3.1). In wetlands with losing hydrologic systems, where surface water percolates downward to recharge groundwater, oxidized sulfur in the form of sulfate (SO_4^{2-}) is introduced to reducing conditions within wetland soils, where it can be utilized by microbes. One reaction that commonly occurs in freshwater systems is:

$$CH_3COO^-_{(aq)} + SO_4^{2-}{}_{(aq)} \rightarrow HS^-_{(aq)} + 2HCO_3^-{}_{(aq)} \qquad (1)$$

(Lovely and Klug, 1986). The sulfide generated in these porewaters can undergo processes such as sulfide oxidation through contact with dissolved oxygen (equation 4) or sulfide mineralization with ferrous iron (equation 5):

$$HS^-_{(aq)} + 2O_{2(aq)} \rightarrow H^+_{(aq)} + SO_4^{2-}{}_{(aq)} \text{ (Boudreau, 1991)} \qquad (4)$$

$$Fe^{2+}_{(aq)} + HS^-_{(aq)} \leftrightarrows FeS_{(s)} + H^+_{(aq)} \text{ (Rickard, 1995)} \qquad (5)$$

Additionally, there is growing interest in other less commonly recognized Fe and S reactions in freshwater wetlands, due to their potential in supporting “cryptic” sulfur cycling (described further below). In these reactions, sulfide oxidation can occur coupled with ferric oxide reduction, resulting in iron sulfides and elemental S (equation 6).

Elemental sulfur produced from this reaction can undergo further transformations via reaction with sulfide to form polysulfides (equation 7) or through biotic disproportionation (equation 8).

$2HS^{-}_{(aq)} + FeOOH_{(s)} + H^{+}_{(aq)} \rightarrow S^{0}_{(aq)} + FeS_{(s)} + H_2O_{(l)}$ (Thamdrup et al., 1993) (6)

$(x\text{-}1)S^{0}_{(aq)} + HS^{-}_{(aq)} \leftrightarrows Sx^{2-}_{(aq)} + H^{+}_{(aq)}$ (Findlay & Kamyshny, 2017) (7)

$2S^{0}_{(aq)} + 4H_2O_{(l)} \rightarrow HS^{-}_{(aq)} + SO_4{}^{2-}_{(aq)} + 7H^{+}_{(aq)}$ (Thamdrup et al., 1993) (8)

Polysulfides formed in reaction 8 can further react with ferrous Fe to form amorphous Fe sulfide phases (FeS), such as mackinawite. In certain conditions, oxidation of elemental sulfur has been observed (Findlay & Kamyshny, 2017):

$S^{0}_{(aq)} + O_{2(aq)} + H_2O_{(l)} \rightarrow SO_3{}^{2-}_{(aq)} + 2H^{+}_{(aq)}$ (Langmuir, 1997) (10)

$SO_3{}^{2-}_{(aq)} + S^{0}_{(aq)} \rightarrow S_2O_3{}^{2-}_{(aq)}$ (Janssen, Schuhmann, Bak, & Liesack, 1996) (11)

Additionally, oxidation of elemental sulfur by oxygen has been empirically shown to result in the formation of thiosulfate ($S_2O_3{}^{2-}$) (Luther, 1987). In certain conditions, thiosulfate has been shown to either oxidize to $SO_4{}^{2-}$ or disproportionate into HS^- and $SO_4{}^{2}$ (Jørgensen, Zawacki, & Jannasch, 1990). This process essentially completes the reaction loop, wherein $SO_4{}^{2-}$ is formed to continue the S cycle once again.

3.1.3 Cryptic sulfur cycling

Due to the high reactivity of intermediate S phases, reactions in equations 6 through 10 are believed to occur rapidly, with S intermediates transforming into more stable S phases such as $SO_4{}^{2-}$. Thus, these reactions represent a collection of rapid S reactions believed to aid in what is often called a “cryptic” sulfur cycle. The rapid reactions make these S intermediates difficult to measure but have a marked impact on Fe and S cycling. In all but the most sulfate-rich environments, such as marine sediments, it is believed that ferric Fe reduction should outcompete dissimilatory SO_4^{2-} reduction (Froelich et al., 1979; Hoehler, Alperin, Albert, & Martens, 1998; D R Lovley & Phillips, 1987; Patrick & Henderson, 1981). This is based on a commonly used conceptual model applied throughout soil and earth sciences known as the thermodynamic ladder of microbial organic carbon oxidation, which dictates that the order of electron acceptor consumption follows a predictable pattern based on energetic yields (Champ et al., 1979). In low SO_4^{2-} environments, such as freshwater riparian wetlands, it had been assumed that SO_4^{2-} reduction would have little impact on Fe cycling. However, there is a growing body of evidence of a "cryptic" sulfur cycle in freshwater sediments (Figure 3.1), where high SO_4^{2-} reduction rates are supported by intermediate valence S species coupled to Fe reduction (Berg et al., 2019; Findlay & Kamyshny, 2017; Hansel et al., 2015; Ng, Yourd, Johnson, & Myrbo, 2017; Ng et al., *in review*; Wu et al., 2019). However, cryptic S cycling in freshwater wetlands remains poorly understood, prompting further study.

3.1.4 Objective/Hypothesis

Preliminary results presented in this thesis are the start of a multi-year study of Fe-S cycling in dynamic riparian wetland soils. The objective of our study is to work toward a mechanistic understanding of Fe-S-C cycling processes occurring within the hyporheic zone of riparian wetlands. Increased understanding of these processes will lead to the development of more robust reactive-transport modeling codes that can better simulate important wetland functions such as regulating C budgets, nutrient transformations, and the fate and transport of heavy metal contamination.

To reach this objective, we employ hydrogeologic monitoring and geochemical analyses. By comparing geochemical data to hydrologic fluxes, we can develop a better understanding of hydrologic controls on Fe and S redox cycling in wetlands.

3.2 Site Description

3.2.1 General Description of Tims Branch

Our study site is in the Tims Branch riparian wetland, located within the Savannah River Site in Aiken, SC, USA. Tims Branch is part of Argonne National Laboratory's Wetland Hydrobiogeochemistry Scientific Focus Area, whose overarching goal is to "develop a mechanistic understanding of the coupled hydrological, geochemical, and biological processes controlling water quality in wetlands" (https://doesbr.org/research/sfa/sfa_anl.shtml). This site is of interest due to a history of metals contamination, such as Cu, Cr, Pb, and U (Kaplan et al., 2017). A key characteristic of this wetland is an abundance of Fe(III) oxide containing microbial mats, or "flocs", that are heterogeneously distributed throughout the wetland. These flocs are of interest due to their ability to sorb contaminants such as heavy metals. While many areas within this site have experienced contamination, our study focuses on subsites located upstream of a major U-contaminated area (Figure 3.2, adapted from Kaplan et al., 2017) in order to develop a fundamental understanding of Fe-S cycling in wetlands, particularly in the context of the formation of flocs.

Within the upstream control area, we have established a transect of four subsites (referred to collectively as the "Upstream Sites") across about 100m spanning a range of hydrologic and geochemical conditions (Figure 3.3a and b). Our Tributary subsite is a small stream fed by a spring, contains abundant flocs, and appears to have high clay and silt content in upper sediments with a transition to sandy sediments within the top 30cm. The adjacent Stream subsite contains no flocs and contains mostly sandy sediments. Our Wetland subsite contains abundant flocs and has highest silt content compared to the Tributary and Stream sites. Finally, our Sulfide Pond subsite, located directly adjacent to our Wetland site, contained some flocs and emitted a distinct hydrogen sulfide odor. Not only are these sites spatially heterogeneous, but they are also temporally variable, with inundated and non-inundated conditions occurring throughout the year (Figure 3.3a).

In addition to these subsites, two additional subsites were established in August 2019 roughly 50 meters downstream of the original four subsites. These sites, called SCONDS and H2OCON1 and referred to collectively as the "Downstream Sites", are both within a perennial reach of the stream that also contains flocs. SCONDS is a small wetland alongside the perennial stream with abundant flocs near the stream banks. This site emitted a distinct sulfide odor, serving as a motivation for establishing this site. H2OCON1, located upstream of SCONDS, contained mostly sandy sediments and contained some flocs near stream banks. H2OCON1 was located near another established Scientific Focus Area (SFA) subsite, facilitating denser data collection. These sites were established in order to observe hydrologic and geochemical conditions in sites that are inundated throughout the year. Specifically, the establishment of the SCONDS subsite aimed to replicate the Wetland subsite but with perennially inundated conditions, and H2OCON1 aimed to do the same for the Tributary subsite. Since these sites were only recently established, there is no temporal data available, but they still can provide insights into processes that may be happening in streams that typically have standing water year-round.

3.3 Methods

3.3.1 Hydrogeology

In order to investigate Fe and S processes in the context of wetland hydrology, we installed paired surface water gauges and shallow piezometers to examine vertical fluxes in the hyporheic zone. Surface water gauge- piezometer pairs were installed in all sites except the Sulfide Pond, which was too small to instrument. However, due to their proximity, we assumed conditions were similar to the Wetland subsite. Solinst Levelogger Jr. pressure transducers were installed in every surface water gauge and piezometer, allowing us to collect high-resolution (15-minute) temporal surface water and groundwater head data. Manual measurements of groundwater and surface water head were taken at known times to convert pressure transducer data to head values. To observe the changes in groundwater flux over time, head gradient was calculated for the Tributary, Wetland, and Stream sites during times when these sites were inundated. Calculating head gradient allows us to observe changes in the hyporheic flux in these sites over time.

3.3.2 Geochemistry

Our geochemical work can be organized into three types: field sampling measurements, in-lab aqueous-phase analysis, and in-lab solid-phase analysis. Samples were collected from two time periods, in January and August of 2019.

3.3.2.1 Field Measurements

pH, temperature, dissolved oxygen, and Eh were measured in the surface water at each subsite. pH measurements were taken with pH paper in January of 2019, and with a ThermoScientific pH probe in August of 2019. Temperature and dissolved oxygen were measured utilizing a FireSting 3.0 DO probe that was calibrated to atmospheric oxygen concentrations in the field. Surface water Eh measurements were taken using an Oakton EuTech Instruments, Waterproof ORP Testr 10 Eh probe.

3.3.2.2 Sediment sample collection

Sediment cores were collected in duplicate from each site, where possible. Depending on the sampling period, sediment cores were collected utilizing differing coring methods. In January 2019, sediment samples were collected using a gravity corer surrounded by a metal sleeve. However, due to concerns with porewater disruption and sediment shifting, cores were collected using a LacCore Griffith corer (http://lrc.geo.umn.edu/laccore/griffith.html) in August 2019. With both coring methods, sediment cores were collected in polycarbonate tubes, and surface water was poured on top of the core immediately after sampling to prevent oxidation of the sediments. Cores were then sealed with caps and electrical tape in the field for transportation back to the lab. Cores were placed under -20°C upon return to the lab about 1-2 hours after sampling to limit further oxidation and/or microbial activity.

Cores were subsampled within 1 week after sampling, and immediately after core thawing, for a variety of analytes under a nitrogen, anoxic atmosphere within a glove bag. Cores, ranging from 20-35cm in length, were subsampled at 4 intervals at depths depending on core length. Observations of sediment characteristics were recorded during core subsampling (see Appendix). Samples were collected for microbial DNA extraction, solid Fe extraction, acid volatile sulfides (AVS), and synchrotron analysis. Once collected, samples were placed in 40mL silicate tubes with septa caps, flushed with nitrogen, and sealed in anoxic mylar bags for long-term storage.

3.3.2.3 Water sample collection

For aqueous phase investigations, surface water, porewater, and groundwater samples were collected from each subsite. Surface water samples were taken using a syringe and injected into 50 mL falcon tubes (cation/anion) and purged serum vials ranging from 20-50 mL in volume depending on the analyte. When abundant flocs were present, samples were pushed through a 0.2 μm syringe filter prior to injection. Porewater samples were collected from sediment cores from each site using 9 cm Rhizosphere Macro-rhizon samplers. Rhizon samplers were inserted into sediment cores at two intervals, 0-10cm and 10-20cm depth, and these were inserted while the core was covered in plastic wrap to limit oxygen exposure. The rhizons were then connected to vacuum-pumped serum vials via tubing and a needle, both to minimize exposure of porewaters to oxygen and for the collection of in-situ porewaters from sediments. Groundwater samples were collected using a Nalgene vacuum hand pump. Three well volumes were ejected into a bucket, after which groundwater was subsampled for various parameters. All samples were stored under refrigeration prior to analysis. For tables of groundwater geochemistry measurements, see the Appendix.

In many cases, water samples were placed into vacuum-pumped vials to limit exposure to oxygen and maintain sample integrity. Depending on the analyte, sample vials were of different volumes and contained different preservatives. Alkalinity samples were collected in 30mL-50mL clear vials, and cation/anion samples were collected in 20mL clear vials, all without preservatives. Sulfide samples were collected in 20mL clear vials filled with 1mL of 5% w/w $ZnCl_2$ to preserve sulfur speciation. Dissolved methane samples were collected in 20-30mL amber vials containing 0.05g of trisodium phosphate to volatilize dissolved methane into the vial headspace.

3.3.3 Laboratory Analyses

The laboratory analyses described in this section were completed for this thesis, but many more analyses will be completed as part of a later phase of this multi-year project. In future analyses, to observe the dynamics of C cycling in wetlands, total organic carbon (TOC) sediment concentrations and dissolved methane ($CH_{4(aq)}$) analyses will be performed; however due to method development (TOC) and instrument failure ($CH_{4(aq)}$), these were not completed prior to this writing. Additionally, further investigations into S and Fe speciation will include synchrotron analyses of sediments and measurements of aqueous sulfide. The former was beyond the scope of this thesis, and the latter is incomplete due to method development. Finally, microbial investigations were also considered beyond the scope of this thesis but will be completed at a later date.

3.3.3.1 Alkalinity

Alkalinity was measured within 48 hours of sample collection when possible, using a colorimetric titration technique. A Bromocresol green dye was used to indicate the end point of the titration, and samples were titrated with either 1.6 or 0.16M H_2SO_4. Measurements were performed in triplicate. Alkalinity concentrations were calculated based on the volume of H_2SO_4 used via the following equation:

$$ALK\left(\frac{meq}{L}\right) = \frac{\left(\frac{V_a * A}{Vs}\right)}{2 * M_{CaCO3}}$$

where V_a corresponds to volume of H_2SO_4 , A corresponds with a correction factor (1 or 0.1 depending on concentration of H_2SO_4), V_s corresponds to volume of sample in mL, and M_{CaCO3} is the molar mass of calcium carbonate. For plots of alkalinity measurements, see the Appendix.

3.3.3.2 Aqueous Iron

Dissolved ferrous and ferric iron were measured via ferrozine assay modified after Stookey, 1970. 40μL of surface water, porewater, or groundwater sample were diluted in 1.00mL 0.005M ferrozine – 2.5M ammonium acetate reagent then thoroughly mixed. Samples were then allowed to react for 30 minutes and there then analyzed on a Cary 60 UV-vis spectrophotometer at 562 nm for dissolved ferrous Fe. Following this measurement, 40μL of 0.2M hydroxylamine hydrochloride was injected into the sample-ferrozine solution and left to react for an additional 10 minutes. Samples were then run again on a Cary 60 UV-vis spectrophotometer at 562 nm for measurement of total Fe. Unfortunately, sample oxidation was observed by ferric Fe oxide precipitation within vials, and therefore speciated Fe concentrations were deemed to be unreliable. Because of this, results will only show total Fe concentrations.

3.3.3.3 Anions

Surface water, porewater, and groundwater samples for anion analysis were prepared by adding 3.00mL of sample into an IC sample tube and diluting with 3.00mL of nanopore water. Samples were then left in open air under refrigeration for 24 hours, after which they were filtered through 0.2 um filters to remove any precipitates. Anion samples were measured by ion chromatography (IC) using a Metrohm Professional IC Vario 1 AnCat system. Anions were measured using the Metrohm protocol 'AN-S-199' with a 4.25mM sodium bicarbonate eluent; measured anions included chloride (Cl^-), nitrite (NO_2^-), nitrate (NO_3^-), and sulfate (SO_4^{2-}) (Metrohm, 2019a). Cation sampled were prepared same as above and analyzed using Metrohm protocol 'AN-C-103'(Metrohm 2019a). For plots of nitrate+nitrite and cation data, see the Appendix.

3.3.3.4 HCl Fe Extractions

Solid phase ferrous and ferric iron concentrations were measured via a sequential HCl extraction method modified from Bhattacharyya et al., 2018. Sediment subsamples were placed in an anoxic, nitrogen atmosphere, and 2-3 grams of each sample were added to 15mL falcon tubes. Then, 10mL of 0.1M HCl was pipetted into each falcon tube, after which the falcon tubes were inverted for mixing and placed in a fume hood for reaction. After 24 hours of reaction time, the falcon tubes were centrifuged at 4500rpm for 5 minutes. The supernatant was then removed from each falcon tube using a 15mL syringe and placed under refrigeration. Sediments were then injected with 10mL of 6.0M HCl, inverted for mixing, and placed in a fume hood for reaction. After 24 hours, the samples were centrifuged using the same procedure as above, and the supernatant was again extracted and placed under refrigeration.

Once supernatant from both extraction steps was acquired, ferrous and ferric iron concentration were measured via ferrozine assay. 40µL of supernatant was diluted in 1.00mL 0.005M ferrozine – 2.5M ammonium acetate reagent then thoroughly mixed. Samples were then allowed to react for 30 minutes and there then analyzed on a Cary 60 UV-vis spectrophotometer at 562 nm for dissolved ferrous Fe. Following this measurement, 40µL of 0.2M hydroxylamine hydrochloride was injected into supernatant-ferrozine solution and left to react for an additional 10 minutes. Samples were then run again on a Cary 60 UV-vis spectrophotometer at 562 nm for measurement of total Fe. Ferric iron concentrations were calculated by taking the difference of total and ferrous iron concentrations.

3.3.3.5 Acid Volatile Sulfides

The acid volatile sulfide mineral sediment fraction was measured via a 6.0M HCl extraction method modified from Allen et al., 1993. First, 5-10 grams of homogenized sediment were removed from the sample vial and placed into a 250mL Erlenmeyer flask under an anoxic, nitrogen atmosphere within a glove bag. Then, 50mL of anoxic, nanopure water was added to the vials, along with a magnetic stir bar, and then was sealed with parafilm and removed from the glove bag. The Erlenmeyer flasks were then placed on stir plates and sealed with S-free rubber stoppers with 10mL glass pipettes running through the center of the stopper and into the sample slurry. This flask was then attached to an AVS apparatus (Figure 3.4). Gas outflow from this flask led to a container with 75mL of nanopure water for chloride retention. Gas was then diverted to yet another impinger containing silver nitrate trapping solution (0.05M silver nitrate and

0.517M nitric acid). Once the sample flask was attached to the apparatus, the entire system was flushed with nitrogen gas at a flow rate of 1 L/minute for 10 minutes. 15mL as then added to the sample flask, after which flow rate of the nitrogen gas was reduced to 0.2 L/minute for 30 minutes. After 30 minutes, the trapping solution was filtered through a 0.45μm filter that had been dried at 100degC for 30 minutes and pre-weighed. The filter was dried again, then a final weight measurement was taken to determine the mass of precipitated silver sulfide, allowing for the calculation of AVS within the sediment sample.

3.3.3.6 S Speciation: XANES

Samples were prepared and analyzed for S speciation using XANES as reported in Torgeson, 2019. XANES, or x-ray absorption near-edge structure, is a spectroscopic technique in which solid samples are bombarded with x-rays and the absorption of those x-rays by electrons of molecules within the sample are measured. Each molecule has a unique absorption pattern, and information such as characterization and redox state can be obtained from these analyses. XANES analyses on our samples were completed at sector 9-BM at the Advanced Photon Source at Argonne National Laboratory.

3.4 Results/Discussion

3.4.1 Hydrology

Results of surface water and groundwater head (top of screen measured at 70-90 cm depth) show a hydrologically dynamic system across all instrumented sites (Figure 3.5). Surface water gauge pressure transducers were positioned below the sediment-water interface elevation within the PVC pipe. Therefore, surface water head measurements that fall below this interface indicate non-inundated periods and represent water table elevation instead of surface water head. From January to April, there appears to be a clearly defined inundated season, when all sites were inundated, or in other words had standing water. Low January temperatures (Figure 3.6) (National Weather Service) likely led to low evapotranspiration. This combined with high precipitation relative to the rest of the year likely resulted in inundated conditions both leading into and throughout the month of January within our subsites. However, from April to August, there appears to be a non-inundated season when sediments were unsaturated as far as 50cm depth. A rain event occurred in mid-June that temporarily re-inundated the sediments for about 1 month, after which the sediment surface became unsaturated once again. The onset of the non-inundated period corresponds to a precipitation drop and increase in temperatures. While precipitation was high June to August, this was apparently insufficient to counteract increased evapotranspiration due to high temperatures, thereby leading to non-inundated conditions in our subsites throughout much of the summer months. A large rain event occurred approximately 1 week prior to our August sampling period that once again re-inundated the sediment surface. During both the January and August sampling periods, sediments at all sites were inundated.

To determine the direction and magnitude of hyporheic flux, head gradient was calculated for our surface water gauge-piezometer pairs when sites were inundated (Figure 3.7). Positive values correspond to upward flux of groundwater, meaning that the surface water is “gaining”, whereas negative values correspond to downward flux of groundwater, meaning that the surface water is “losing". The Stream subsite generally experiences downward flux throughout the year, whereas the Tributary and Wetland subsites often experience upward flux. While head gradient data can give us an idea of flux direction and relative magnitude within a subsite, data on hydraulic conductivity is needed to determine absolute flux values. Higher hydraulic conductivities often correlate with greater sediment grain size (Freeze and Cherry, 1979), therefore sites with sandier sediments are likely to have higher overall hydraulic conductivity. Sandy sediments were observed in the Stream subsite, while silty sediments were observed in the Tributary and Wetland subsites. With likely higher hydraulic conductivity and greater observed head gradient magnitudes (0.090 at the Stream versus 0.007 and 0.019 at the Tributary and Wetland, respectively), the Stream subsite not only experiences a different flux direction, but the flux magnitude is likely higher than the Tributary or Wetland subsites. While no temporal data exists for the SCONDS and H2OCON1 subsites, manual measurements indicated that both areas were gaining in August.

There appears to be a correspondence between hyporheic flux and the occurrence of flocs in our sites. Subsites with upward flux of groundwater contained flocs, whereas the Stream subsite, which experiences downward flux year-round, shows no signs of flocs (Table 3.1). This observation suggests that the deep groundwater (below the cored depth) has reducing conditions. As this reducing groundwater moves up under gaining conditions, it is bringing in a source of ferrous iron and/or it is allowing for the production of ferrous iron in the shallow organic-rich sediments. The high ferrous iron porewater then advects up to the surface water and oxidizes either abiotically or biotically to form the flocs that we see in our Tributary and Wetland subsites. Our shallow upland groundwater wells are not high in ferrous iron (see Appendix), but these might be positioned too horizontally far from the subsites and shallow to be representative of the deep groundwater that flows up into the hyporheic zone. Table 3.2 details vertical hydraulic gradient for the subsites with upward flux (Wetland, Tributary, H2OCON1 and SCONDS) during the August sampling. Head gradients were highest in the Wetland and H2OCON1 subsites, while head gradients in the Tributary and SCONDS sites were lower by a factor of 2. This helps to explain the difference in abundance of flocs between the Wetland and Tributary subsites – the Wetland subsite contained abundant flocs, likely due to a higher magnitude upward flux (assuming hydraulic conductivity are similar between the two sites), and the Tributary subsite contained less flocs than the Wetland site due to a lower magnitude upward flux. In contrast, floc density was similar between the two downstream subsites, indicating that perennial inundation may hinder the effect of flux magnitude on floc formation. Surface water and porewater chemistry and sediment geochemistry are examined in the following sections to test the hypothesis of different redox conditions in the gaining versus losing subsites.

3.4.2 pH, Eh, Temperature, and Dissolved Oxygen

Table 3.3 summarizes field measurements taken in the surface water during both sampling periods. Between sampling periods, pH appears to have increased by 2 units across all sites. This is not a realistic change, and instead likely reflects inaccuracies due to using pH paper in January. Surface water temperature closely follows seasonal atmospheric conditions, and changes in dissolved oxygen concentrations between the two sampling periods are likely due to differences in oxygen saturation driven by these temperature differences. Finally, increases in Eh suggest more oxidizing conditions in August in all subsites except the Wetland subsite, where Eh measurements decreased between the two sampling periods. More oxidizing surface waters in August is consistent with the non-inundated conditions preceding the August sampling. An opposing trend in Eh at the Wetland subsite compared to other subsites seems unlikely, and we believe that there may have been an error in the Wetland Eh measurement in August. The depth of the Eh meter in the surface waterways not standardized, and Eh measurements may have been taken from deeper surface waters in the Wetland subsite than in other subsites, causing an aberrantly low Eh measurement.

3.4.3 Porewater chemistry

3.4.3.1 Chloride

Chloride data (Figure 3.8) can provide information on physical processes at different subsites and different sampling times.

Comparing data across Upstream subsites, it appears that the floc sites consistently have higher chloride concentrations than the no-floc Stream subsite. This can likely be attributed to hydrologic differences; the Stream subsite experiences year-round downward flux, whereas the Tributary, Wetland, and presumably Sulfide Pond subsites often experience upward flux. Higher concentrations of chloride in these latter subsites likely correspond with a deeper groundwater source of chloride, which would be expected to have higher concentrations due to evapotranspiration than surface water. Chloride concentrations for Downstream subsites fall within the range of concentrations seen in all August samples; however, data from multiple time periods are needed to draw more conclusive observations for these sub-sites.

When comparing chloride concentrations across the two sampling periods, there is up to a 2-fold increase in chloride concentrations from January to August, which we attribute to greater evaporation from the streambed during the non-inundated period that preceded the August sampling. While there was a rain event one week prior to the August sampling period that re-inundated the sediments, this was likely insufficient to completely dilute increases in chloride concentration due to evaporation. This increase provides an important baseline for comparing January and August datasets, because any increases in analyte concentrations beyond this 2-fold increase represent processes beyond evaporation effects.

3.4.3.2 Aqueous Iron

Aqueous Fe concentrations are plotted as total iron in Figure 3.9. Due to the low solubility of ferric Fe, most of the total dissolved Fe concentrations is considered to be ferrous Fe.

Comparing Upstream subsites within each sampling period yields a clear pattern – the no-floc Stream subsite consistently has low dissolved Fe concentration compared to floc sites. The differences in total dissolved Fe between floc and no-floc sites is likely hydrologically driven – a consistent low upward flux from deep, anoxic groundwater (deeper than our sampling techniques reach) could bring with it high dissolved Fe concentrations that can then be used in the production of flocs and freshly precipitated Fe oxides when it reaches the upper sediments and surface water. Higher concentrations of aqueous Fe may also be formed in situ in the floc sites due to reductive dissolution of ferric Fe oxides within the sediment interval sampled with our coring techniques. In nearly all cores, dissolved Fe increases with depth, which can be attributed to more oxidizing conditions in the surface water and upper sediments resulting in Fe oxidation – and therefore Fe oxide precipitation – whereas deeper sediments would have more reducing conditions in which iron reductively dissolves. This trend does not appear in Stream subsite samples, indicating that the Stream subsite sediments may experience more oxidizing conditions due to downward flux of oxygenated surface water during inundated periods and due to exposure to the atmosphere during non-inundated periods.

August total dissolved Fe concentrations were higher than January by a factor of 2 to 5, depending on the site. While a 2-fold increase at the Stream subsite can be explained by evaporation, a 5-fold increase seen in Wetland, Sulfide Pond, and Tributary subsites indicates the occurrence of redox processes. An increase in total dissolved Fe in August may seem counterintuitive given the long non-inundated period in the late spring through summer – unsaturated sediments would likely have allowed oxidation of ferrous iron and precipitation of ferric Fe oxides. However, a week-long rain event preceded our August sampling period and re-inundated the subsites, apparently allowing reducing conditions to return in deeper sediments. Increases in total dissolved Fe with depth are consistent with this hypothesis, as more reducing conditions likely occur at depths farther from the oxygenated surface water. Higher aqueous Fe concentrations in August (after one week of re-inundation) compared to January (presumably during sustained inundated conditions) may be explained by lower magnitude upward flux in floc sites during the August sampling period compared to January, which could have allowed for increased accumulation of dissolved Fe. This great accumulation may have occurred because the amount of Fe being released due to reductive dissolution of ferric oxides exceeds the amount that escapes the system due to the low magnitude upward flux of water in August, resulting in a net increase in total dissolved Fe within floc sites. These results underscore the transience of aqueous data – even though this sampling period was preceded by a long non-inundated period, a rain event that occurred just a week before our sampling period triggered a switch in redox conditions.

Total dissolved Fe in the Downstream subsites follow a unique pattern, with concentrations increasing from surface water to 0-10cm depth and decreasing from 0-10 cm to 10-20cm. Overall Fe concentrations as these sites were very low compared to August measurements from the upstream subsites. Low total dissolved Fe concentrations may suggest an oxidizing environment; however, these subsites are located within a perennial, gaining stream, so sediments are often or perpetually saturated, making the occurrence of oxidizing conditions unlikely. Instead, one explanation may be that under perennial inundation, sediments do not re-oxidize, and ferric Fe oxides may deplete. The small reservoir of Fe oxides may result in less production of ferrous Fe. Evidence to support this hypothesis can be found in solid Fe extraction data, as discussed in the next section. Without temporal hydrologic and geochemical data, it is difficult to make further conclusions about these subsites.

3.4.3.3 Solid Phase Fe

Speciated solid Fe data are shown for the 0.1 M and 6.0 M HCl extractions (Figure 3.10 and 3.11). Data presented in Figures 3.10 and 3.11 represent one of two replicate cores taken from each site, with data from other replicate cores shown in the

Appendix. It is important to note that Fe extraction results were qualitatively similar across these replicates.

By recording cumulative precipitation and dissolution in the streambed, solid phase data represent geochemical conditions over longer time scales than moving porewater. The 6.0 M HCl Fe extraction data support the hypothesis of oxidation during the non-inundated period preceding our August sampling: 6.0 M HCl extractable ferric Fe increased dramatically (up to an order of magnitude) between January and August samples. This suggests oxidation and in situ precipitation of ferric Fe oxides during the non-inundated period. Additionally, there is an increase in HCl extractable ferrous Fe in both 0.1 and 6.0 M HCl extraction results, especially at the subsites with highest August aqueous Fe concentrations (Wetland and Sulfide Pond), which may have precipitated during the transition from oxic to reducing conditions following the late-August rain event which re-inundated sediments. Finally, high concentrations of HCl extractable ferric Fe at depth can be explained by the presence of abundant ferric Fe oxide coated root systems (Figure 3.12), which appear to remain stable even where conditions in the bulk porewater are reducing.

The lack of increase in ferric Fe in our 0.1 M extraction in August samples is unexpected. Freshly precipitated Fe oxide phases are often extracted in concentrations more dilute than 6.0 M HCl (Bhattacharyya et al., 2018; Raiswell, Canfield, & Berner, 1994; Tucci & Gammons, 2015; Voelz, Johnson, Chun, Arnold, & Penn, 2019), while 6.0 M HCl is more commonly used to target more recalcitrant forms (Raiswell, Canfield, & Berner, 1994; Voelz, Johnson, Chun, Arnold, & Penn, 2019). It appears that our first-step HCl extraction strength of 0.1 M was too weak to extract the freshly precipitated ferric oxides. Indeed, many other studies use 0.5M HCl concentrations for extraction of amorphous Fe oxides (Bhattacharyya, Schmidt, Stavitski, & Enid, 2018; Hansel, Benner, Nico, & Fendorf, 2004; Heron, Crouzet, Bourg, & Christensen, 1994; Sutherland, 2002). It is likely that in our results, our 6.0 M HCl extraction was removing fresh ferric Fe phases that would have been removed at HCl strengths greater than 0.1 M and considerably lower than 6.0 M.

6.0 M HCl extractable ferric Fe concentrations were low in subsites H2OCON1 and SCONDS compared to other August measurements. These observations seem to support the hypothesis that these subsites are continuously reducing due to perennial inundation of the sediments. 0.1 M HCl extractable Fe is dominantly ferrous, and concentrations for the SCONDS subsite are similar to measurements made for Wetland subsite measurements. H2OCON1 extraction concentrations were higher than those measured at Tributary and Stream subsites, suggesting that more 0.1 M HCl extractable Fe is present in perennial equivalents to the Tributary and Stream subsites.

3.4.3.4 Sulfate

Evidence for oxidation occurring during the non-inundated period can also be seen in porewater sulfate data (Figure 3.13). Between January and August, sulfate concentrations increased by a factor of 5 in the surface water, to over an order of magnitude in the 0-10cm sampling interval, and a factor of 5 in the 10-20cm sampling interval. These concentration increases are beyond what can be explained by evaporation alone, suggesting that sulfide oxidation occurred in these sediments, likely during the non-inundated period. However, this large increase in sulfate concentration is limited to the floc containing subsites; Stream subsite sulfate concentrations changed the least between sampling periods, and the increase in sulfate within this site appears to be within the range of what can be explained just evaporation effects. Low sulfate concentrations at depth compared to the upper profile during August sampling support the hypothesis of a transition back to reducing conditions after re-inundation of sediment, which apparently is allowing sulfate reduction to occur at depth. This trend is in agreement with patterns seen in total dissolved iron concentrations, which are low in upper sediments and higher in low sediments. A transition from oxidizing to reducing conditions in the lower profile will appear as an increase in total dissolved Fe due to reductive Fe dissolution but will appear as a decrease in sulfate concentrations due to sulfate reduction. However, Fe concentrations in 0-10cm profile in August are still higher than those in January, indicating that while conditions are more reducing in the lower portion than in the upper portion, conditions in the upper profile are still sufficiently reducing to cause reductive dissolution of ferric oxides. Sulfate requires more reducing conditions to reduce than Fe, which may explain why sulfate concentrations in August remain higher than in January throughout the profile, despite the return of reducing conditions.

When comparing across subsites, clear patterns can be seen between the Upstream subsites. The no-floc Stream subsite shows low sulfate concentrations throughout both sampling periods. Consistently low sulfate concentrations in the Stream subsite in August may indicate less S redox activity in the Stream subsite compared to floc subsites. Sulfate concentrations at H2OCON1 and SCONDS are low compared to other August measurements, and do not increase in the 0-10cm interval like other floc sites. Low sulfate concentrations in these subsites could be due to their location within a perennial stream – if sediments at these sites are perpetually saturated, there is no mechanism for S oxidation like there is in the floc subsites. The low sulfate concentrations could also be due to a lack of solid ferric Fe within these subsites, as sulfide oxidation can become coupled with ferric Fe reduction in "cryptic" S cycling. As stated in section 4.3.3, low concentrations of ferric Fe solid phases within H2OCON1 and SCONDS subsites are attributed to perennially inundated conditions limiting exposure of sediments to the atmosphere.

3.4.3.5 AVS

Solid AVS concentrations (Figure 3.15 and 3.16) are interpreted here as sediment metal sulfides, which we assume to correspond with Fe sulfide phases. While this method is able to achieve 90% extraction of Fe, Cd, and Zn sulfides (Allen, Fu, & Deng, 1993), this assumption of mostly Fe sulfide is supported by the abundance of Fe within our subsites. Further work is needed to determine Cd and Zn concentrations within our subsites to evaluate the presence of Cd and Zn sulfides.

Between sampling periods, AVS concentrations show small but noticeable changes, but there appears to be little correspondence between depth and AVS concentrations. Concentrations of AVS are slightly lower in August than in January, again supporting the hypothesis of sediment oxidation during the non-inundated period. This corresponds with an increase in aqueous sulfate concentrations within floc-containing sites – likely caused by the dissolution and oxidation of solid AVS phases. AVS concentrations in the Stream subsite appear to have changed very little, which supports the hypothesis of there being less redox activity in the Stream subsite as compared to the floc subsites. AVS concentrations within H2OCON1 and SCONDS (Figure 3.17) are similar to other subsites for the August sampling period, indicating that while these may be reducing systems, there is not appreciably more AVS compared to other subsites, where oxic conditions were believed to have occurred during the non-inundated time. Data from additional times are needed before further conclusion can be made about H2OCON1 and SCONDS.

3.4.3.6 S Speciation – XANES

While extractions can be informative, they are operationally defined and do not provide concrete information on phases present in sediment samples. For this reason, we have started analyzing samples through spectroscopic techniques, namely XANES (Figure 3.18). January sediment samples were analyzed for S speciation. Across all sites, a high proportion of S species can be attributed to sulfur intermediates, providing evidence for a "cryptic" sulfur cycle. In particular, the presence of thiosulfate in the floc sites is intriguing, as thiosulfate is a S intermediate known to disproportionate as a step within "cryptic" sulfur cycling. Notably, there is a lack of thiosulfate in the Stream subsite, possibly indicating that cryptic sulfur cycling may not be as important there – which seems consistent with the consistently low sulfate and dissolved Fe concentrations there. Additionally, the presence of L-Cystine and L-Methionine represent an organic pool of S intermediates. The implications of this are still unclear but will be investigated as this research continues.

3.4.4 Synthesis

Together, the geochemical data from the different subsites provide a multi-month to transient picture of processes affecting floc production. Solid-phase data capture a longer time period and provide evidence that the 4-month non-inundated period preceding the August sampling caused oxidation of the sediments in the Upstream subsites. Solid HCl extractable ferric Fe increased in all Upstream cores between January and August sampling periods, indicating oxidation of ferrous Fe and the precipitation of ferric Fe oxide phases. AVS concentrations decreased within floc sites between sampling periods as well, indicating the oxidation of solid sulfide phases.

The aqueous results from January to August also indicated redox activity in the floc sites. Specifically, sulfate and total dissolved iron concentrations increased in the floc sites beyond the 2-fold increase seen in chloride measurements due to evaporation effects alone. The increase in sulfate concentrations is consistent with the oxidation of sulfide minerals during the non-inundated period, as observed in the AVS results. Further, lower sulfate concentrations in deeper sediments compared to upper sediments indicate a spatial redox gradient – it appears that deeper sediments returned to reducing conditions as the sediments become re-inundated the week before the August sampling, causing sulfate to once again reduce. This redox gradient and return to reducing conditions at the floc subsites is also apparent in total dissolved Fe concentrations, which are higher in the lower sediments than upper sediments, presumably due to greater reductive dissolution of ferric iron oxide at depth. However, unlike the sulfate data, the aqueous Fe results indicate a return to reducing conditions throughout the profile; concentrations are higher in both the upper and lower profile in August compared to January. It is likely that if reducing conditions persisted after the August sampling, the upper profile would become sufficiently reducing such that sulfate concentrations in the upper profile would also begin to decrease. The return of reducing conditions to the sediments – especially lower portions that are farther from oxygenated surface waters - highlights the transience of aqueous data: while there was a non-inundated period that exposed pore spaces to the atmosphere for several months, inundation for a week prior to our August sampling was apparently enough to lead to the return of reducing conditions in the aqueous phase.

When comparing across subsites, patterns also emerge between the Upstream subsites. Floc subsites, which often experience gaining conditions, consistently contain higher and more dynamic sulfate and dissolved Fe concentrations than the Steam subsite. Higher dissolved Fe concentrations indicate that there is a source of Fe to the floc subsites, either through upward flux of deep, anoxic groundwater with high Fe concentrations or due to reductive dissolution of ferric oxides that are replenished in the upper sediments during non-inundated periods. Consistently low sulfate concentrations in the losing Stream subsite indicates a lack of S redox activity, which is supported by similar AVS concentrations between January and August sampling periods, and likely results from constant oxidizing conditions due to the downward flux of oxygenated surface water. The presence of thiosulfate at the floc subsites but not at the no-floc Stream subsite provide evidence that coupled Fe and S redox processes are occurring at the floc subsites via "cryptic" S cycling. The Downstream subsites provide interesting insight into the effects of perennial inundation on Fe redox. These sites experience perpetually reducing conditions due to inundation, but ferrous Fe concentrations remain low in these sites, possibly due to a lack of Fe oxide replenishment. Overall, more data is needed from the Downstream sites to provide more substantive conclusions.

3.5 Conclusions

3.5.1 Summary

The Tims Branch riparian wetland is a hydrologically dynamic system, with spatially heterogeneous features and temporally variable conditions. Hydrology plays a significant role in controlling redox conditions within the Tims Branch wetland. Subsites experiencing upward flux consistently show the presence of flocs, and the occurrence of inundated and non-inundated periods results in dynamic redox conditions at the sites with flocs. At the floc sites, non-inundated periods result in oxidation of Fe and S, causing precipitation of ferric oxide phases and oxidation of acid volatile sulfide phases, while inundated periods result in higher AVS concentrations due to sulfate reduction as well as the reductive dissolution of ferric Fe phases. Low magnitude upward flux appears to allow for the accumulation of aqueous Fe, due to a higher ratio of Fe oxide reductive dissolution to out-flux to the surface water. High aqueous Fe concentrations advecting to oxidizing surface water is likely is a key to dense floc formation, which may have implications for metal contaminant immobilization.`

Perennial streams within the Tims Branch wetland provide intriguing datasets that differ from conditions within more seasonal streams and wetlands. Year-round sediment inundation facilitates the occurrence of reducing conditions, and the lack of a non-inundated period in these sites appears to limit the oxidation of ferrous Fe and sulfide phases.

Evidence suggests that coupled Fe-S processes occur within the Tims Branch wetland. The presence of AVS minerals at low concentrations in all sub-sites (compared to total extractable Fe) indicates some coupling between ferrous Fe and sulfide. The presence of S intermediates, specifically the presence of thiosulfate in floc sites, indicates that 'cryptic' sulfide oxidation occurs coupled with Fe reduction.

3.5.2 Future work

These results represent just the start of a multi-year study in which we will observe spatially and temporally dynamic hydrologic and geochemical conditions within the Tims Branch wetland. Additional analyses are planned for the future to build a more robust dataset, including Fe and S speciation, microbial analyses, and carbon analyses. The ultimate objective of this project is to develop a mechanistic understanding of Fe-S-C cycling in this dynamic wetland, with the overarching goal of implementing findings into reactive-transport models. Developing more robust reactive transport models will lead to better predictions of the fate and transport of heavy metal contaminants, as well as Fe-S-C budgets within these wetlands over time.

4.0 Conclusions

These studies into two instances of surface water – groundwater interaction highlight the importance of developing an understanding the underlying hydrologic and geochemical processes occurring within them. Within shallow aquifers downgradient from nutrient-impacted lakes, a reactive-transport model implemented with seasonal temperature variability indicated that As release mechanisms are temperature-dependent. Above MCL concentrations of aqueous As were simulated during warm periods, and below MCL concentrations were simulated during cold periods. Additionally, these aqueous As concentrations could not be replicated within simulations where temperature was averaged to a single value. Within a geochemically dynamic wetland in Aiken, SC, variable hydrologic conditions driven by seasonal conditions were found to have a significant impact on porewater geochemistry within the hyporheic zone. Sites which experienced periods of inundation and non-inundation experienced higher aqueous and solid Fe concentrations, as well as elevated sulfate, when compared to their perennially inundated counterparts, which may have implications on the formation of Fe oxide microbial mats that are believed to help filter contaminants such as U. Additionally, the presence of Fe oxide microbial mats appears to be tied to hyporheic flux direction, with sites experiencing upward flux containing microbial mats, and those experiencing downward flux did not. Finally, the presence of S intermediates within microbial mat sites indicate the presence of "cryptic" sulfur cycling. These studies show that surface water and groundwater cannot be treated as separate pools, and that the interactions between surface water and groundwater can have lasting impacts on water quality and human health.

5.0 Tables

Variable	Value	Source
Hydraulic conductivity (K)	36.3 m/d	Walter et al 2016
Head gradient (dh/dx)	0.035 (unitless)	Walter et al 2016
Porosity (n)	0.39 (unitless)	Smith et al 2013
Tortuosity (T*)	0.5 (unitless)	Bear 1972
Molecular diffusion coefficient	8.64×10^{-5} m^2/day	Li and Gregory, 1974
Longitudinal dispersivity	1 m	Zheng & Bennett, 2002
Horizontal transverse dispersivity	0.018 m	Garabadien et al., 1991
Vertical transverse dispersivity	0.0015 m	Garabadien et al., 1991

Table 2.1: Summary of flow and transport input parameters and their corresponding sources.

Variable	Surface Water Concentration (M) (1st grid cell)	Porewater Concentration (M) (2nd to 50th grid cells)
As(3)	0	2.1 e -36
As(5)	0	5 e -07
C(4)	8.1 e -05	7.8 e -05
Cl(-)	7.2 e -04	6.6 e -04
Fe(2)	0	2.0 e -24
K	3.7 e -05	3.7 e -05
Na	6.2 e -04	6.9 e -04
O(0)	8.8 e -04	8.8 e -04
P	0	0
Si	0	0
pH	7	7.2
pe	15	14

Table 2.2: Aqueous phase initial concentrations, post PHREEQC equilibration. Concentrations given in mol/L (M).

Arsenic (As^{3+}, As^{5+})		
Reaction	**Log K**	**Source**
$Hfo\_wOH + H_3AsO_4 = Hfo\_wH_2AsO_4 + H_2O$	8.61	Dzombak & Morel, 1990
$Hfo\_wOH + H_3AsO_4 = Hfo\_wHAsO_4^- + H_2O + H^+$	2.81	Dzombak & Morel, 1990
$Hfo\_wOH + H_3AsO_4 = Hfo\_wAsO_4^{-2} + H_2O + 2H^+$	-40.7	Dzombak & Morel, 1990
$Hfo\_wOH + H_3AsO_4 = Hfo\_wOHAsO_4^{-3} + 3H^+$	-10.12	Dzombak & Morel, 1990
$Hfo\_wOH + H_3AsO_3 = Hfo\_wH_2AsO_3 + H_2O$	5.41	Dzombak & Morel, 1990
Phosphate(PO_4^{3-})		
Reaction	**Log K**	**Source**
$Hfo\_wOH + PO_4^{-3} + 3H^+ = Hfo\_wH_2PO_4 + H_2O$	31.29	Dzombak & Morel, 1990
$Hfo\_wOH + PO_4^{-3} + 2H^+ = Hfo\_wHPO_4^- + H_2O$	25.39	Dzombak & Morel, 1990
$Hfo\_wOH + PO_4^{-3} + H^+ = Hfo\_wPO_4^{-2} + H_2O$	17.72	Dzombak & Morel, 1990
Ferrous Fe (Fe^{2+})		
Reaction	**Log K**	**Source**
$Hfo\_wOH + Fe^{+2} = Hfo\_wOFe^+ + H^+$	-2.98	Appelo et al.,2002
$Hfo\_wOH + Fe^{+2} + H_2O = Hfo\_wOFeOH + 2H^+$	-11.55	Appelo et al., 2002
$Hfo\_wOH + Fe^{+2} = Hfo\_wOFe^+ + H^+$	-2.5	Dzombak & Morel, 1990
Carbonate (CO_3^{2-})		
Reaction	**Log K**	**Source**
$Hfo\_wOH + CO_3^{-2} + H^+ = Hfo\_wCO_3^- + H_2O$	12.78	Appelo et al., 2002
$Hfo\_wOH + CO_3^{-2} + 2H^+= Hfo\_wHCO_3 + H_2O$	20.37	Appelo et al., 2002
Sulfate (SO_4^{2-})		
Reaction	**Log K**	**Source**
$Hfo\_wOH + SO_4^{-2} + H^+ = Hfo\_wSO_4^- + H_2O$	7.78	Dzombak & Morel, 1990
$Hfo\_wOH + SO_4^{-2} = Hfo\_wOHSO_4^{-2}$	0.79	Dzombak & Morel, 1990
Calcium (Ca^{2+})		
Reaction	**Log K**	**Source**
$Hfo\_wOH + Ca^{+2} = Hfo\_wOCa^+ + H^+$	-5.85	Dzombak & Morel, 1990
Magnesium (Mg^{2+})		
Reaction	**Log K**	**Source**
$Hfo\_wOH + Mg^{+2} = Hfo\_wOMg^+ + H^+$	-4.6	Dzombak & Morel, 1990

Table 2.3: Summary of sorption reactions included in the database of our reactive transport model.

Parameter	Parameter Description	Value	Source
$k_{aerobic}$,9°C	First order aerobic organic carbon degradation rate parameter at 9°C	$4.4e^{-8}$/hr	Repert et al., 2020
$k_{anaerobic}$ / $k_{aerobic}$	Ratio between anaerobic and aerobic first order organic carbon degradation rate parameter	$1e^{-6}$	Stoliker et al, 2016
dT multiplier, aerobic	Change in aerobic degradation rate per change in temperature of 10°C	x5 per dT = 10°C	Modified from Repert et al., 2020
dT multiplier, anaerobic	Change in anaerobic degradation rate per change in temperature of 10°C	x5 per dT = 10°C	Doug Kent, Deborah Repert, personal communication

Table 2.4: Summary of Organic Carbon degradation measurements which informed the development of our Arrhenius model.

Site/Location	January 2019	August 2019
Tributary	Gaining	Gaining
Stream	Losing	Losing
Wetland	Gaining	Gaining
H2OCON1	-	Gaining
SCONDS	-	Gaining

Table 3.1: Summary of hyporheic flux direction in Tims Branch subsites for both January and August sampling periods. Gaining indicates upward flux, whereas losing indicates downward flux.

Site/Location	Head Gradient (dh/dz)
Tributary	0.00734
Wetland	0.01909
H2OCON1	0.03579
SCONDS	0.00875

Table 3.2: Summary of head gradient values for floc subsites measured during August sampling period.

Site/Location	pH		Temperature (°C)		Eh		Dissolved Oxygen (mg/L)	
	Jan 2019	*Aug 2019*	*Jan 2019*	*Aug 2019*	*Jan 2019*	*Aug 2019*	*Jan 2019*	*Aug 2019*
Tributary	4.4	6.14	11.8	23.7	225	249	11.34	8.365
Stream	4.4	6.74	10.3	25.3	247	391	11.67	8.185
Wetland	4.2	5.57	12	23.8	257	197	11.23	8.45
Sulfide Pond	4.5	5.56	11	23.8	140	414	11.33	8.334
H2OCON1	-	6.34	-	24.3	-	192	-	8.3
SCONDS	-	6.24	-	24.1	-	382	-	8.373

Table 3.3: Summary of subsite surface water measurements of pH, temperature, Eh, and dissolved oxygen across both sampling periods.

6.0 Figures

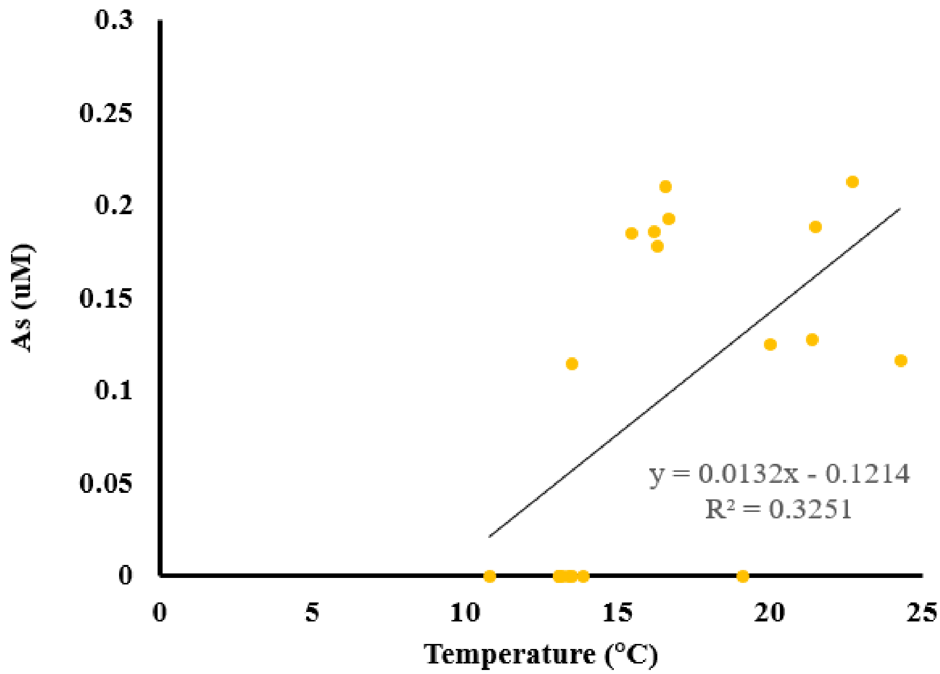

Figure 2.1: Arsenic concentrations downgradient from hypereutrophic Santuit Pond. A positive value for slope in linear regression suggests a possible positive correlation between mobile arsenic concentrations and temperature.

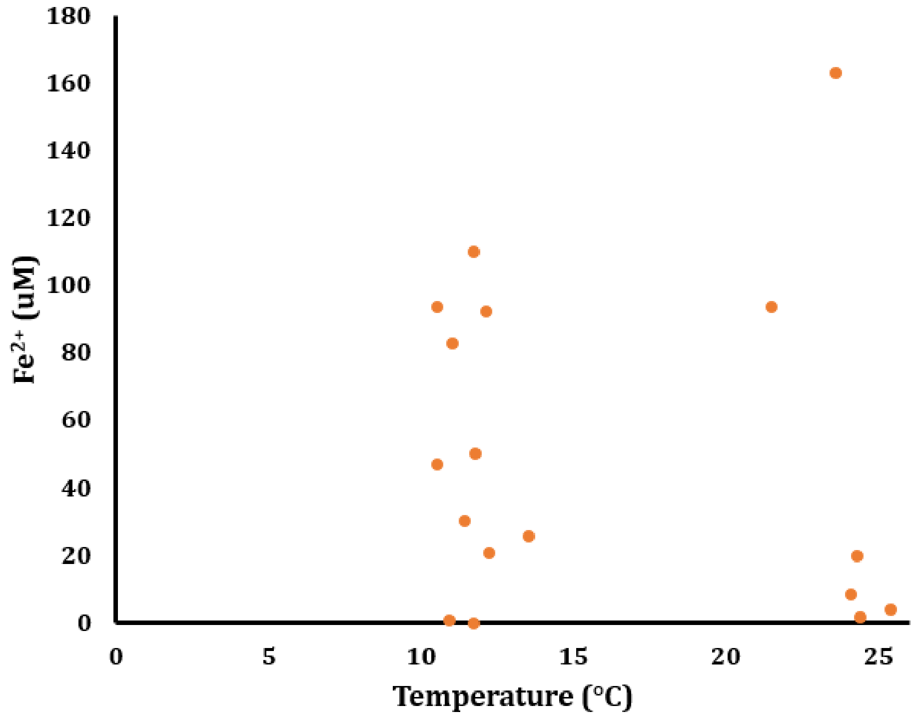

Figure 2.2: Observed ferrous Fe concentrations downgradient of Santuit Pond. Samples were taken from multi-level sampling well M229 – 30 meters downgradient from Santuit Pond.

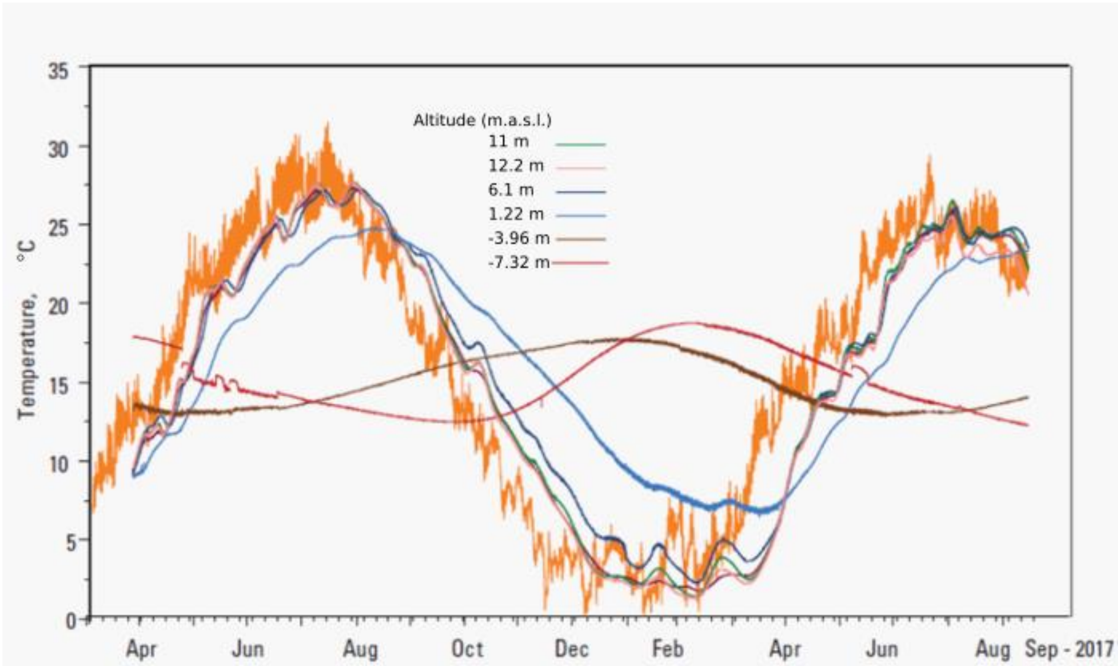

Figure 2.3: Temperature data from Ashumet Pond from April 2016 to September 2017 (adapted from Hull et al., 2019). Surface water (orange line) has a seasonal temperature variation between 2 and 27°C. Depths for temperature data at the multi-level sampling well F722, located about 10 meters horizontally from the lake shore, are shown in meters above sea level (m.a.s.l.). The surface water-groundwater interface and water table in well F722 are at 12.5 m.a.s.l.. Data indicate that shallow groundwater temperatures (e.g., green and light red lines) follow a similar pattern as the surface water temperatures. Deeper groundwater (e.g., light blue, brown, and dark red lines) have increasingly stable groundwater temperatures at greater depths (≤1.22 m.a.s.l.).

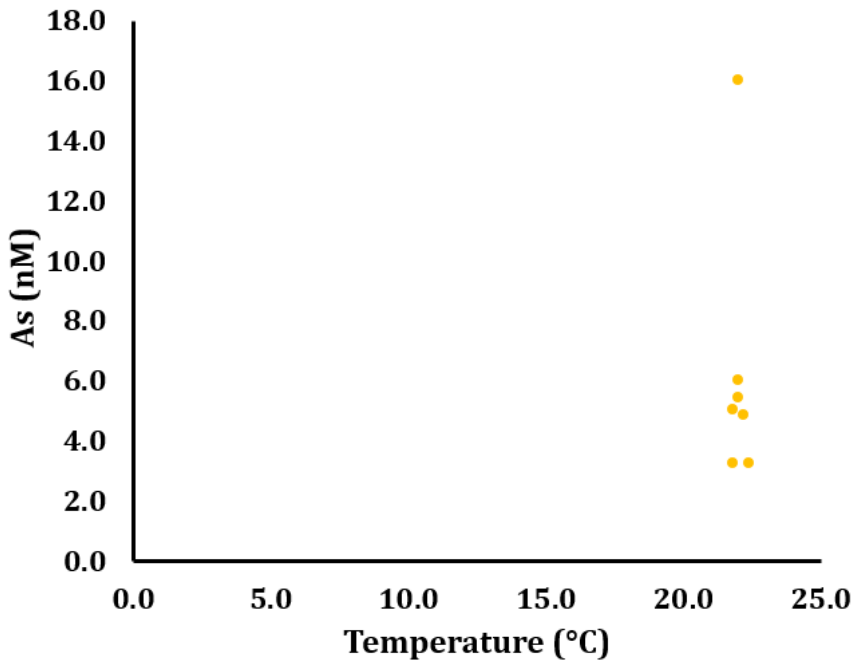

Figure 2.4: Concentrations of arsenic from porewaters downgradient of mesotrophic Ashumet Pond (well F722, 15 meters downgradient) in Cape Cod, Massachusetts (USA). Arsenic concentrations downgradient from Ashumet Pond are several orders of magnitude lower than those downgradient from Santuit Pond.

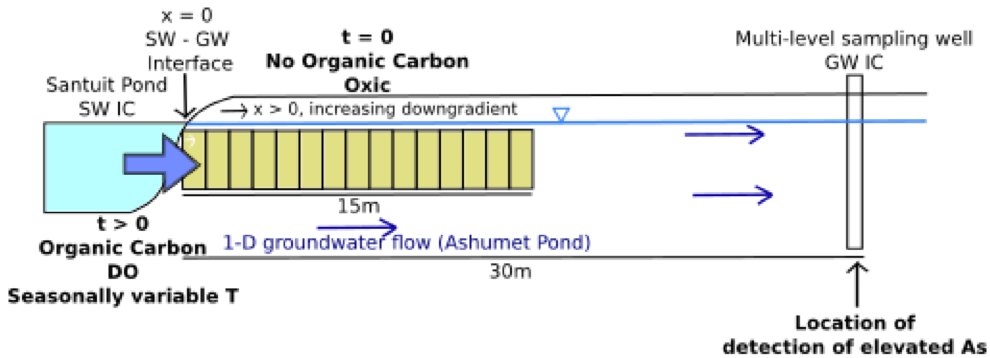

Figure 2.5: Schematic representation of conceptual model and data sources. "SW" indicates surface water, "GW" indicates groundwater, and "IC" indicates initial conditions.

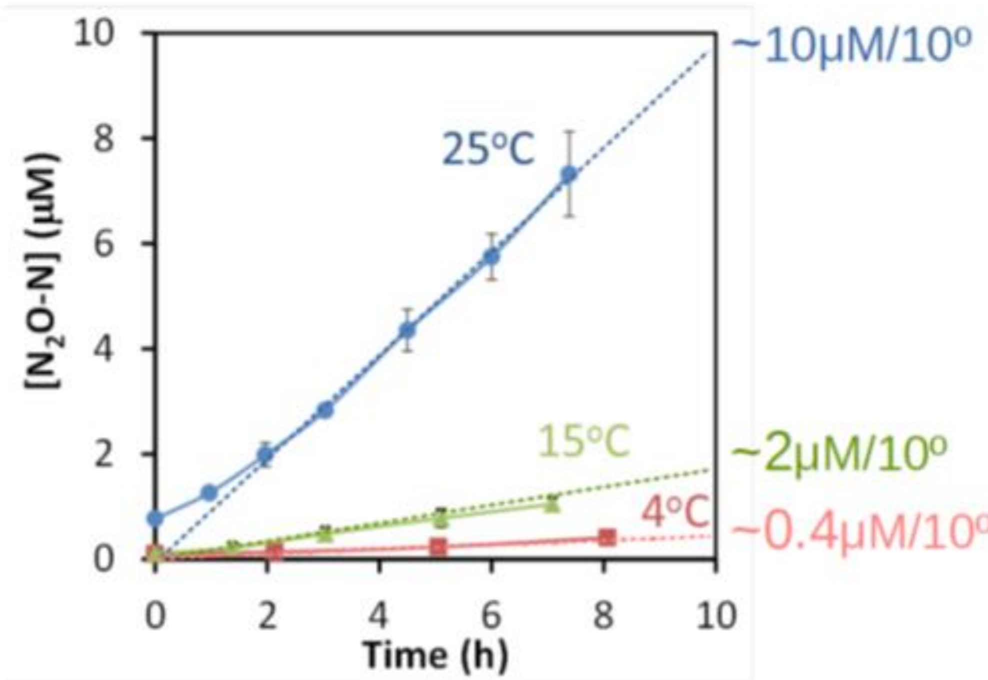

Figure 2.6: Results from an anaerobic organic carbon degradation (coupled with nitrate reduction) experiment indicate a 5-fold increase in degradation rate per 10°C increase in temperature. (Doug Kent, personal communication)

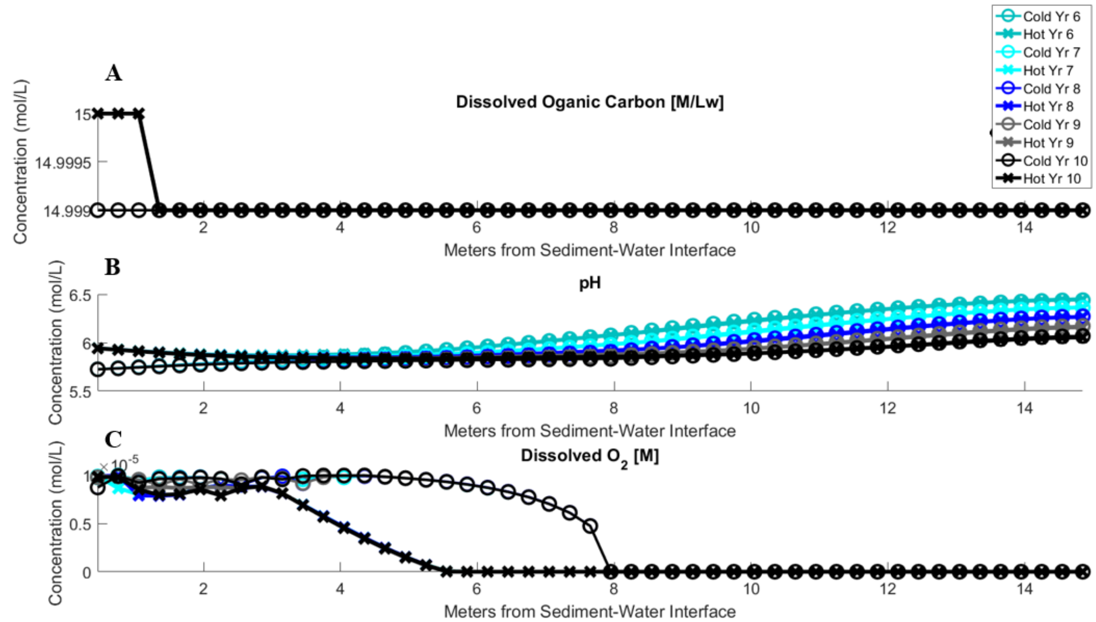

Figure 2.7: Summary of results from final 5 years of model simulation. Results for labile organic carbon (A), pH (B), and dissolved oxygen (C) are shown. Plots display 2nd to 50th gridcells and do not include surface water conditions.

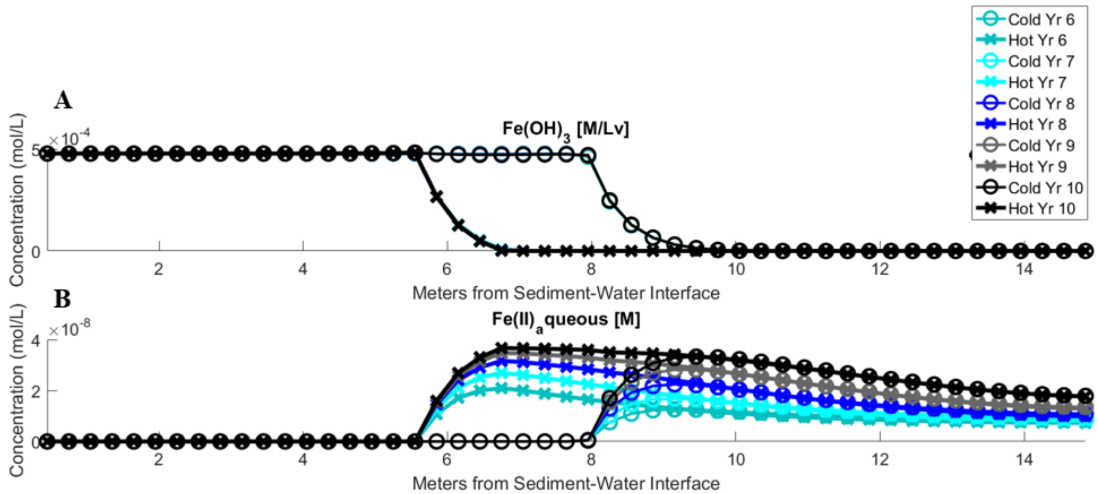

Figure 2.8: Summary of results from final 5 years of model simulation. Results for hydrous ferric oxide minerals (A) and aqueous ferrous iron (B) are shown. Plots display 2nd to 50th gridcells and do not include surface water conditions.

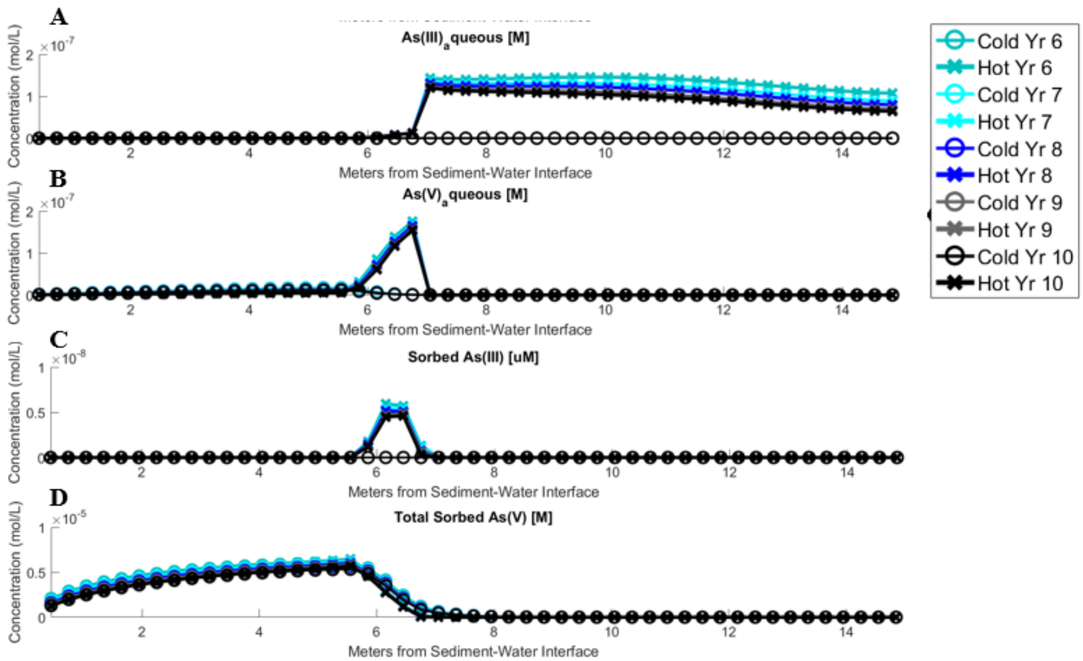

Figure 2.9: Summary of results from final 5 years of model simulation. Results for aqueous arsenite (A), aqueous arsenate (B), sorbed arsenite (C), and sorbed arsenate (D) are shown. Plots display 2nd to 50th gridcells and do not include surface water conditions.

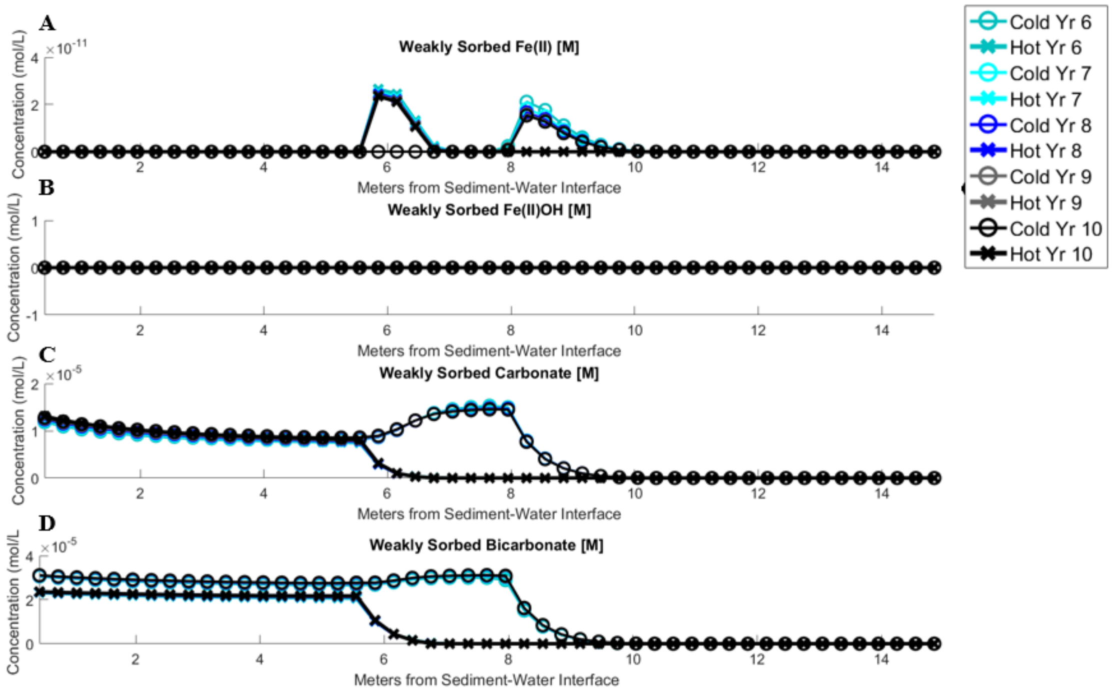

Figure 2.10: Summary of results from final 5 years of model simulation. Results for sorbed Fe(II) (A), sorbed Fe(II)OH (B), sorbed carbonate (C), and sorbed bicaronate (D) are shown. Plots display 2nd to 50th gridcells and do not include surface water conditions.

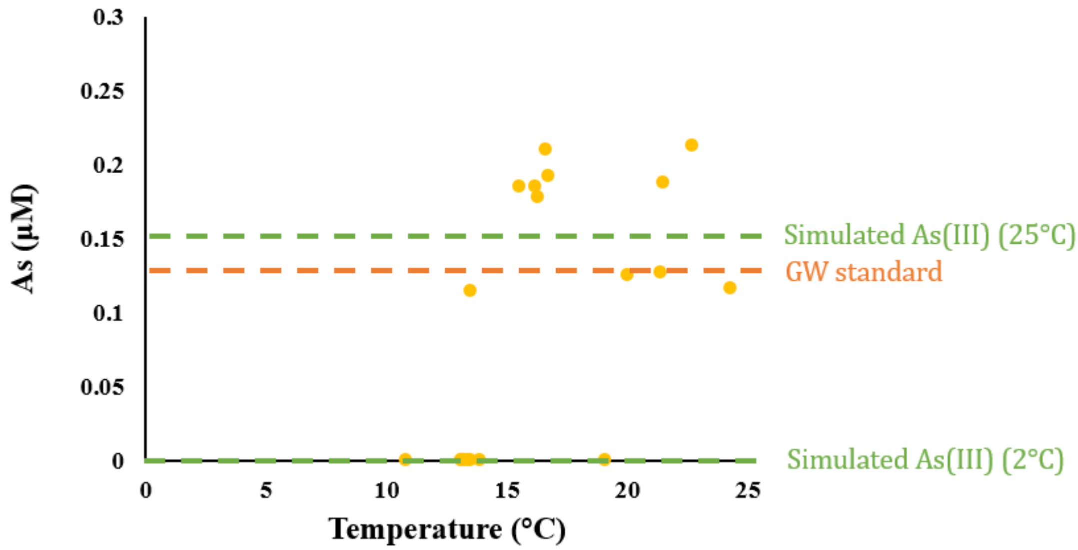

Figure 2.11: A comparison between simulated mobile As(III) concentrations and concentrations observed from multi-level sampling well M229 – 30 meters downgradient from Santuit Pond.

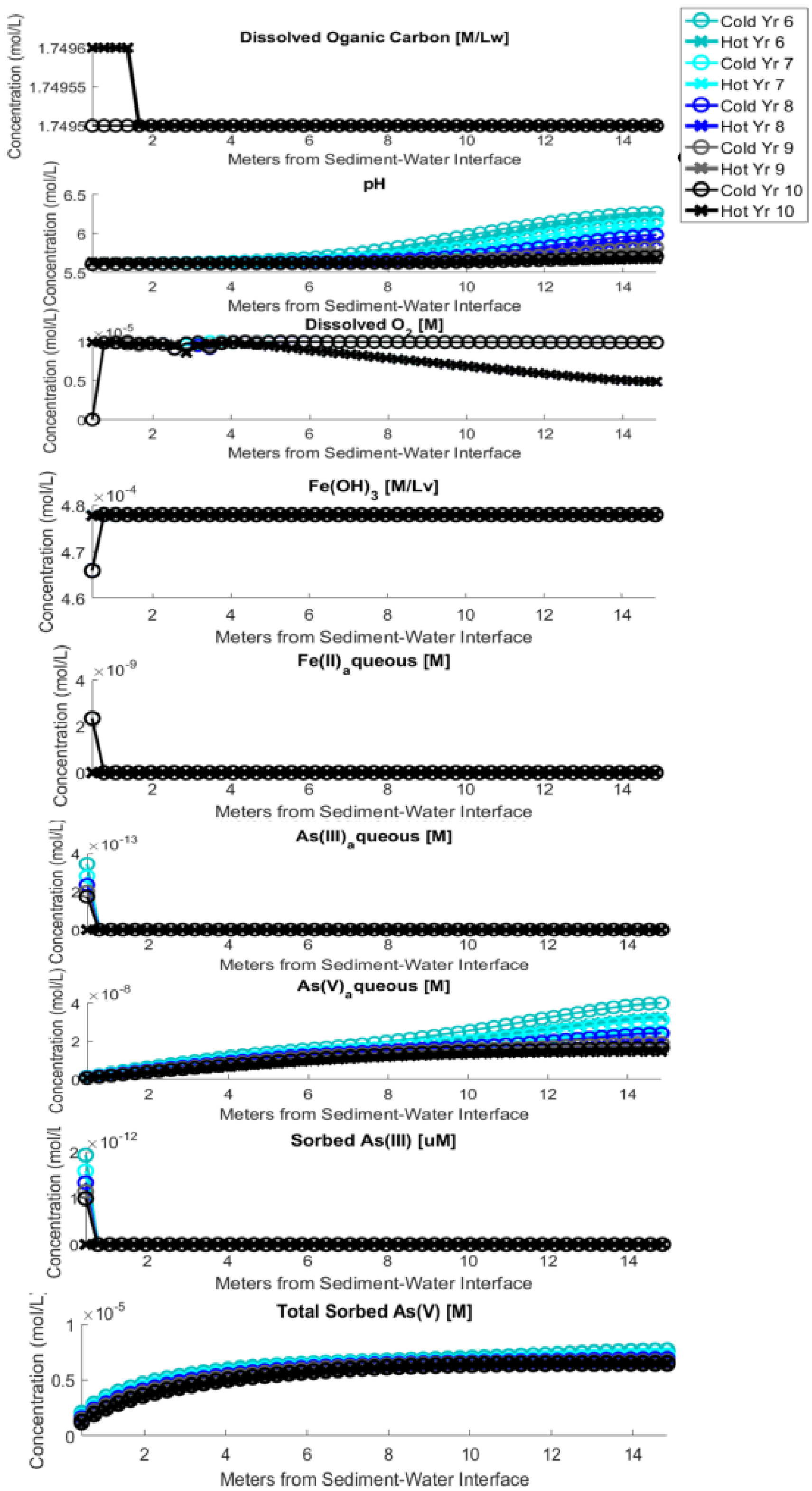

Figure 2.12: Simulation results for a non-eutrophic lake scenario with lower organic carbon concentrations.

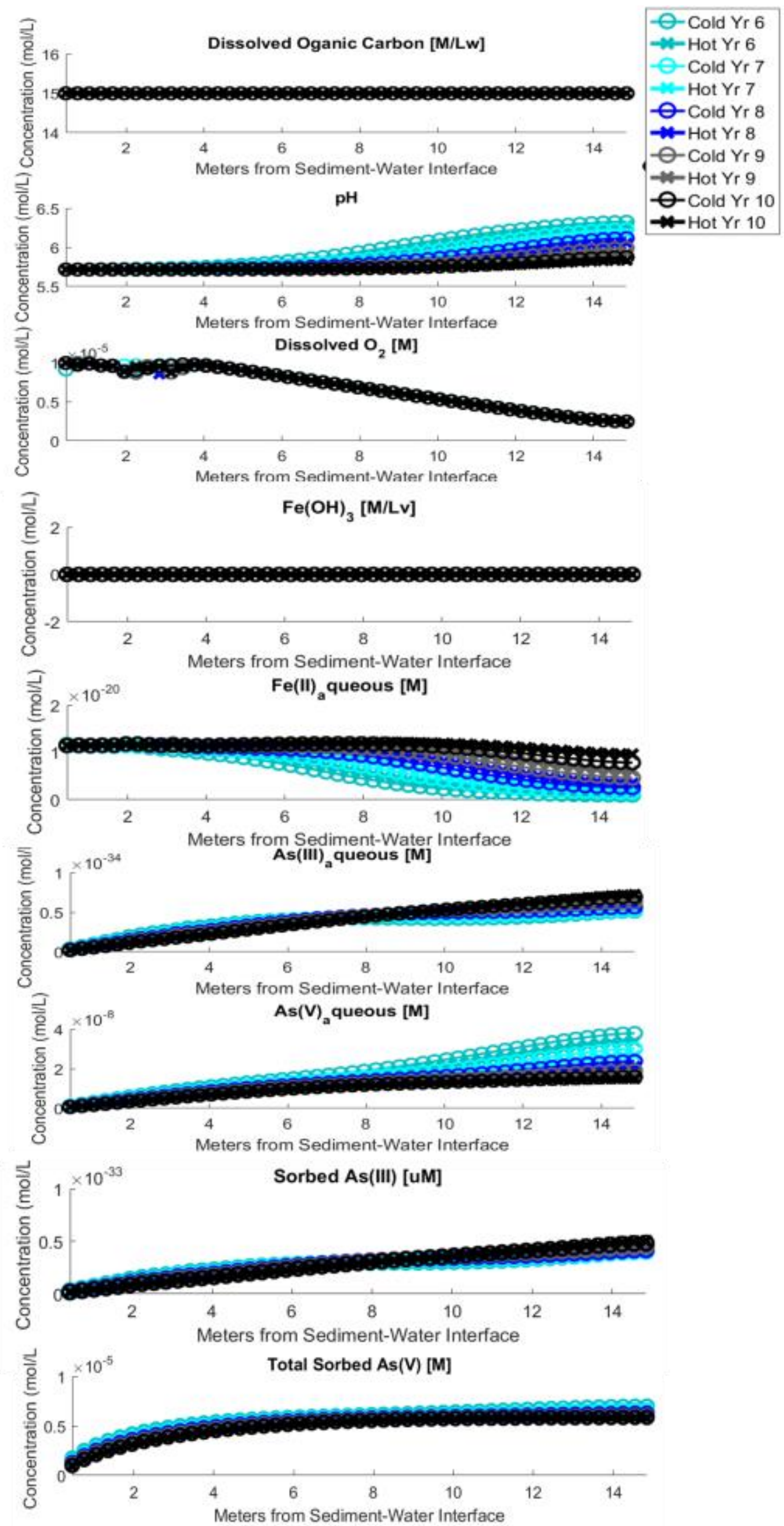

Figure 2.13: Simulation results for a constant temperature scenario with temperature set to 13.5°C.

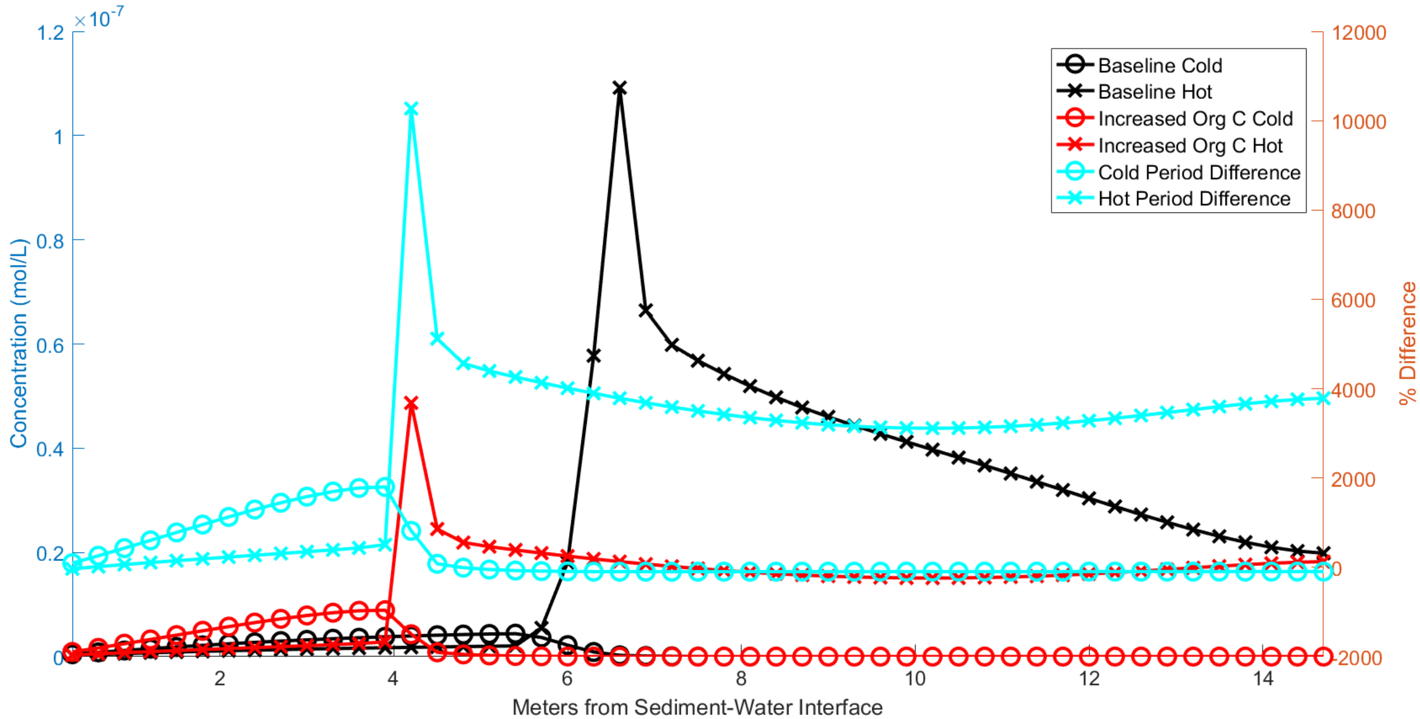

Figure 2.14: Assessment of model sensitivity to increased organic carbon concentrations. For this test, organic carbon was increased by 67%.

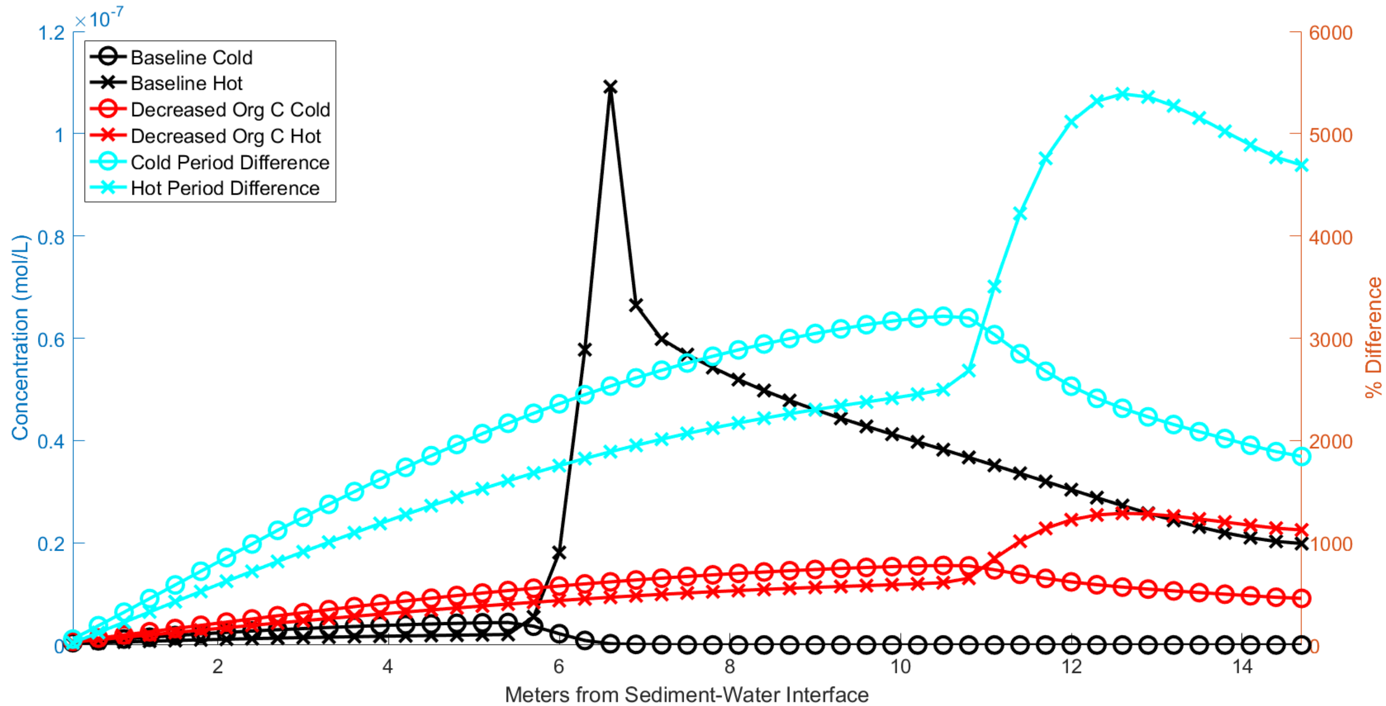

Figure 2.15: Assessment of model sensitivity to decreased organic carbon concentration. For this test, organic carbon was decreased 67%

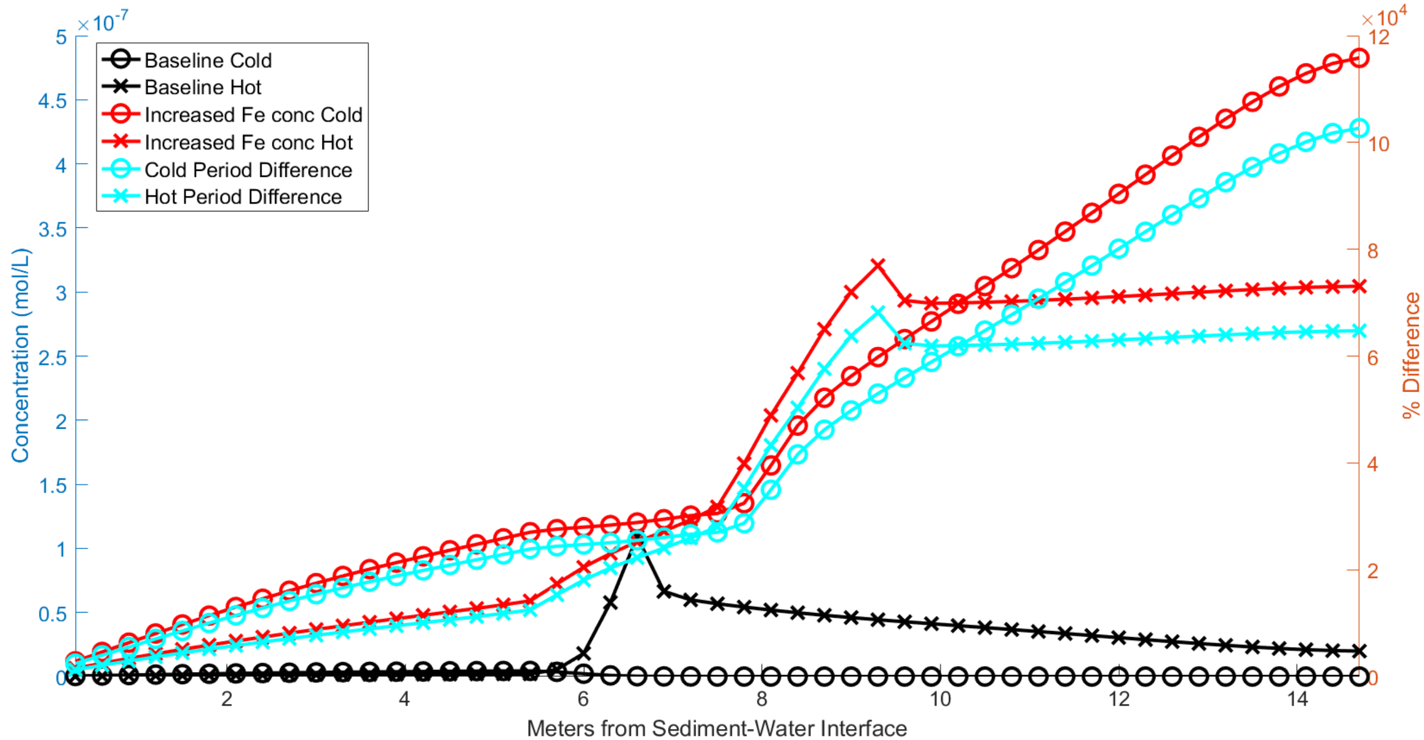

Figure 2.16: Assessment of model sensitivity to Fe mineral concentration. For this test, Fe mineral concentration was increased by an order of magnitude.

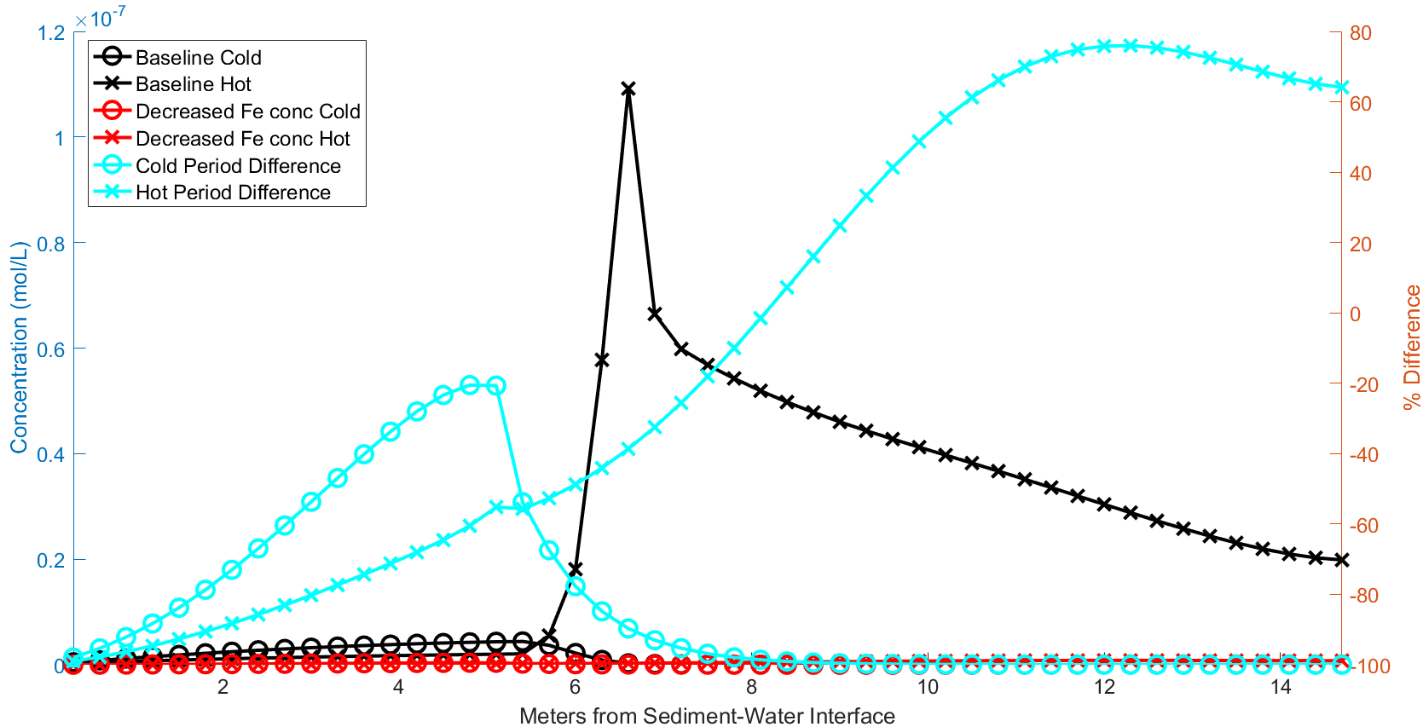

Figure 2.17: Assessment of model sensitivity to Fe mineral concentration. For this test, Fe mineral concentration was decreased by an order of magnitude.

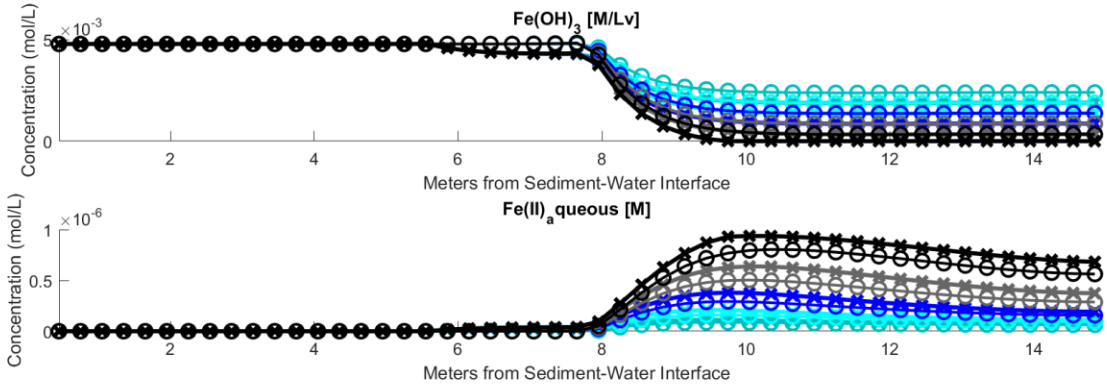

Figure 2.18: Model results from sensitivity test simulation with Fe oxide concentration increased by an order of magnitude. Fe^{2+} concentrations more closely match observations than base model simulations and are higher by 2 orders of magnitude.

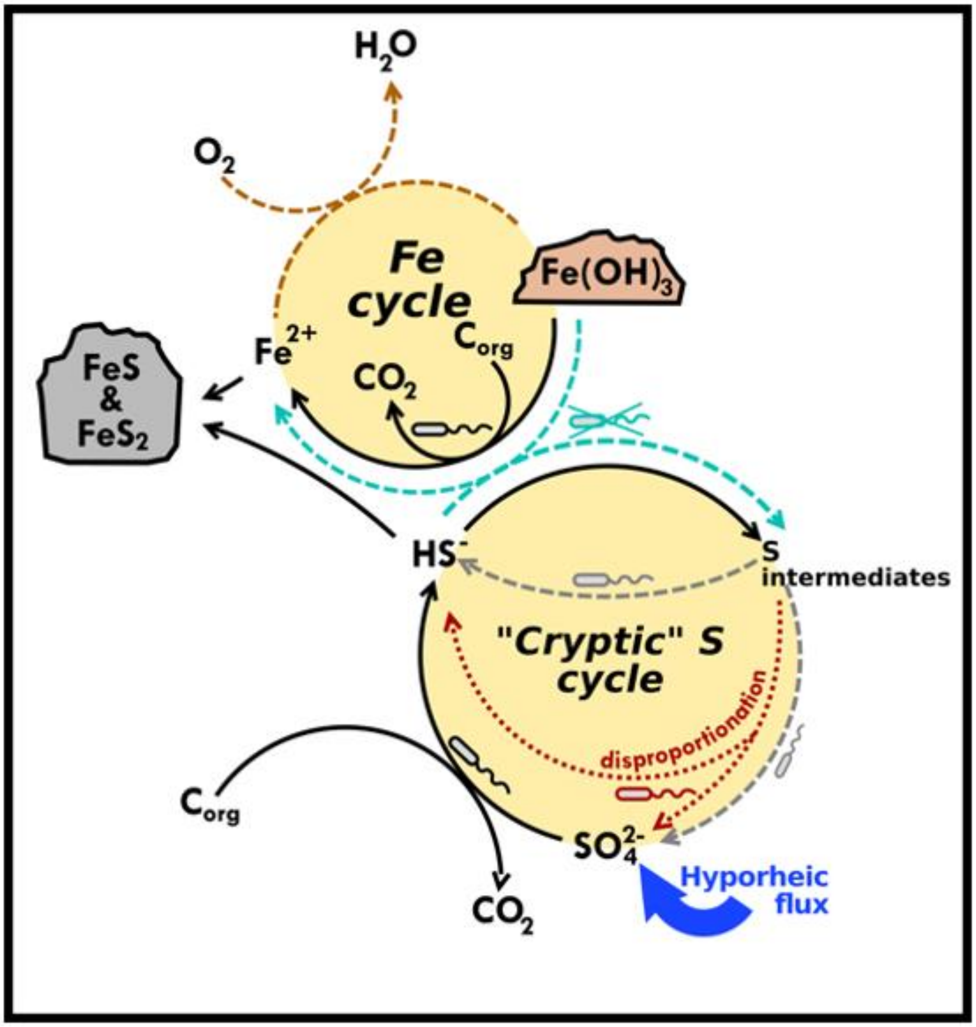

Figure 3.1: Proposed conceptual model for Fe-S cycling in wetlands (adapted from Flynn et al., 2014).

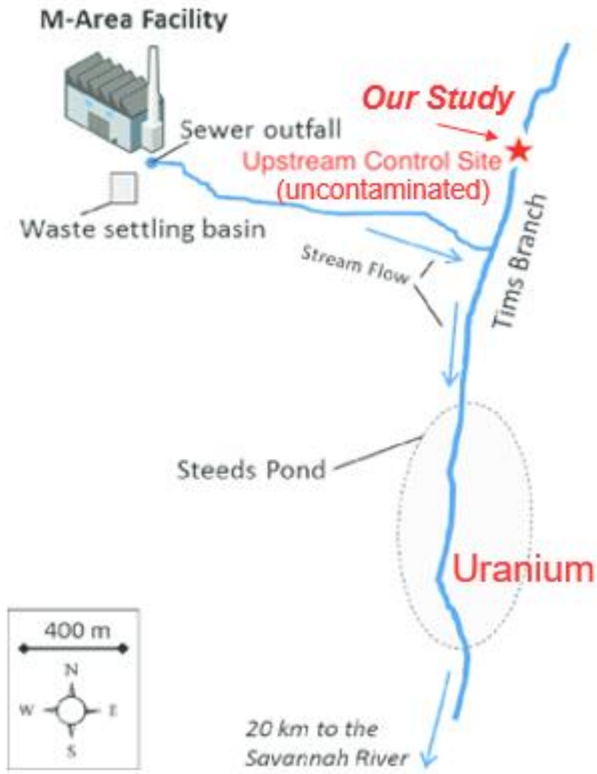

Figure 3.2: Schematic representation of Argonne SFA site. Our site is located within the upstream control site, which is upstream of contaminated areas (adapted from Kaplan et al., 2017).

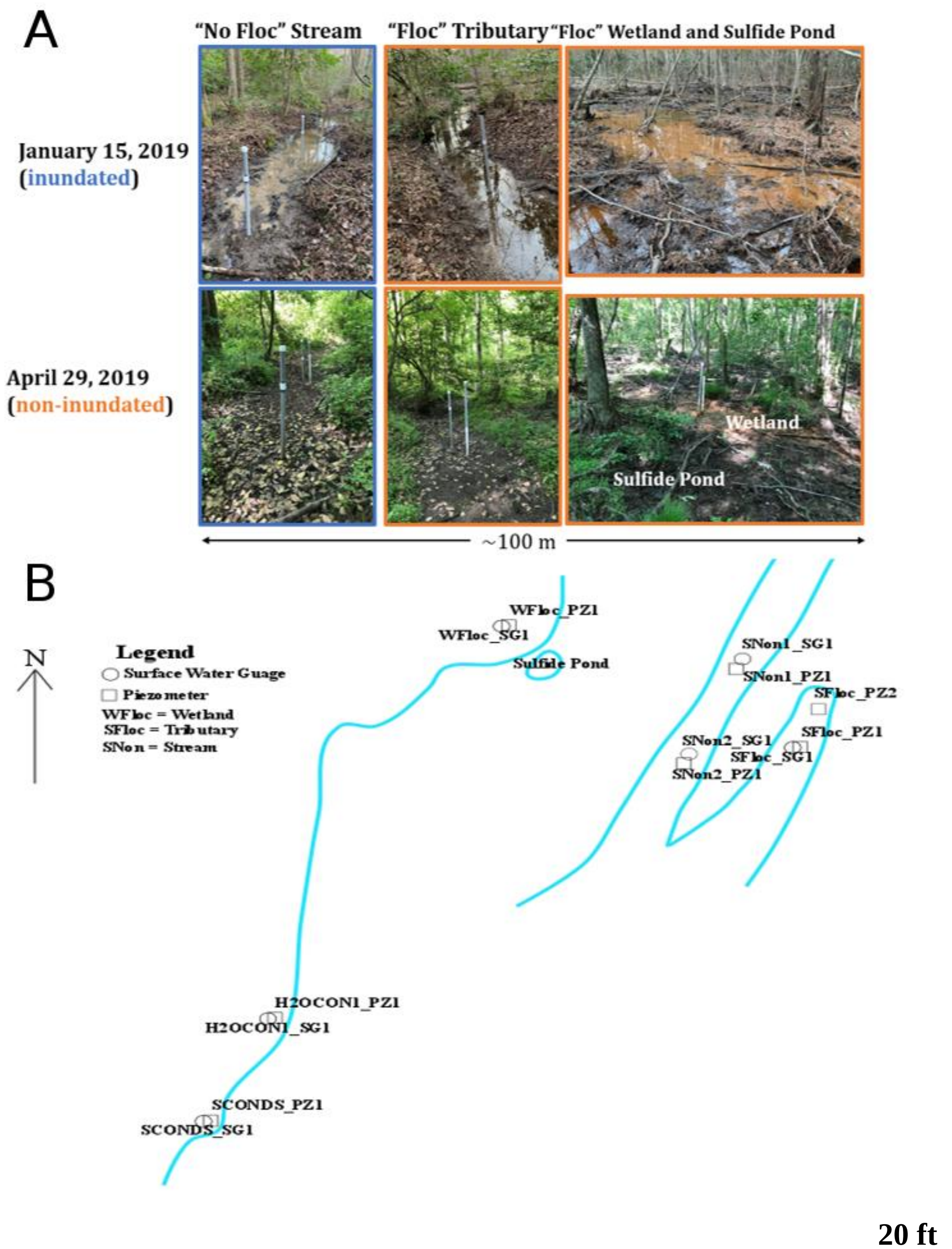

Figure 3.3: (A): Photos of Tims Branch subsites from two time periods: January 15th, 2019 and April 29th, 2019. From left to right, the geochemical gradient between sites can be seen, with no flocs occurring in the Stream subsite and abundant flocs occurring in the Wetland subsite. From top to bottom, hydrologic variability can be seen, with periods of inundated and non-inundated sediment occurring throughout the year. **(B):** Schematic map of site locations and locations of hydrologic equipment.

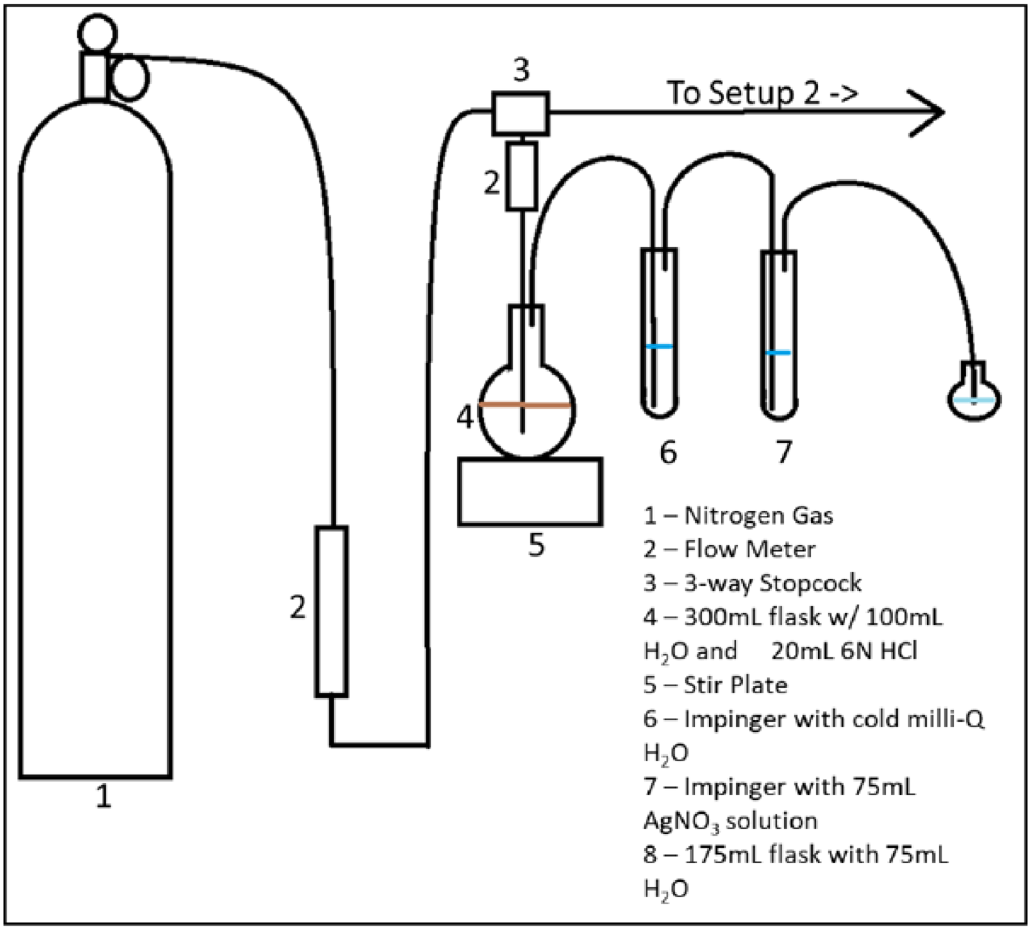

Figure 3.4: Schematic of apparatus used for acid volatile sulfide extraction. Modified from Allen et al., 1993 (Image credit: Joshua Torgeson).

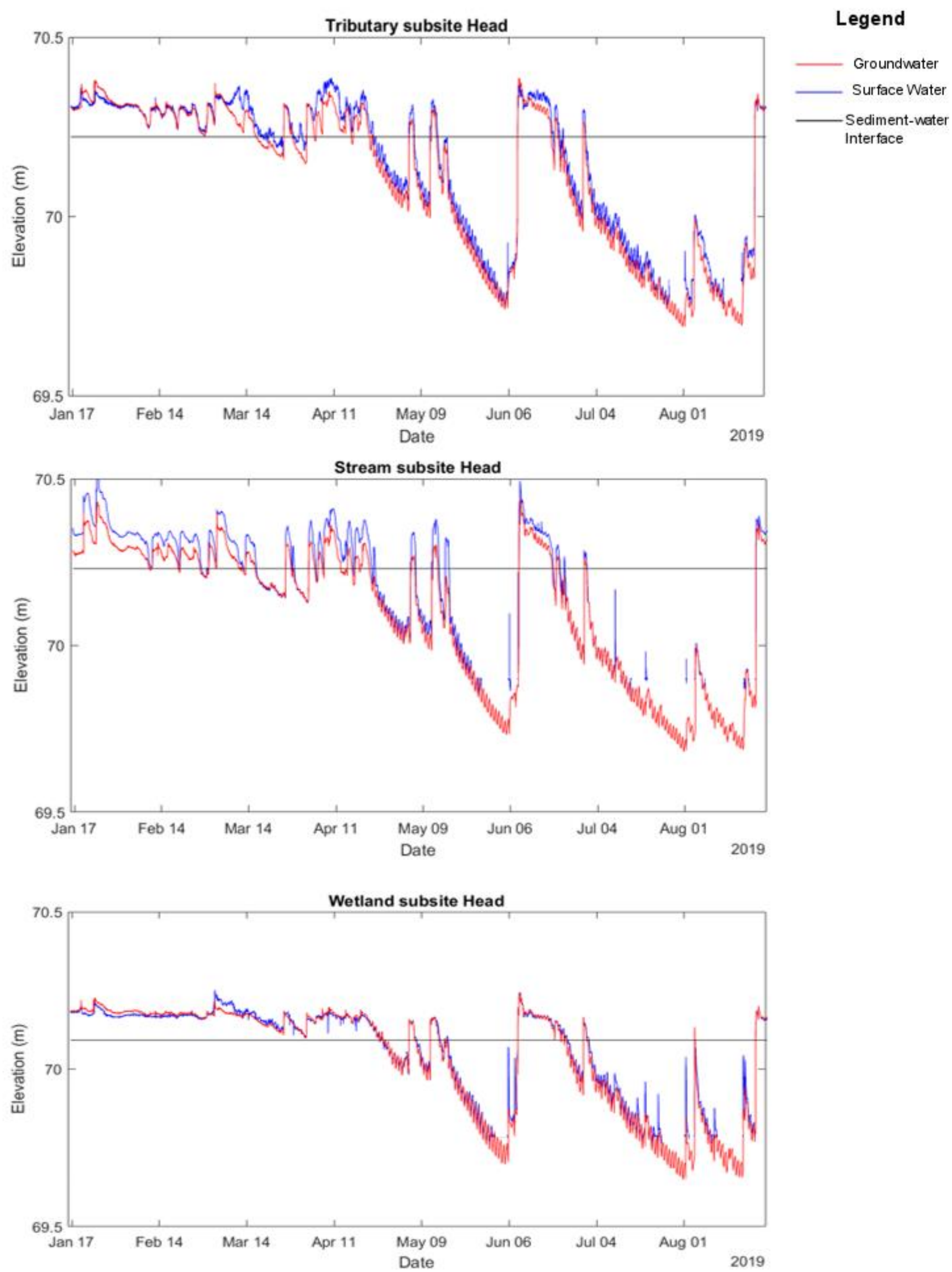

Figure 3.5: Plots of head over time for Upstream subsites.

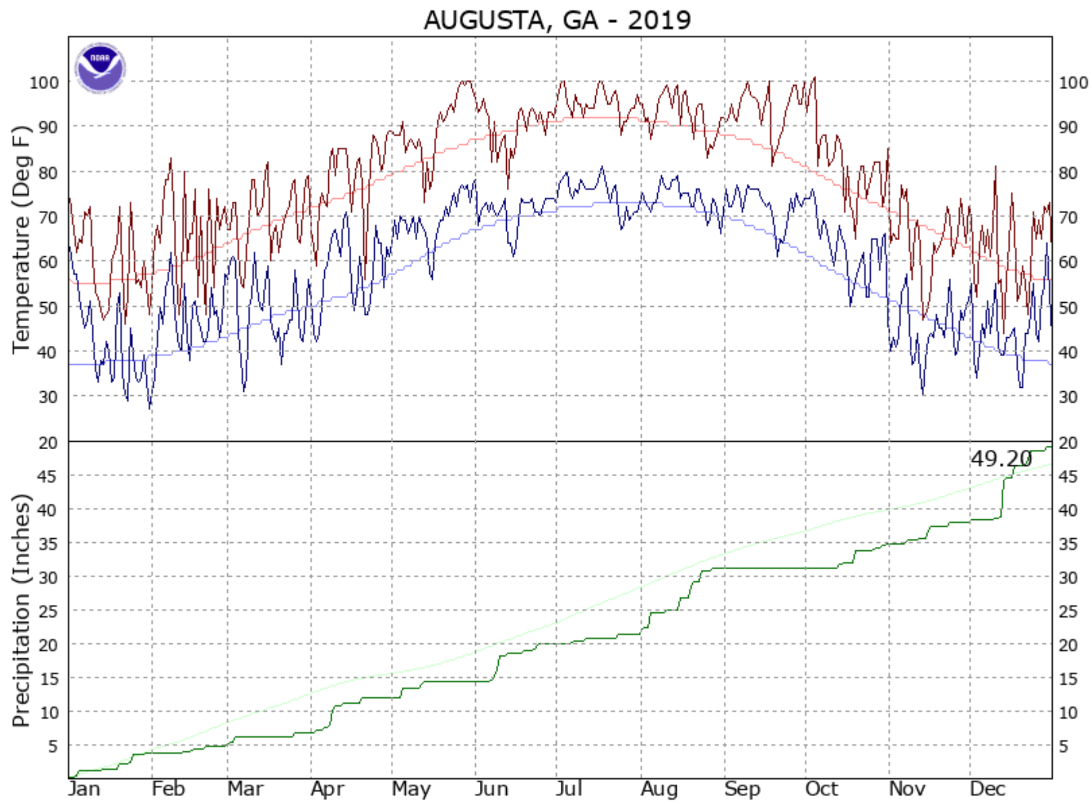

Figure 3.6: High (red) and low (blue) daily temperature data and cumulative precipitation data for nearby city of Augusta, GA. (National Weather Service).

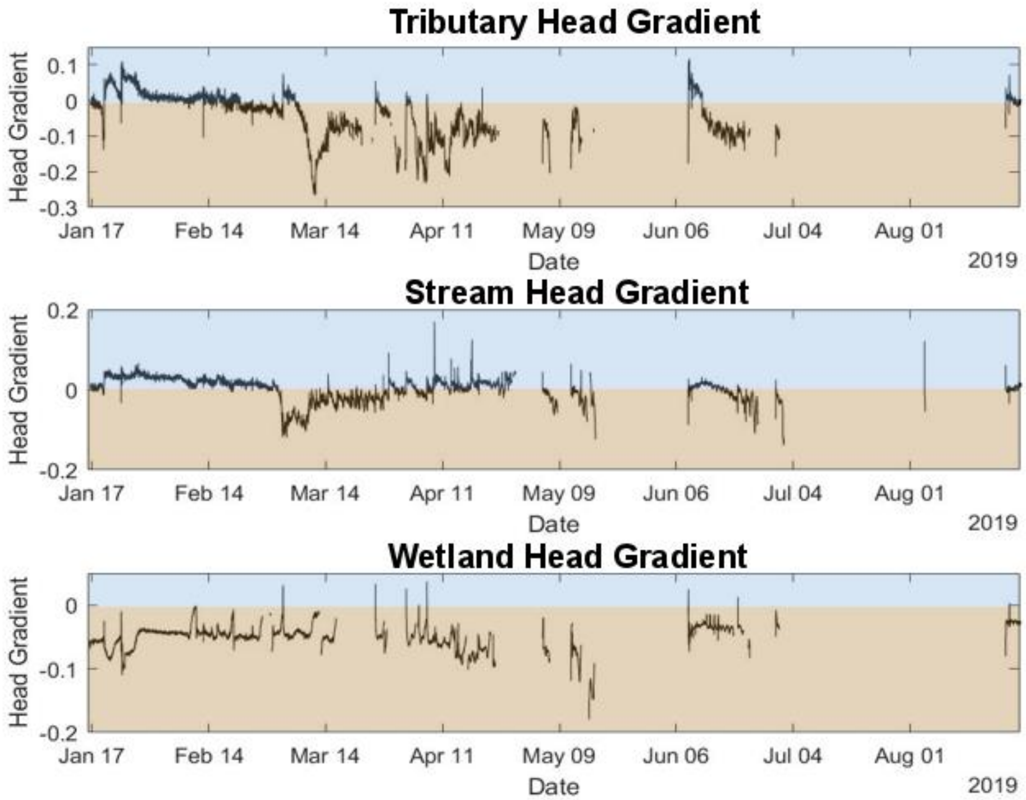

Figure 3.7: Head gradient plots for Tributary, Stream, and Wetland subsites. Head gradient only calculated when subsites were inundated. Positive head gradient values (blue region) correspond with upward flux while negative head gradient values (brown region) correspond with downward flux.

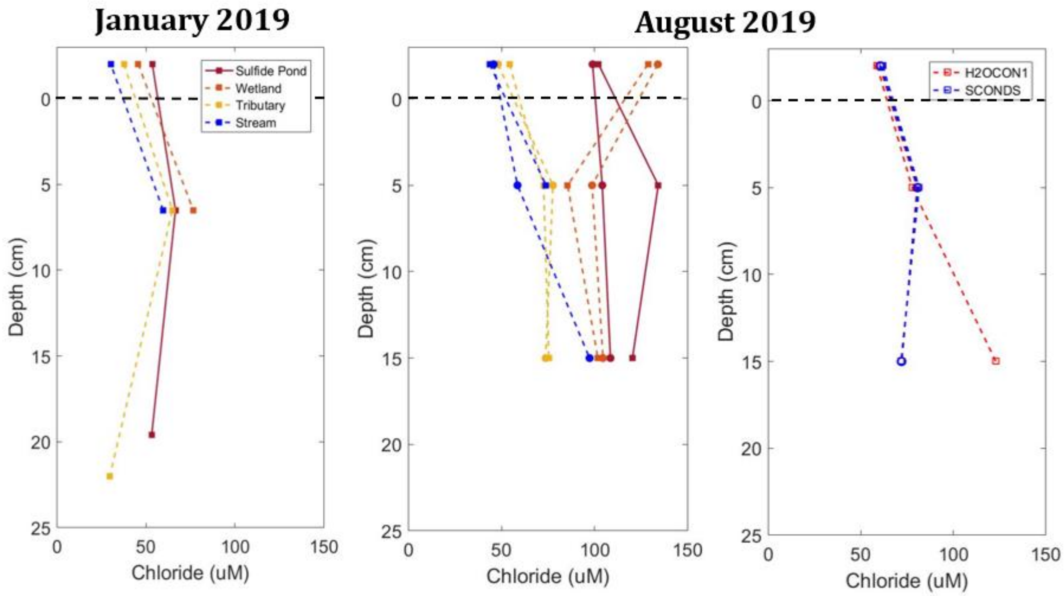

Figure 3.8: Chloride concentrations for Upstream site set for January 2019 and for both Upstream and Downstream site sets for August 2019. Black, dashed line indicates the sediment-water interface; data plotted above this line are surface water, while data plotted below this line are porewater.

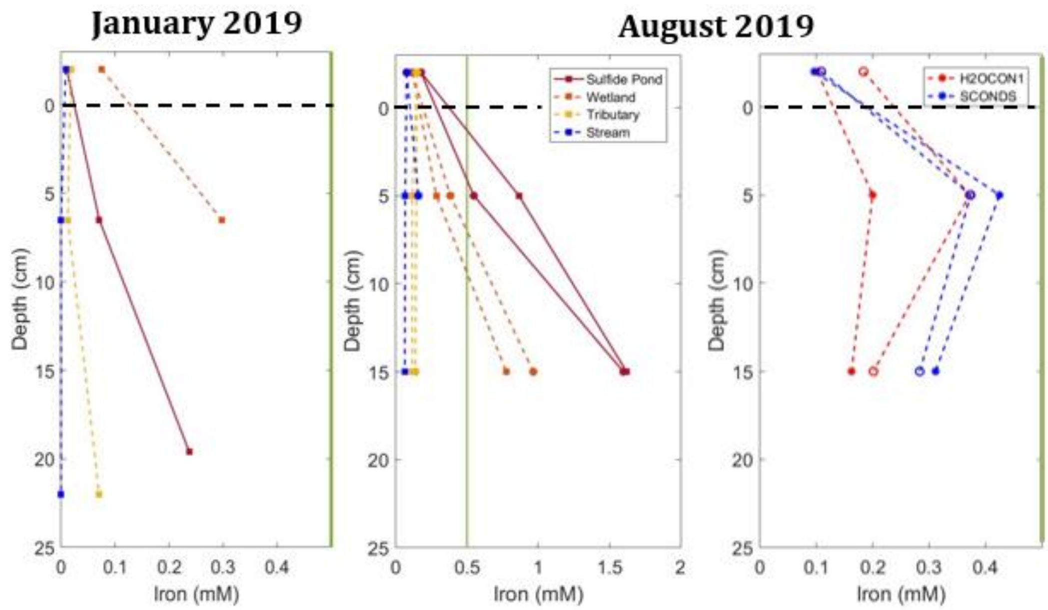

Figure 3.9: Dissolved total iron concentrations for Upstream site set for January 2019 and for both Upstream and Downstream site sets for August 2019. Black, dashed line indicates the sediment-water interface; data plotted above this line are surface water data, while data plotted below this line are porewater data. Green line is at the same concentration for all plots.

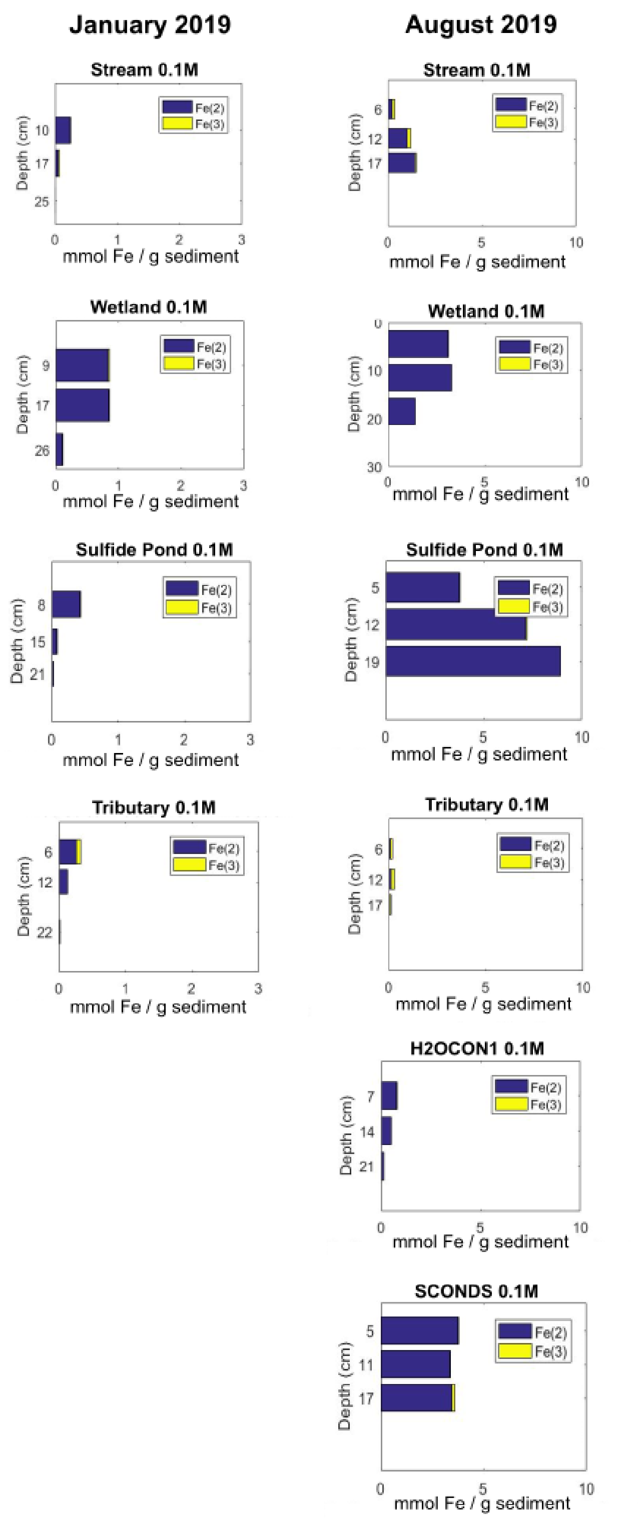

Figure 3.10: 0.1M HCl Extraction for sediment Fe phases for Upstream site set in January 2019 (right), and both Upstream and Downstream site sets in August 2019 (left).

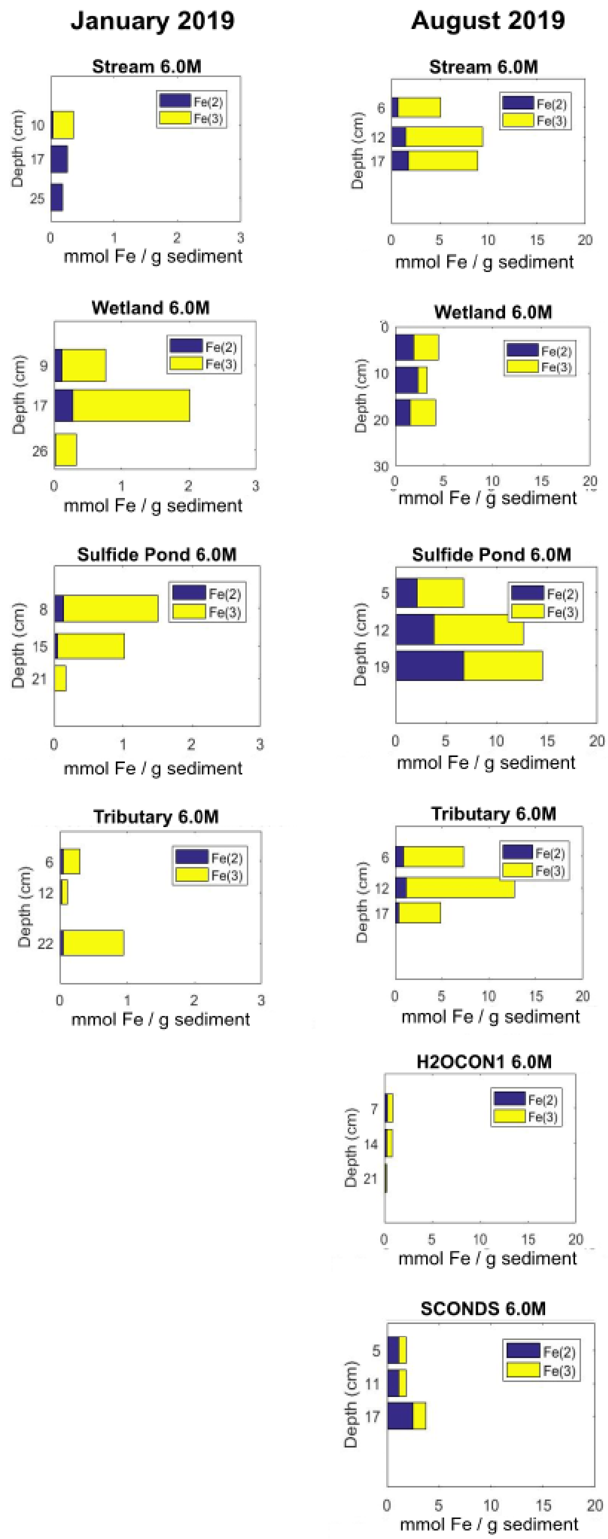

Figure 3.11: 6.0M HCl Extraction for sediment Fe phases for Upstream site set in January 2019 (right), and both Upstream and Downstream site sets in August 2019 (left).

Figure 3.12: Ferric Fe oxide coated roots seen at depth in several cores within the Tims Branch wetland.

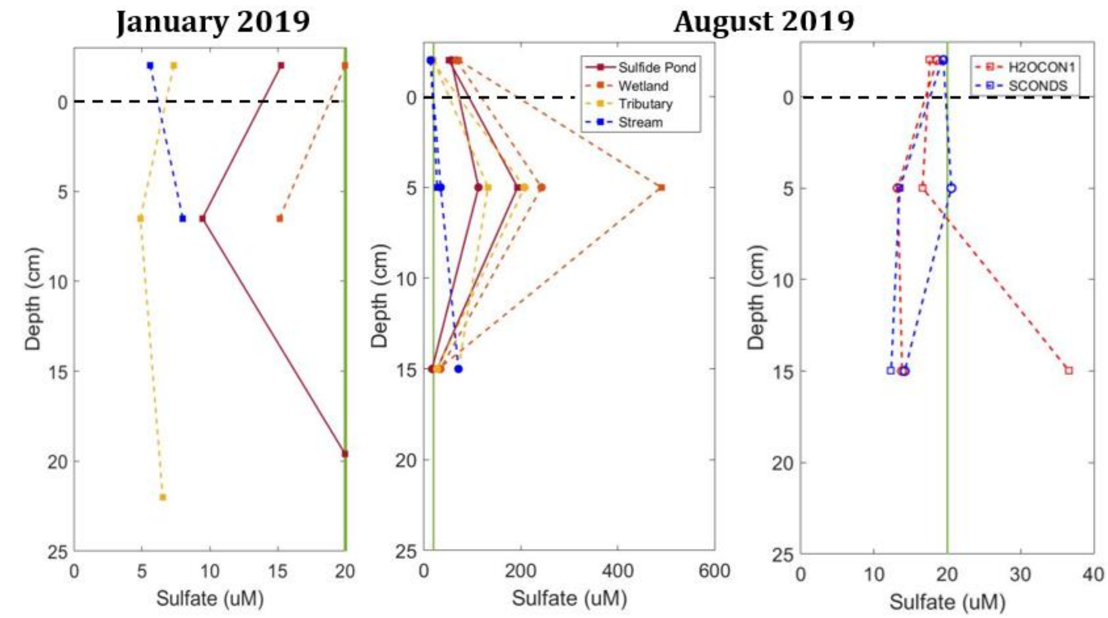

Figure 3.13: Sulfate concentrations for Upstream site set for January 2019 and for both Upstream and Downstream site sets for August 2019. Black, dashed line indicates the sediment-water interface, data plotted above this line are surface water, while those plotted below are porewater. Green line is at the same concentration for all plots.

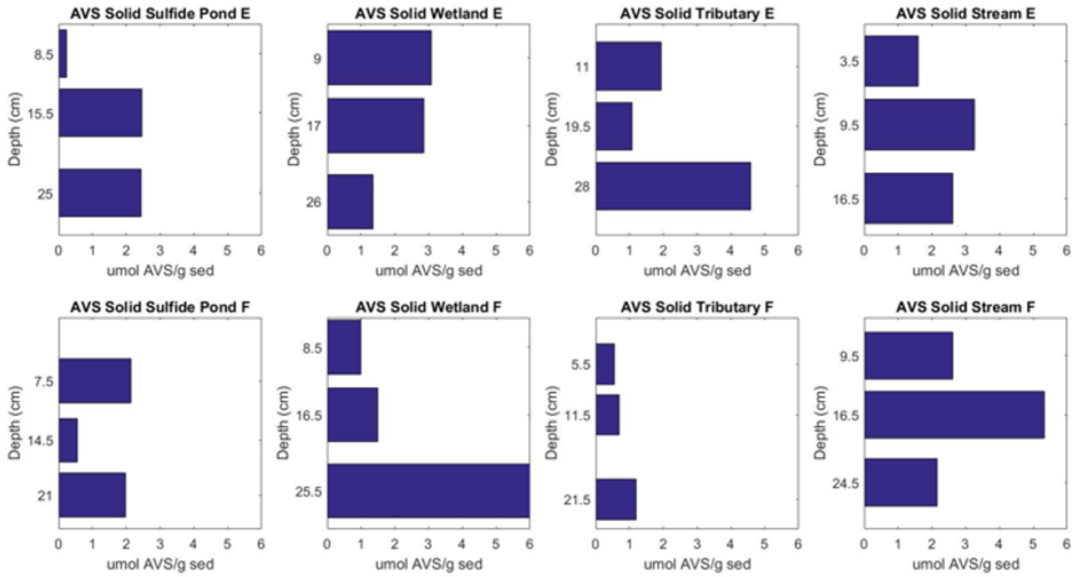

Figure 3.14: Acid volatile sulfide concentrations for Upstream site set sediments for January 2019.

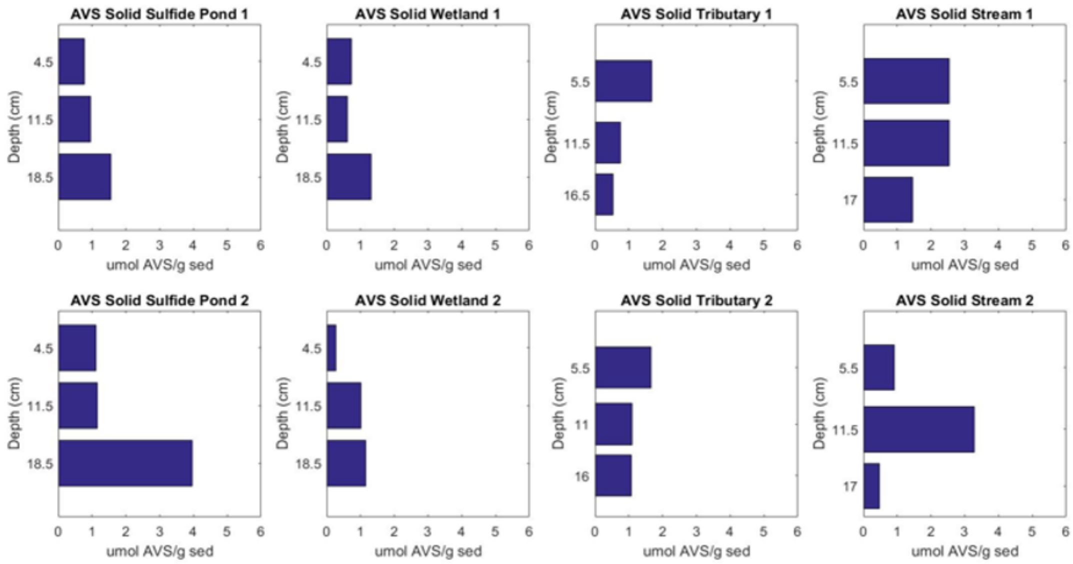

Figure 3.15: Acid volatile sulfide concentrations for Upstream site set sediments for August 2019.

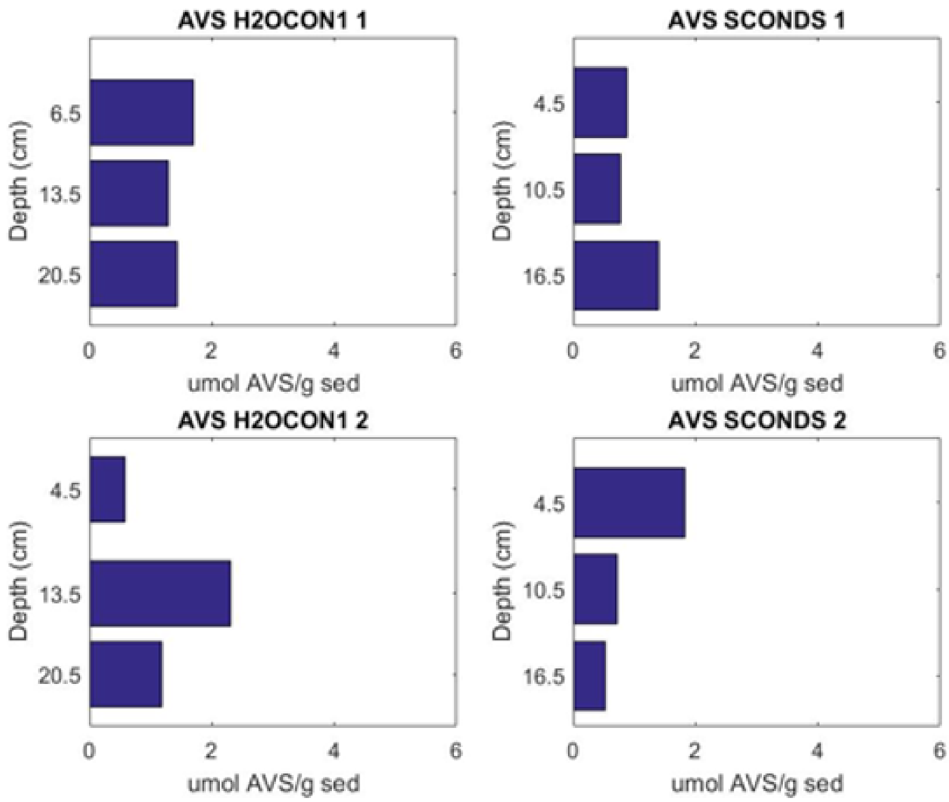

Figure 3.16: Acid volatile sulfide concentrations for Downstream site set sediments for August 2019.

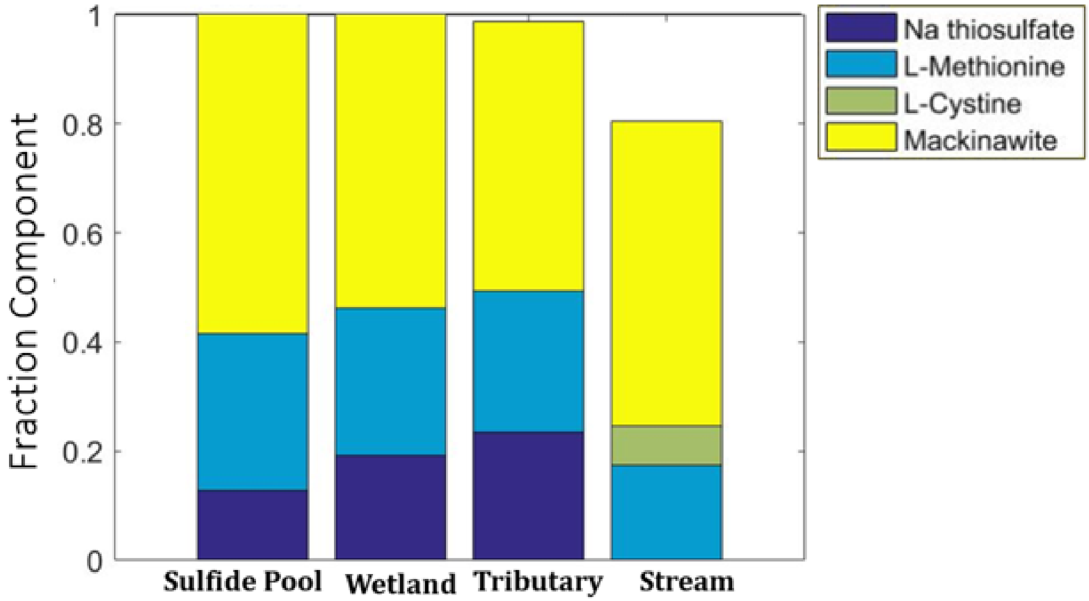

Figure 3.17: S speciation data for Upstream site set sediments for January 2019.

7.0 Appendix

Analyte	Value
Alkalinity	0.047 meq/L
Total Fe(aq)	0.1132 mM
Sulfate	15.7 µM
Chloride	53.34 µM
Nitrite+Nitrate	9.09 µM

Table A1: Summary of geochemistry measurements for samples collected from shallow groundwater well located near Tributary subsite. Values shown are averages from duplicate samples.

Table A.2: Summary of sediment observations during subsampling of January cores.

January 2019			
Subsite	**Interval**	**Replicate**	**Observations**
Tributary	0-2cm	E	sand/clay mix, abundance of leaf/root plant organic matter
	3-8cm	E	some leafy/root organic matter, clay/sand mix, relatively homogenous
	9-14cm	E	little organic matter, homogenous sand/clay mix
	19-28cm	E	transition from sand/clay mix to sand @20 cm, sharp transition gradient
	0-2cm	F	clayey with some sand, very little plant/organic matter, dark brown (clay/OC?)
	7-15cm	F	Clayey, with sand pockets, rings of oxidized iron around sand pockets
	17-22cm	F	Transition to dominantly sandy sed, some pockets of oxidized Fe
	24-32cm	F	Transition from sandy to clayey @28cm,darker color on bottom
Stream	0-5cm	E	clay/sand mix, leaf litter, roots near top of section
	7-12cm	E	sand/clay mix, relatively homogenous
	14-19cm	E	sand/clay mix 14-15 cm, sharp transition to dominant sand @ 15 cm
	22-27cm	E	sand, appears to be large fraction quartz, small pockets of clay sized particles
	0-2cm	F	clay/sand mix, some leaf matter/twigs present
	3-5cm	F	clay/sand mix, very little organic matter, relatively homogenous
	7-12cm	F	clay/sand mix, very little organic matter, slow transition to dominant sand starting at 9 cm depth
	14-19cm	F	sand with very small clay fraction
Wetland	0-4cm	F	clayey, dark brown, roots and other undigested plant matter present
	6-11cm	F	Clayey, dark brown, some undigested and digested plant matter, some sand mixed with clay
	13-20cm	F	Clayey, dark brown in upper part, transition to sandy layer @18cm
	22-29cm	F	Sandy quartz grains, rust staining (Fe oxide coating?) little to no undigested plant matter
Sulfide Pond	0-12cm	E	clay/sand mix, some root/leaf plant matter (undigested OC), more root matter than previous section, pockets of oxidized Fe
	14-20cm	E	clay/sand mix, some root/leaf plant matter (undigested OC), more sand, more root matter than previous section, pockets of oxidized Fe
	22-30cm	E	transition from sand/clay mix to sand at 24 cm, sand-quartz grains, abundant roots at clay/sand transition
	0-4cm	F	clay/sand mix, dark brown, lots of undigested plant material (leaf matter)
	6-11cm	F	Clay/sand mix, dark brown, digested and undigested plant material (leaf matter, humus)
	13-18cm	F	Clay/sand mix @ 13 cm, transition from clay sand mist to dominant sand @~16.5 cm
	20-30cm	F	Sandy, porous, some roots present (undigested plant matter)

Table A.3: Summary of sediment observations during subsampling of January core.

August 2019			
Subsite	**Interval**	**Replicate**	**Observations**
Tributary	0-2cm	1	Mucky, silty, abundant roots, Fe oxide
	3-8cm	1	Sandy, several pockets of oxidized Fe
	9-14cm	1	Sandy, several pockets of oxidized Fe
	15-18cm	1	Shift to sand/silt mix @15cm
	0-2cm	2	Sandy with Fe oxide throughout, saturated
	3-8cm	2	Sandy with Fe oxide throughout, saturated
	9-13cm	2	Sandy with Fe oxide throughout, saturated
	15-18cm	2	Sandy with Fe oxide throughout, saturated
Stream	0-14cm	1	silt/sand mix, abundant roots, pockets of Fe(III) mineral
	14-19cm	1	silt/sand mix, less roots, pockets of Fe(III) mineral
	Entire core	2	silt/sand mix, abundant roots, twigs throughout
Wetland	Entire core	1	0-10cm has reddish hue, homogenous core: silty/clayey texture, roots throughout though density greater in upper 10cm
	Entire core	2	0-10cm has reddish hue, homogenous core: silty/clayey texture, roots throughout though density greater in upper 10cm
Sulfide Pond	Entire core	1	Mixture of silt and clay, organic rich (leaves, roots, undigested organic matter), roots to end of core, some rusted roots throughout, but most in upper 7cm, relatively homogenous
	Entire core	2	Mixture of silt and clay, transition to sand at 20-23cm, organic rich (leaves, roots, undigested organic matter), roots to end of core, some rusted roots throughout, but most in upper 7cm, relatively homogenous
H2OCON1	0-2cm	1	silt/sand mix, leaves, twigs and roots
	2-7cm	1	silt/sand mix, leaves, twigs and roots, less organic matter
	11-16cm	1	silt in upper portion, transition to sand at 13cm
	18-23cm	1	homogenous sand
	Entire core	2	silt/sand mix, sand lens at 18cm, plant matter rich 0-14cm, leaf matter at top of core, well mixed, homogenous
SCONDS	Entire core	1	Mucky, undigested plant material, saturated, silty texture
	0-2cm	2	Mucky, silty (maybe some clay), lots of organic (plant, debris)
	2-7cm	2	Less plant matter (stops at 5cm), silty
	8-13cm	2	Less plant matter, silty
	14-19cm	2	silty on top, transitions to homogenous sand at 16cm, roots throughout

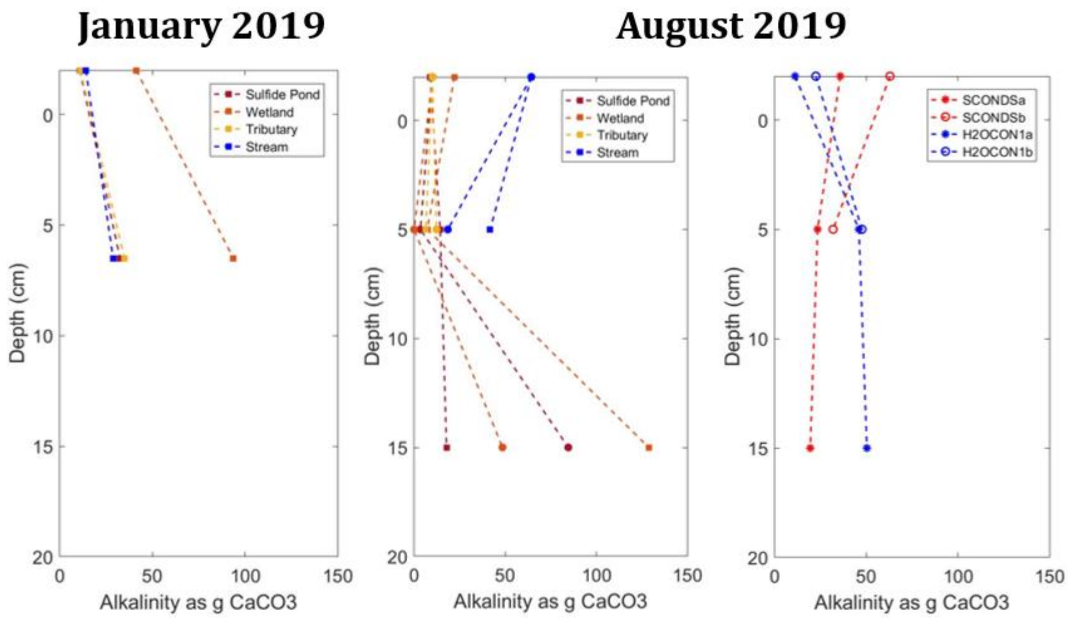

Figure A.1: Alkalinity measurements for Upstream site set for January 2019 and for both Upstream and Downstream site sets for August 2019.

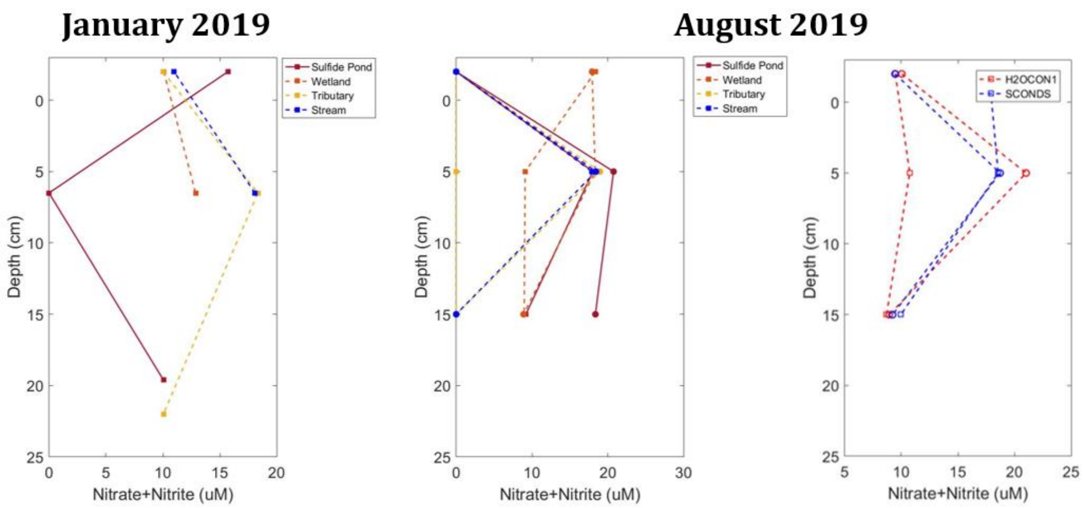

Figure A.2: Nitrate+Nitrite measurements for Upstream site set for January 2019 and for both Upstream and Downstream site sets for August 2019.

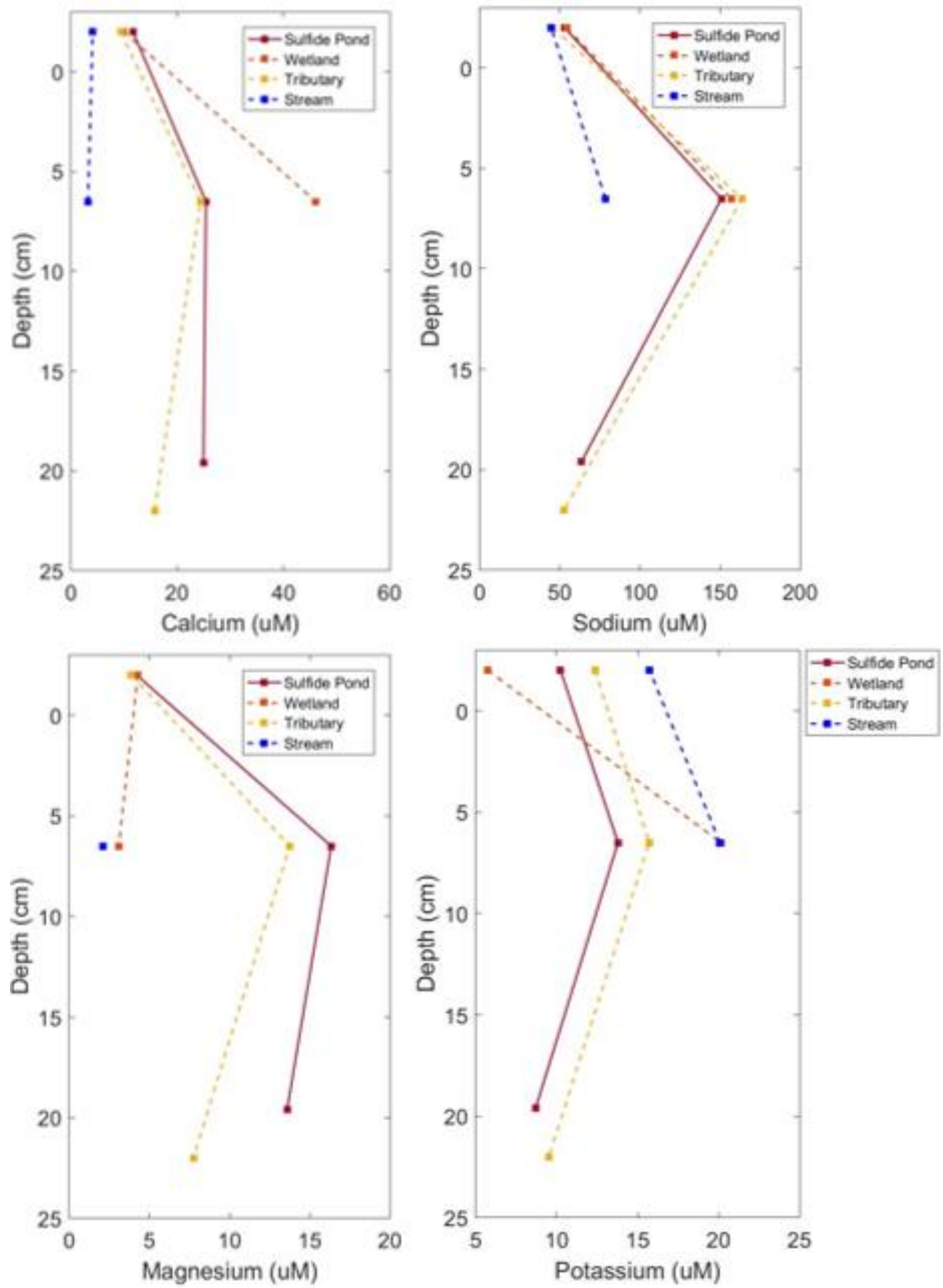

Figure A.3: Calcium, sodium, magnesium, and potassium concentrations for surface water and porewater samples collected in January 2019.

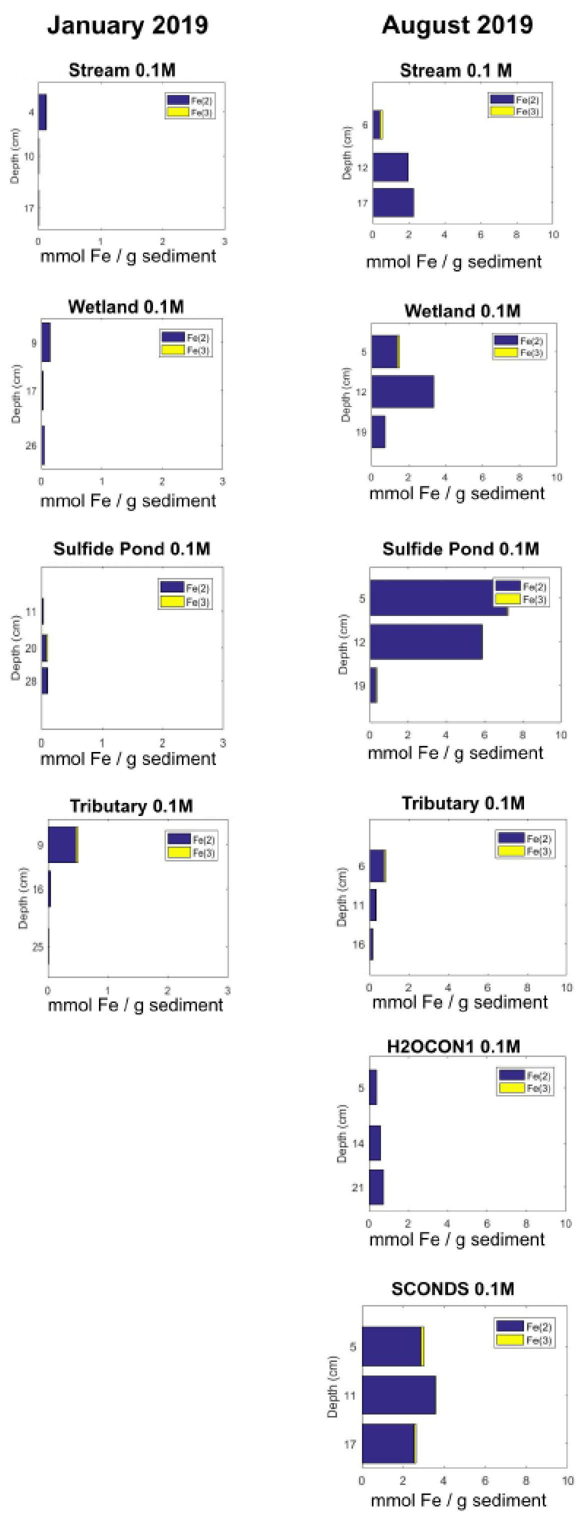

Figure A.4: 0.1M HCl Extraction for sediment Fe phases for Upstream site set in January 2019 (right), and both Upstream and Downstream site sets in August 2019 (left). Data are for replicate samples.

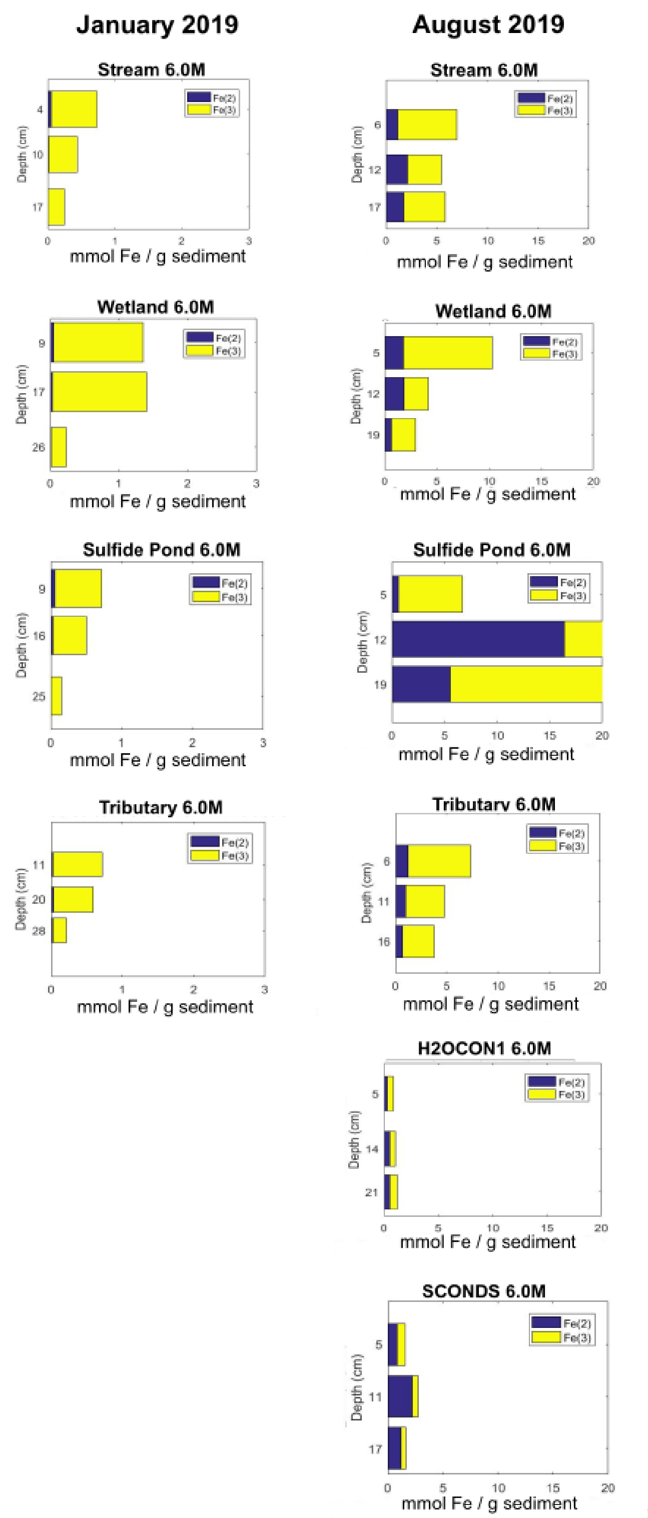

Figure A.5: 6.0M HCl Extraction for sediment Fe phases for Upstream site set in January 2019 (right), and both Upstream and Downstream site sets in August 2019 (left). Data are for replicate samples.

7.0 References

Al-Sid-Cheikh, M., Pédrot, M., Dia, A., Guenet, H., Vantelon, D., Davranche, M., … Delhaye, T. (2015). Interactions between natural organic matter, sulfur, arsenic and iron oxides in re-oxidation compounds within riparian wetlands: NanoSIMS and X-ray adsorption spectroscopy evidences. *Science of the Total Environment*, *515–516*, 118–128. https://doi.org/10.1016/j.scitotenv.2015.02.047

Allen, H. E., Fu, G., & Deng, B. (1993). Analysis of acid-volatile sulfide (AVS) and simultaneously extracted metals (SEM) for the estimation of potential toxicity in aquatic sediments. *Environmental Toxicology and Chemistry*, *12*(8), 1441–1453. https://doi.org/10.1002/etc.5620120812

Anibas, C., Fleckenstein, J. H., Volze, N., Buis, K., Verhoeven, R., Meire, P., & Batelaan, O. (2009). Transient or steady-state? Using vertical temperature profiles to quantify groundwater – surface water exchange. *Hydrological Processes*, *2177*(March), 2165–2177. https://doi.org/10.1002/hyp

Appelo, C. A. J., Van Der Weiden, M. J. J., Tournassat, C., & Charlet, L. (2002). Surface complexation of ferrous iron and carbonate on ferrihydrite and the mobilization of arsenic. *Environmental Science and Technology*, *36*(14), 3096–3103. https://doi.org/10.1021/es010130n

Arai, Y., Sparks, D. L., & Davis, J. A. (2004). Effects of Dissolved Carbonate on Arsenate Adsorption and Surface Speciation at the Hematite-Water Interface. *Environmental Science and Technology*, *38*(3), 817–824. https://doi.org/10.1021/es034800w

Arnosti, C., Jorgenson, B. B., Sagemann, J., & Thamdrup, B. (1998). Temperature dependence of microbial degradation of organic matter in marine sediments : polysaccharide hydrolysis , oxygen consumption , and sulfate reduction. *Marine Ecology Progress Series*, *165*, 59–70.

Ascar, L., Ahumada, I., & Richter, P. (2008). Influence of redox potential (Eh) on the availability of arsenic species in soils and soils amended with biosolid. *Chemosphere*, *72*(10), 1548–1552. https://doi.org/10.1016/j.chemosphere.2008.04.056

Ayuso, S. V., Acebes, P., López-archilla, A. I., Montes, C., & Guerrero, C. (2007). Environmental factors controlling the spatiotemporal distribution of microbial communities in a coastal , sandy aquifer system (Doñana , southwest Spain). https://doi.org/10.1007/s10040-008-0397-8

Bardini, L., Boano, F., Cardenas, M. B., Revelli, R., & Ridolfi, L. (2012). Nutrient cycling in bedform induced hyporheic zones. *Geochimica et Cosmochimica Acta*, *84*, 47–61. https://doi.org/10.1016/j.gca.2012.01.025

Barrett, P. M., Hull, E. A., Burkart, K., Hargrave, O., Mclean, J., Taylor, V. F., … Neumann, R. B. (2019). Contrasting arsenic cycling in strongly and weakly stratified contaminated lakes : Evidence for temperature control on sediment – water arsenic fluxes. *Limnology and Oceanography*, *64*, 1333–1346. https://doi.org/10.1002/lno.11119

Bauer, M., & Blodau, C. (2006). Mobilization of arsenic by dissolved organic matter from iron oxides, soils and sediments. *Science of the Total Environment*, *354*(2–3), 179–190. https://doi.org/10.1016/j.scitotenv.2005.01.027

Bauer, M., Fulda, B., & Blodau, C. (2008). Groundwater derived arsenic in high carbonate wetland soils: Sources, sinks, and mobility. *Science of the Total Environment*, *401*(1–3), 109–120. https://doi.org/10.1016/j.scitotenv.2008.03.030

Berg, J. S., Jézéquel, D., Duverger, A., Lamy, D., Laberty-Robert, C., & Miot, J. (2019). Microbial diversity involved in iron and cryptic sulfur cycling in the ferruginous, low-sulfate waters of Lake Pavin. *PLoS ONE*, *14*(2), 1–21. https://doi.org/10.1371/journal.pone.0212787

Bhattacharyya, A., Schmidt, M. P., Stavitski, E., & Enid, C. (2018). Organic Geochemistry Iron speciation in peats : Chemical and spectroscopic evidence for the co-occurrence of ferric and ferrous iron in organic complexes and mineral precipitates. *Organic Geochemistry*, *115*, 124–137. https://doi.org/10.1016/j.orggeochem.2017.10.012

Boano, F., Harvey, J. W., Marion, A., Packman, A. I., Revelli, R., Ridolfi, L., & Worman, A. (2014). Hyporheic flow and transport processes: Mechanisms, models, and biogeochemical implications. *Reviews of Geophysics*, *52*, 603–679. https://doi.org/10.1002/2012RG000417.Received

Bonte, M., Breukelen, B. M. Van, & Stuyfzand, P. J. (2013). Temperature-induced impacts on groundwater quality and arsenic mobility in anoxic aquifer sediments used for both drinking water and shallow geothermal energy production. *Water Research*, *47*(14), 5088–5100. https://doi.org/10.1016/j.watres.2013.05.049

Bose, P., & Sharma, A. (2002). Role of iron in controlling speciation and mobilization of arsenic in subsurface environment. *Water Research*, *36*(19), 4916–4926. https://doi.org/10.1016/S0043-1354(02)00203-8

Boudreau, B. P. (1991). Modelling the sulfide-oxygen reaction and associated pH gradients in porewaters. *Geochimica et Cosmochimica Acta*, *55*(1), 145–159. https://doi.org/10.1016/0016-7037(91)90407-V

Boulton, A. J., Findlay, S., Marmonier, P., Stanley, E. H., & Valett, H. M. (1998). THE FUNCTIONAL SIGNIFICANCE OF THE HYPORHEIC ZONE IN STREAMS AND RIVERS. *Annual Review of Ecology and Systematics*, *29*, 59–81.

Brechbühl, Y., Christl, I., Elzinga, E. J., & Kretzschmar, R. (2012). Competitive sorption of carbonate and arsenic to hematite: Combined ATR-FTIR and batch experiments. *Journal of Colloid and Interface Science*, *377*(1), 313–321. https://doi.org/10.1016/j.jcis.2012.03.025

Briggs, M. A., Lautz, L. K., Hare, D. K., & González-Pinzón, R. (2013). Relating hyporheic fluxes, residence times, and redox-sensitive biogeochemical processes upstream of beaver dams. *Freshwater Science*, *32*(2), 622–641. https://doi.org/10.1899/12-110.1

Briggs, M. A., Lautz, L. K., Mckenzie, J. M., Gordon, R. P., & Hare, D. K. (2012). Using high-resolution distributed temperature sensing to quantify spatial and temporal variability in vertical hyporheic flux, *48*, 1–16. https://doi.org/10.1029/2011WR011227

Burke, V., Greskowiak, J., Asmuß, T., Bremermann, R., Taute, T., & Massmann, G. (2014). Temperature dependent redox zonation and attenuation of wastewater-derived organic micropollutants in the hyporheic zone. *Science of the Total Environment, The*, *482–483*, 53–61. https://doi.org/10.1016/j.scitotenv.2014.02.098

Charlet, L., Chakraborty, S., Appelo, C. A. J., Roman-Ross, G., Nath, B., Ansari, A. A., … Mallik, S. B. (2007). Chemodynamics of an arsenic “hotspot” in a West Bengal aquifer: A field and reactive transport modeling study. *Applied Geochemistry*, *22*(7), 1273–1292. https://doi.org/10.1016/j.apgeochem.2006.12.022

Constantz, J., Eddy-Miller, C. A., Wheeler, J. D., & Essaid, H. I. (2013). Streambed exchanges along tributary streams in humid watersheds. *Water Resources Research*, *49*(4), 2197–2204. https://doi.org/10.1002/wrcr.20194

Coston, J. A., Fuller, C. C., & Davis, J. A. (1995). Pb2+ and Zn2+ adsorption by a natural aluminum- and iron-bearing surface coating on an aquifer sand, *59*(17), 3535–3547. Retrieved from papers3://publication/uuid/EEE9AFA5-4AAB-45B9-B125-3F9B5C402C74

Davidson, E. A., & Janssens, I. A. (2006). Temperature sensitivity of soil carbon decomposition and feedbacks to climate change. *Nature*. https://doi.org/10.1038/nature04514

Engelhardt, I., Piepenbrink, M., Trauth, N., Stadler, S., Kludt, C., Schulz, M., … Ternes, T. A. (2011). Comparison of tracer methods to quantify hydrodynamic exchange within the hyporheic zone. *Journal of Hydrology*, *400*(1–2), 255–266. https://doi.org/10.1016/j.jhydrol.2011.01.033

Engelhardt, I., Prommer, H., Schulz, M., Vanderborght, J., Schu, C., & Ternes, T. A. (2014). Reactive Transport of Iomeprol during Stream-Groundwater Interactions. https://doi.org/10.1021/es403194r

Erickson, M. L., & Barnes, R. J. (2005a). Glacial sediment causing regional-scale elevated arsenic in drinking water. *Ground Water*, *43*(6), 796–805. https://doi.org/10.1111/j.1745-6584.2005.00053.x

Erickson, M. L., & Barnes, R. J. (2005b). Well characteristics influencing arsenic concentrations in ground water. *Water Research*, *39*(16), 4029–4039. https://doi.org/10.1016/j.watres.2005.07.026

Farquhar, M. L., Charnock, J. M., Livens, F. R., & Vaughan, D. J. (2002). Mechanisms of arsenic uptake from aqueous solution by interaction with goethite, lepidocrocite, mackinawite, and pyrite: An X-ray absorption spectroscopy study. *Environmental Science and Technology*, *36*(8), 1757–1762. https://doi.org/10.1021/es010216g

Fierer, N., Colman, B. P., Schimel, J. P., & Jackson, R. B. (2006). Predicting the temperature dependence of microbial respiration in soil : A continental-scale analysis, *20*(June). https://doi.org/10.1029/2005GB002644

Findlay, A. J., & Kamyshny, A. (2017). Turnover rates of intermediate sulfur species (Sx2-, S0, S2O32-, S4O62-, SO32-) in anoxic freshwater and sediments. *Frontiers in Microbiology*, *8*(DEC). https://doi.org/10.3389/fmicb.2017.02551

Fuller, C. C., & Harvey, J. W. (2000). Reactive Uptake of Trace Metals in the Hyporheic Zone of a Mining-Contaminated Stream , Pinal Creek , Arizona. *Environmental Science and Technology*, *34*(7), 1150–1155. https://doi.org/10.1021/es990714d

Gandy, C. J., Smith, J. W. N., & Jarvis, A. P. (2007). Attenuation of mining-derived pollutants in the hyporheic zone : A review, *373*, 435–446. https://doi.org/10.1016/j.scitotenv.2006.11.004

Goldberg, S., & Johnston, C. T. (2001). Mechanisms of Arsenic Adsorption on Amorphous Oxides Evaluated Using Macroscopic Measurements, Vibrational Spectroscopy, and Surface Complexation Modeling. *Journal of Colloid and Interface Science*, *234*(1), 204–216. https://doi.org/10.1006/jcis.2000.7295

Gutknecht, J. L. M., Goodman, R. M., & Balser, T. C. (2006). Linking soil process and microbial ecology in freshwater wetland ecosystems. *Plant and Soil*, *289*(1–2), 17–34. https://doi.org/10.1007/s11104-006-9105-4

Hansel, C. M., Benner, S. G., Nico, P., & Fendorf, S. (2004). Structural constraints of ferric (hydr)oxides on dissimilatory iron reduction and the fate of Fe(II). *Geochimica et Cosmochimica Acta*, *68*(15), 3217–3229. https://doi.org/10.1016/j.gca.2003.10.041

Hansel, C. M., Lentini, C. J., Tang, Y., Johnston, D. T., Wankel, S. D., & Jardine, P. M. (2015). Dominance of sulfur-fueled iron oxide reduction in low-sulfate freshwater sediments. *ISME Journal*, *9*(11), 2400–2412. https://doi.org/10.1038/ismej.2015.50

Harvey, C. F., Swartz, C. H., Badruzzaman, A. B. M., Keon-Blute, N., Yu, W., Ali, M. A., … Ahmed, M. F. (2002). Arsenic mobility and groundwater extraction in Bangladesh. *Science*, *298*(5598), 1602–1606.

https://doi.org/10.1126/science.1076978

Hatch, C. E., Fisher, A. T., Revenaugh, J. S., Constantz, J., & Ruehl, C. (2006). Quantifying surface water – groundwater interactions using time series analysis of streambed thermal records : Method development, *42*(Table 1), 1–14. https://doi.org/10.1029/2005WR004787

Heron, G., Crouzet, C., Bourg, A. C. M., & Christensen, T. H. (1994). Speciation of Fe(II) and Fe(III) in Contaminated Aquifer Sediments Using Chemical Extraction Techniques. *Environmental Science and Technology*, *28*(9), 1698–1705. https://doi.org/10.1021/es00058a023

Hull, R.B., Briggs, M.A., LeBlanc, D.R., Armstrong, D.A., and McCobb, T.D., 2019, Temperature and seepage data from the nearshore bottom sediments of five groundwater flow-through glacial kettle lakes, western Cape Cod, Massachusetts, 2015-18: U.S. Geological Survey data release, https://doi.org/10.5066/P9QLIFWV.

Jakobsen, R., & Cold, L. (2007). Geochemistry at the sulfate reduction-methanogenesis transition zone in an anoxic aquifer-A partial equilibrium interpretation using 2D reactive transport modeling. *Geochimica et Cosmochimica Acta*, *71*(8), 1949–1966. https://doi.org/10.1016/j.gca.2007.01.013

Janssen, P. H., Schuhmann, A., Bak, F., & Liesack, W. (1996). Disproportionation of inorganic sulfur compounds by the sulfate-reducing bacterium Desulfocapsa thiozymogenes gen, nov., sp. nov. *Archives of Microbiology*, *166*(3), 184–192. https://doi.org/10.1007/s002030050374

Jørgensen, B. B., Zawacki, L. X., & Jannasch, H. W. (1990). Thermophilic bacterial sulfate reduction in deep-sea sediments at the Guaymas Basin hydrothermal vent site (Gulf of California). *Deep Sea Research Part A, Oceanographic Research Papers*, *37*(4), 695–710. https://doi.org/10.1016/0198-0149(90)90099-H

Jung, H. U. N. B. O. K., Charette, M., & Zheng, Y. (2009). Study of Reactive Transport of Groundwater Arsenic in a Coastal Aquifer. *Environmental Science and Technology*, *43*(14), 5333–5338.

Kaplan, D. I., Buettner, S. W., Li, D., Huang, S., Koster, P. G., Groos, V., … Jaff, P. R. (2017). Applied Geochemistry In situ porewater uranium concentrations in a contaminated wetland : Effect of seasons and sediment depth *, *85*, 128–136. https://doi.org/10.1016/j.apgeochem.2016.11.017

Kent, D. B., & Fox, P. M. (2004). The influence of groundwater chemistry on arsenic concentrations and speciation in a quartz sand and gravel aquifer. *Geochemical Transactions*, *5*(1), 1–12. https://doi.org/10.1063/1.1738211

Lamers, L. P. M., van Diggelen, J. M. H., Op Den Camp, H. J. M., Visser, E. J. W., Lucassen, E. C. H. E. T., Vile, M. A., … Roelofs, J. G. M. (2012). Microbial transformations of nitrogen, sulfur, and iron dictate vegetation composition in wetlands: A review. *Frontiers in Microbiology*, *3*(APR), 1–12.

https://doi.org/10.3389/fmicb.2012.00156

Lautz, L. K., Kranes, N. T., & Siegel, D. I. (2010). Heat tracing of heterogeneous hyporheic exchange adjacent to in-stream geomorphic features, *3086*(May), 3074–3086. https://doi.org/10.1002/hyp.7723

Lautz, L. K., & Siegel, D. I. (2006). Modeling surface and ground water mixing in the hyporheic zone using MODFLOW and MT3D. *Advances in Water Resources*, *29*(11), 1618–1633. https://doi.org/10.1016/j.advwatres.2005.12.003

Lloyd, J., & Taylor, J. A. (1994). On the Temperature Dependence of Soil Respiration. *Functional Ecology*, *8*(3), 315–323.

Luther, G. W. (1987). Pyrite oxidation and reduction: Molecular orbital theory considerations. *Geochimica et Cosmochimica Acta*, *51*(12), 3193–3199. https://doi.org/10.1016/0016-7037(87)90127-X

Lynch, S. F. L., Batty, L. C., & Byrne, P. (2014). Environmental Risk of Metal Mining Contaminated River Bank Sediment at Redox-Transitional Zones, 52–73. https://doi.org/10.3390/min4010052

Mandal, B. K., & Suzuki, K. T. (2002). Arsenic round the world : a review. *Talanta*, *58*, 201–235.

Manning, B. A., & Goldberg, S. (1996). Modeling Competitive Adsorption of Arsenate with Phosphate and Molybdate on Oxide Minerals. *Soil Science Society of America Journal*, *60*(1), 121. https://doi.org/10.2136/sssaj1996.03615995006000010020x

Mitra, S., Wassmann, R., & Vlek, P. L. G. (2005). An appraisal of global wetland area and its organic carbon stock. *Current Science*, *88*(1), 25–35.

Mitsch, W. J., Bernal, B., Nahlik, A. M., Jørgensen, S. E., & Brix, H. (2013). Wetlands , carbon , and climate change, 583–597. https://doi.org/10.1007/s10980-012-9758-8

National Weather Service. Columbia, SC Weather Forecast Office. https://www.weather.gov/cae/cliplotdnl2019. Retrieved January 6th,2019.

Nagorski, S. A., & Moore, J. N. (1999). Arsenic mobilization in the hyporheic zone of a stream, *35*(11), 3441–3450.

Neubauer, S. C., Emerson, D., & Megonigal, J. P. (2002). Life at the energetic edge: Kinetics of circumneutral iron oxidation by lithotrophic iron-oxidizing bacteria isolated from the wetland-plant rhizosphere. *Applied and Environmental Microbiology*, *68*(8), 3988–3995. https://doi.org/10.1128/AEM.68.8.3988-3995.2002

Neumann, R. B., Seyfferth, A. L., Teshera-levye, J., & Ellingson, J. (2017). Soil Warming Increases Arsenic Availability in the Rice Rhizosphere. *Agricultural & Environmental Letters, 2*(1). https://doi.org/10.2134/ael2017.02.0006

Ng, G.-H. C., Yourd, A. R., Johnson, N. W., & Myrbo, A. E. (2017). Modeling hydrologic controls on sulfur processes in sulfate-impacted wetland. *Journal of Geophysical Research*, *122*, 2435–2457. https://doi.org/10.1002/2017JG003822

Ng, Gene-Hua Crystal, Bekins, B. A., Cozzarelli, I. M., Baedecker, M. J., Bennett, P. C., Amos, R. T., & Herkelrath, W. N. (2015). Reactive transport modeling of geochemical controls onsecondary water quality impacts at a crude oil spill site nearBemidji, MN. *Water Resources Research*, *51*, 4156–4183. https://doi.org/10.1002/2015WR016964.Received

Nicholas, S. L., Erickson, M. L., Woodruff, L. G., Knaeble, A. R., Marcus, M. A., Lynch, J. K., & Toner, B. M. (2017). Solid-phase arsenic speciation in aquifer sediments: A micro-X-ray absorption spectroscopy approach for quantifying trace-level speciation. *Geochimica et Cosmochimica Acta*, *211*, 228–255. https://doi.org/10.1016/j.gca.2017.05.018

Nordstrom, D. K. (2002). Worldwide occurrences of arsenic in ground water. *Science*, *296*(5576), 2143–2145. https://doi.org/10.1126/science.1072375

Oremland, R., & Stolz, J. (2003). The Ecology of Arsenic. *Science*, *300*(5621), 939–944.

Pierce, M. L., & Moore, C. B. (1980). Adsorption of Arsenite on Amorphous Iron Hydroxide from Dilute Aqueous Solution, 214–216. https://doi.org/10.1021/es60162a011

Pierce, M. L., & Moore, C. B. (1982). ADSORPTION OF ARSENITE AND ARSENATE ON AMORPHOUS IRON HYDROXIDE, *16*.

Postma, D., & Jakobsen, R. (1996). Redox zonation : Equilibrium constraints on the Fe (III)/ SO4-reduction interface. *Geochimica et Cosmochimica Acta*, *60*(17), 3169–3175.

Postma, Dieke, Larsen, F., Minh Hue, N. T., Duc, M. T., Viet, P. H., Nhan, P. Q., & Jessen, S. (2007). Arsenic in groundwater of the Red River floodplain, Vietnam: Controlling geochemical processes and reactive transport modeling. *Geochimica et Cosmochimica Acta*, *71*(21), 5054–5071. https://doi.org/10.1016/j.gca.2007.08.020

Prommer, H., Barry, D. A., & Davis, G. B. (2002). Modelling of physical and reactive processes during biodegradation of a hydrocarbon plume under transient groundwater flow conditions. *Journal of Contaminant Hydrology*, *59*(1–2), 113–131. https://doi.org/10.1016/S0169-7722(02)00078-5

Radu, T., Subacz, J. L., Phillippi, J. M., & Barnett, M. O. (2005). Effects of dissolved carbonate on arsenic adsorption and mobility. *Environmental Science and Technology*, *39*(20), 7875–7882. https://doi.org/10.1021/es050481s

Raiswell, R., Canfield, D. E., & Berner, R. A. (1994). A comparison of iron extraction methods for the determination of degree of pyritisation and the recognition of iron-limited pyrite formation, *111*, 101–110.

Rau, G. C., Andersen, M. S., Mccallum, A. M., & Acworth, R. I. (2010). Analytical methods that use natural heat as a tracer to quantify surface water – groundwater exchange , evaluated using fi eld temperature records, 1093–1110. https://doi.org/10.1007/s10040-010-0586-0

Rau, G. C., Andersen, M. S., Mccallum, A. M., Roshan, H., & Acworth, R. I. (2014). Heat as a tracer to quantify water flow in near-surface sediments. *Earth Science Reviews*, *129*, 40–58. https://doi.org/10.1016/j.earscirev.2013.10.015

Raven, K. P., Jain, A., & Loeppert, R. H. (1998). Arsenite and Arsenate Adsorption on Ferrihydrite : Kinetics , Equilibrium , and Adsorption Envelopes, *32*(3), 344–349. https://doi.org/10.1021/es970421p

Repert, D.A., Smith, R.L., and LeBlanc, D.R., 2020, Determination of the effect of temperature (Q10) on rates of oxygen consumption in surface sediments collected from Ashumet Pond on Cape Cod, MA (2016): U.S. Geological Survey data release, https://doi.org/10.5066/P9SPP01Q.

Rickard, D. (1995). Kinetics of FeS precipitation: Part 1. Competing reaction mechanisms. *Geochimica et Cosmochimica Acta*, *59*(21), 4367–4379. https://doi.org/10.1016/0016-7037(95)00251-T

Roden, E. E., Wetzel, R. G., & Dec, N. (2007). Organic Carbon Oxidation and Suppression of Methane Production by Microbial Fe (III) Oxide Reduction in Vegetated and Unvegetated Freshwater Wetland Sediments Organic carbon oxidation and suppression of methane production by microbial Fe (II1) oxide r. *Limnology*, *41*(8), 1733–1748.

Runkel, R. L., & Kimball, B. A. (2002). Evaluating remedial alternatives for an acid mine drainage stream: Application of a reactive transport model. *Environmental Science and Technology*, *36*(5), 1093–1101. https://doi.org/10.1021/es0109794

Scanlon, B. R., & Cook, P. G. (2002). Preface Theme issue on groundwater recharge, 3–4. https://doi.org/10.1007/s10040-001-0175-3

Simmler, M., Bommer, J., Frischknecht, S., Christl, I., Kotsev, T., & Kretzschmar, R. (2017). Reductive solubilization of arsenic in a mining-impacted river floodplain : Influence of soil properties and temperature. *Environmental Pollution*, *231*. https://doi.org/10.1016/j.envpol.2017.08.054

Singh, A. J. S., & Gupta, S. R. (1977). Plant Decomposition and Soil Respiration in Terrestrial Ecosystems. *Botanical Review*, *43*(4), 449–528.

Smedley, P. L., & Kinniburgh, D. G. (2002). A review of the source, behaviour and distribution of arsenic in natural waters. *Applied Geochemistry*, *17*(5), 517–568.

https://doi.org/10.1016/S0883-2927(02)00018-5

Smith, A. H., Lingas, E. O., & Rahman, M. (2000). Contamination of drinking-water by arsenic in Bangladesh : a public health emergency, *78*(9).

Smith, R. L., Repert, D. A., Barber, L. B., & Leblanc, D. R. (2013). Long-term groundwater contamination after source removal — The role of sorbed carbon and nitrogen on the rate of reoxygenation of a treated-wastewater plume on Cape Cod , MA , USA. *Chemical Geology*, *337–338*, 38–47. https://doi.org/10.1016/j.chemgeo.2012.11.007

Sophocleous, M. (2002). Interactions between groundwater and surface water : the state of the science. *Hydrogeology Journal*, *10*, 52–67. https://doi.org/10.1007/s10040-001-0170-8

Stern, N., Ginder-vogel, M., Stegen, J. C., Arntzen, E., Kennedy, D. W., Larget, B. R., & Roden, E. (2017). Colonization Habitat Controls Biomass Composition, and Metabolic Activity of Attached Microbial Communities in the Columbia River Hyporheic Corridor. *Applied and Environmental Microbiology*, *83*(16), 1–18.

Stoliker, D. L., Repert, D. A., Smith, R. L., Song, B., LeBlanc, D. R., McCobb, T. D., … Kent, D. B. (2016). Hydrologic Controls on Nitrogen Cycling Processes and Functional Gene Abundance in Sediments of a Groundwater Flow-Through Lake. *Environmental Science and Technology*, *50*(7), 3649–3657. https://doi.org/10.1021/acs.est.5b06155

Sutherland, R. A. (2002). Comparison between non-residual Al, Co, Cu, Fe, Mn, Ni, Pb and Zn released by a three-step sequential extraction procedure and a dilute hydrochloric acid leach for soil and road deposited sediment. *Applied Geochemistry*, *17*(4), 353–365. https://doi.org/10.1016/S0883-2927(01)00095-6

Thamdrup, B., Finster, K., Hansen, J. W., & Bak, F. (1993). Bacterial disproportionation of elemental sulfur coupled to chemical reduction of iron or manganese. *Applied and Environmental Microbiology*, *59*(1), 101–108.

Voelz, J. L., Johnson, N. W., Chun, C. L., Arnold, W. A., & Penn, R. L. (2019). Quantitative Dissolution of Environmentally Accessible Iron Residing in Iron-Rich Minerals : A Review. *ACS Earth and Space Chemistry*, *3*, 1371–1392. review-article. https://doi.org/10.1021/acsearthspacechem.9b00012

Wallis, I., Prommer, H., Pichler, T., Post, V., B. Norton, S., Annable, M. D., & Simmons, C. T. (2011). Process-based reactive transport model to quantify arsenic mobility during aquifer storage and recovery of potable water. *Environmental Science and Technology*, *45*(16), 6924–6931. https://doi.org/10.1021/es201286c

Weber, F., Hofacker, A. F., Voegelin, A., & Kretzschmar, R. (2010). Temperature Dependence and Coupling of Iron and Arsenic Reduction and Release during Flooding of a Contaminated Soil. *Environmental Science & Technology*, *44*(1), 116–

122.

Welch, A., Lico, M., & Hughes, J. (1988). Arsenic in Ground Water of the Western United States. *Ground Water*, *26*(3), 333–347.

Welch, A., Westjohn, D. B., Helsel, D., & Wanty, R. (2000). Arsenic in Ground Water of the United States: Occurrence and Geochemistry. *Ground Water*, *38*(4), 589–604.

Williamson, C. E., Morris, D. P., Pace, M. L., & Olson, O. G. (1999). Dissolved organic carbon and nutrients as regulators of lake ecosystems: Resurrection of a more integrated paradigm. *Limnology and Oceanography*, *44*(3part2), 795–803. https://doi.org/10.4319/lo.1999.44.3_part_2.0795

Winter, T. C., Harvey, J. W., Franke, O. L., & Alley, W. M. (1998). Ground Water U . S . Geological Survey Circular 1139.

Wu, S., Zhao, Y., Chen, Y., Dong, X., Wang, M., & Wang, G. (2019). Sulfur cycling in freshwater sediments: A cryptic driving force of iron deposition and phosphorus mobilization. *Science of the Total Environment*, *657*, 1294–1303. https://doi.org/10.1016/j.scitotenv.2018.12.161

Zarnetske, J. P., Haggerty, R., Wondzell, S. M., Bokil, V. A., & González-Pinzón, R. (2012). Coupled transport and reaction kinetics control the nitrate source-sink function of hyporheic zones. *Water Resources Research*, *48*(11), 1–15. https://doi.org/10.1029/2012WR011894

Zhang, S., Kent, D. B., Elbert, D. C., Shi, Z., Davis, J. A., & Veblen, D. R. (2011). Mineralogy, morphology, and textural relationships in coatings on quartz grains in sediments in a quartz-sand aquifer. *Journal of Contaminant Hydrology*, *124*(1–4), 57–67. https://doi.org/10.1016/j.jconhyd.2011.02.003

Zheng, C., and G. D. Bennett (2002), Applied Contaminant Transport Modeling, 2nd ed., 621 pp., John Wiley, Hoboken, N. J.